DEVELOPMENT AND PROGRESSION OF AEOLIAN BLOWOUTS ON PADRE ISLAND NATIONAL SEASHORE

A Thesis

by

MALLORIE ELIZABETH JEWELL

Submitted to the Office of Graduate Studies of
Texas A&M University
in partial fulfillment of the requirements for the degree of

MASTER OF SCIENCE

Chair of Committee,	Chris Houser
Committee Members,	Mark Everett
	Rusty Feagin
	Vatche Tchakerian
Head of Department,	Vatche Tchakerian

August 2013

Major Subject: Geography

ABSTRACT

This study characterizes the development and migration of blowouts within Padre Island National Seashore (PAIS). A combination of aerial photographs and Light Detection and Ranging (LIDAR) are used to track the migration of eighteen blowouts, while Ground-penetrating Radar (GPR) is used to investigate the subsurface at two smaller sites in the study area. This data, coupled with beach morphology and changing anthropogenic factors, helps understand why the dune blowouts develop and are restricted to a particular section of the National Seashore.

Aerial Photographs taken at least twice a decade since 1969 were used to track blowouts. Each blowout was digitized in order to understand its morphometric characteristics by studying its length, width, area, segmentation, perimeter, and the width of the neck, when present, through the foredune. The velocity and direction of movement were also calculated. Cluster analysis was used to analyze the blowouts using these morphological variables. Based on this data, blows appear to group into two morphologically different clusters. Blowouts grouped into Cluster 1 are longer, thinner, have smaller perimeters and areas, smaller throat widths, and are furthest from the beach access road. A lower dune elevation leads to a larger wave runup to crest height ratio. A larger ratio suggests that the dunes are more easily overtopped during large storms, thus scarping, a precursor to blowout development, is increased. Cluster 2 blowouts tend to be longer, wider, and stabilized faster leading to a more undulated perimeter in addition to a smaller wave runup potential due to a higher dune elevation.

Historically blowouts covered the entire northern portion of PAIS. In the 1970's the portion of the beach north of Park Road 22 was designated as non-driving. Since then all blowouts in this section have revegetated, while, blowouts in the driving section are still active. Beach driving pulverizes seaweed leading to less deposition along the dune toe and therefore a lower elevation of the backshore. As a result there is a greater wave runup in storms leading to an increase in susceptibility to scarping, and therefore, blowouts.

Despite the fact that storms are the primary mechanism for blow development, anthropogenic effects, such as vehicle traffic, flatten the beach profile allowing for lower areas to become inundated during storms. This, along with decreased sediment budget and increased storm frequency increases the potential for blowouts to form events and leave the island vulnerable to an increased rate of sea level rise.

GPR surveys were completed at two sites; an active blowout with a foredune that is not completely reestablished (Site 1) and a blowout that is stabilized by vegetation (Site 2). Six GPR surveys were completed at Site 1 and four surveys were completed at Site 2 that show the preservation of historic phases, surfaces, and facies used to interpret sequences and compare to aerial photography and LiDAR data. Site 1 moves through five phases that begin in 1969 and end at the present location, while Site 2 moves through three active phases and then ends in a fourth phase by becoming completely stabilized with vegetation in 2010.

ACKNOWLEDGEMENTS

I would like to thank my committee chair, Dr. Chris Houser, for his excellent leadership and my committee members, Dr. Mark Everett, Dr. Rusty Feagin, and Dr. Vatche Tchakerian, for their guidance and support throughout the course of this research.

Secondly I would like to thank all of my fellow graduate students who acted as field assistants: Sarah Trimble, D. Ryan Arnott, Tess Rentschlar, Christy Swann, and Patrick Barrineau; as well as my undergraduate assistants: David Hoffman, Janelle Randolph, Stephen Nguyen, and Bradley Morales. Without them I would not have been able to collect the massive amounts of data required for this research. I would also like to extend my gratitude to Brad Weymer, whose expertise in the processing of ground-penetrating radar data was immensely helpful.

Additional thanks goes out to my friends and colleagues in the department who made my time at Texas A&M University a great experience. I would also like to thank the Padre Island National Seashore Park Service, who graciously allowed me the opportunity to collect the data for this project.

Finally, I want to extend my gratitude to my parents, for their continued support of me and their encouragement, as well as my boyfriend, for his continued and unwavering support in my pursuit of this degree.

NOMENCLATURE

GHCND	Global Historical Climatology Network - Daily
GPR	Ground-Penetrating Radar
LiDAR	Light Detection and Ranging
NOAA	National Oceanic and Atmospheric Administration
PAIS	Padre Island National Seashore
USDA	United States Department of Agriculture
USGS	United States Geological Survey

TABLE OF CONTENTS

Page

LIST OF FIGURES

Page

LIST OF TABLES

Page

1. INTRODUCTION

Recent evidence suggests that development of dune blowouts and migration of parabolic dunes to the backbarrier shoreline may be a mechanism through which barrier islands transgress in response to relative sea level rise (Hoyt 1967, Otvos 1970, Davidson-Arnott 2005, Garrison et al. 2010). Blowouts develop in areas where variable vegetation cover and dune height increase the potential for foredune erosion. When major storms scrape the dune base, transporting sediment leeward, the foredune migrates landward and this migration is accelerated with the development of blowouts. This is accentuated even more by an increase in wind velocity, wave runup during tropical storms, or anthropogenic disturbances (Gares and Nordstrom 1988, Gares 1992, Bate and Ferguson 1996, Hesp 2002, Davidson-Arnott 2005).

The initial breach along the dune line is caused by erosion and scarping which allows sediment to be funneled landward into the vegetated dune field (Gares 1992, Hesp 2002). Wind converges through the neck of the blowout, eroding sediment and transporting it into the backbarrier, and covering any vegetation that is present. This process continues to increase the size of the blowout, with direction and velocity of blowout movement dependent on the dominant wind direction. Over time, the foredune rebuilds, allowing vegetation to stabilize the entrance (the throat) of the blowout. With the front stabilized, the depositional lobe can then move landward. The depositional lobe continues to move as long as the rate at which it moves landward is faster than the rate at

which it vegetation recolonizes (Jungerius et al. 1981, Gares 1992, Hesp and Hyde 1996, Hesp 2002, Levin 2011).

It is possible that the foredune breach may never completely recover, or that reactivation may occur post-stabilization if there is an increase in storms, anthropogenic forcing, or a decrease in precipitation (Leatherman 1979). When this occurs, both the probability of continued scarping and the size of the blowout will increase (Hesp 2002).

Padre Island National Seashore (PAIS) was founded "to save and preserve, for purposes of public recreation, benefit, and inspiration, a portion of the diminishing seashore of the Unites States that remains undeveloped…" (Weise and White 1980, page 6). The National Parks Service (NPS) is tasked with the management of the Seashore in order to: 1) serve the visitor, 2) preserve the resource and 3) administer the area (NPS 1973). Developing an understanding of when these blowouts originally formed, their present location, and evolution since the 1960's allows for a better understanding of the geomorphic processes taking place as well how visitors, storms, and climate affect the management of the island as a resource. Erosion removes sand and vegetation from the foredune leaving it vulnerable during storms. The purpose of this study is to develop an understanding of how blowouts on PAIS have developed and evolved over the past 50 years. This study will examine aerial photographs, LIDAR and GPR data in conjunction with climatic, geomorphologic and anthropogenic affects to understand the changes and migration patterns of these blowouts. The objectives are to:

1) Quantify the spatial and temporal evolution and distribution of blowouts and parabolic dunes on North Padre Island

2) Relate temporal and spatial evolution of blowouts and parabolic dunes to variations in climate (i.e. temperature, precipitation, storm chronology), beach and dune morphology, and anthropogenic forcing

3) Characterize internal structure of blowouts two representative blowouts using GPR surveys and aerial photography to develop a model of blowout phases

The objectives are discussed following an initial study site description that details the establishment of the Padre Island as a National Seashore and the island's initial geological formation. This first section provides a study of the historical and spatial progression of blowouts through aerial photography, and encompasses the first two objectives. The second section focuses on the internal structure of two smaller study sites within the larger study area, and accomplishes objective 3.

2. STUDY AREA

At 182 kilometers long, Padre Island (Figure 1) is the longest barrier island in the United States, extending along the Texas gulf coast from Corpus Christi Bay in the north to the Rio Grande Delta (Weise and White, 1980). After failed efforts to establish a state park on the island between 1936 and 1955, Texas Senator Ralph Yarborough introduced a new bill to Congress in 1958 to that would help protect the Island (Brezina 2005). In 1962, Congress passed *Public Law 87-712* making the northern 105 km of the island a national seashore to "*save and preserve, for purposes of public recreation, benefit, and inspiration, a portion of the diminishing seashore of the United States that remains undeveloped..."* as cited in Mathewson and Cole (1980) and Weise and White (1980). The National Seashore was dedicated in April of 1968 after over 130,000 acres in five different south Texas counties were procured (NPS 2010, Brezina 2005). Prior to the formation of the National Seashore, the Island's natural boundaries (Laguna Madre to the West, Mansfield Channel to the South, and the Gulf of Mexico to the East) had acted as great natural boundaries for ranchers to graze cattle. With the establishment of the National Seashore, grazing cattle from the King and Dunn ranch were removed and no cattle have inhabited the island since the 1970s - allowing for vegetation regrowth. Today the main use of the island is tourism, with a smaller number of visitors maintining the oil and gas facilities (NPS 2010).

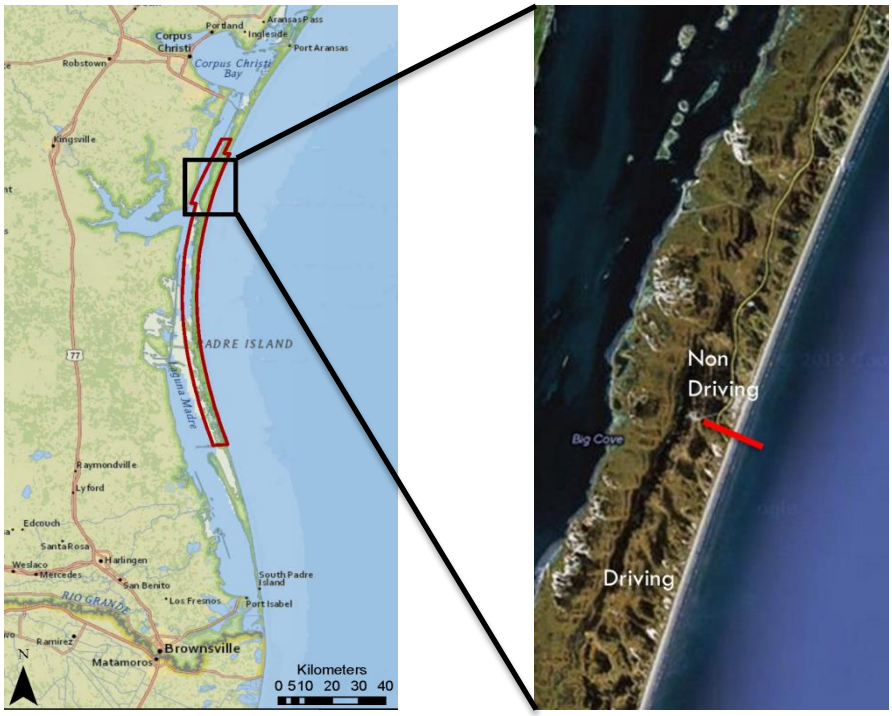

Figure 1- Study Area on Padre Island National Seashore

2.1 GEOLOGY/GEOMORPHOLOGY

Modern barrier islands like Padre Island are found along broad, passive continental margins, comprising 5,700 kilometers of the world's coastline with roughly 3,200 kilometers of that being found along the coast of North America. These long and narrow islands are controlled by both wind and wave action leading to a smooth ocean facing shoreline with a complex shoreline on the lagoon side with the internal structure depending on climate, sediment supply and tidal range (Dickenson et al. 1972). Padre Island is 182 km long and varies in width from 4 kilometer at the northern end to 1 kilometer further south down the island. Offshore multiple bars lead to a dissipative profile. Dune height decreases from North to South except for the areas of Little Shell

and Big Shell which have the highest and most continuous foredune. The low dune heights at the southern end of the island lead to frequent washover and higher erosion rates then on the northern end where the foredune is higher and more continuous (Weise and White 1980). Though it is a geologically young barrier island, the sediment that created the island was deposited on the continental shelf long before the existence of today's Padre Island.

During the Sangamon Stage in the Pleistocene (125,000 to 110,000 years ago), sediments began depositing on the continental shelf by the ancient Brazos-Colorado and Rio Grande rivers. In addition, an interglacial highstand caused mean sea level to be higher than its present level, allowing the coastal plain and a set of barrier islands to develop. After this warm period, the Wisconsin glacial period allowed glacial environments to dominate the northern portion of the North American continent. As the ice moved southward mean sea level dropped, causing progradation of fluvial environments that incised and eroded previously deposited deltaic muds and marginal marine sediments in order to keep up with the falling sea level. Around 18,000 BP the glaciers began to melt, releasing massive amounts of water that was being stored on the continent. This melting lead to a rapid sea level rise that lasted for ~13,500 years until it finally began to slow down and reach a level 90 to 120 m lower than what we experience today. As this rapid influx of water into the world's ocean basins slowed, sea level reached the segmented portions of the deltas along the Texas Gulf coast causing barrier islands to develop. The amount of sediment emanating from the Rio Grande, Colorado, and Brazos Rivers was enough for the barrier islands to keep up with the sea level rise

and not become inundated (Otvos 1970, Morton 1977, Weise and White 1980, Morton et al. 1994, NPS 2010).

Approximately 4,500 years ago sea level reached a level about 4.6 m below the current level and the longshore transport of sediments caused the islands to coalesce. Padre Island National seashore sits at a confluence of littoral drifts along the Texas coast. The northern end of the island, which is higher and wider than the rest of the island, is derived from fluvial sediment transported from the northeast by offshore currents, while the southern end has sediment deposition mainly from the Rio Grande. These fluvial sediments are from submerged ancestrial delta and barrier island deposits. Longshore drift moved sediment from areas of high sediment accumulation to areas of lower accumulation, resulting in connections between ancient barriers and forming the modern barrier system around 2,400 years ago (Otvos 1970, Morton 1977, Weise and White 1980, Morton 1994, NPS 2010).

While longshore drift led to progradation of Padre during the late Holocene, washover fans facilitated sediment movement to the back of the island and caused retrogradation. According to Garrison et al. (2010), nearly one third of the island's growth during this period comes from the sediment moved landward from storm derived washover deposits. Storms have had major impacts on how Padre Island has evolved since its formation; however, storms during periods of sea level highstand have had the most effect on the island. When a highstand occurs, the height of the foredune ridges is reduced, allowing for an erosional, inundation prone environment during extreme storms (Garrison et al. 2010). These storms create washover as their storm surge breaches the

foredune. However, in areas of higher, more continuous foredunes, where wave runup cannot overtop the foredune but still impacts it, there is scarping that can lead to blowouts. Compared to daily aeolian transport processes on the islands, these storms move much more sediment in a shorter amount of time and therefore represent the dominant way by which the island transgresses (Godfrey and Godfrey 1973, Leatherman 1979, Morton and Sallenger 2003, and Sallenger 2000). As sediment moves toward the back of the island it begins to back step, because of the abundant amount of sediment being supplied to the island at this time the island could continuously move sediment into the backshore. This process allows Padre to keep up with both that increase in sea level and with subsequent highstands (Morton 1977, Garrison et al. 2010).

Storms and sea level rise are still acting upon the island today. Since 1851, 136 storms have passed within 320 kilometers of the study site on Padre Island (NOAA 2012). The hurricane force winds of these storms can extend over a diameter of 40 to 250 kilometers from the center of the storm, while tropical storm force winds can extend up to 500 kilometers from the center (NOAA 2012). Including both hurricane and tropical storm force winds, about 250 storms have impacted the study site since 1851 (NOAA 2012). Recent evidence suggests dune blowouts and migrating parabolic dunes may be a mechanism through which the island transgresses in response to relative sea level rise. However the more frequently storms impact the less study area the less likely the foredune will have time to recover leading to a lower overall dune height. This decrease will inhibit seaward progradation in the future because less sediment will be

available for transport (Hoyt 1967, Otvos 1970, Davidson-Arnott 2005, Garrison et al. 2010).

Under the current conditions, Padre will begin to move from equilibrium into a transgressive state as subsequent storms erode and scarp the dune line (Morton 1977, Leatherman 1979, Davidson-Arnott 2005, Garrison et al. 2010). The decrease in sediment supply will lead to increased erosion, because the rise in sea level would normally scarp the foredune and create blowouts, but the lack of sediment supply means that the foredune will not recover to its original size following blowout inception. The process of transgression will increasingly have too little sediment to increase the islands height relative to sea level as it back steps. As a result the foredunes will be lower in height and more prone to scarping with the next increase in wave run up. In this way, if sea level rise continues to increase at an accelerated rate, it could amplify erosion of the island if the rate of sea level rise increases without a competent sediment supply (Hoyt 1967, Otvos 1970, Leatherman 1979, Davidson-Arnott 2005, Garrison et al. 2010).

3. MORPHOMETRIC ANALYSIS AND CONTROLS OF AEOLIAN BLOWOUTS WITHIN PADRE ISLAND NATIONAL SEASHORE

3.1 INTRODUCTION

Coastal dune blowouts have been documented in the scientific record since 1898 (Cowles 1898). However, it is only in the past few decades that study of blowouts has shifted from the basic understanding of development to how they affect the sediment transport on coastal barrier islands (Jungerius et al. 1981, Gares 1992, Psuty 1992, Hesp and Hyde 1996, Hesp 2002, Levin 2011). With rising sea level at the end of the Holocene and modern eustatic rise, the occurrence of extreme storms leads to increased wave runup eroding or breaching the foredune through washover or blowouts. These features are responsible for transgression of the barrier island. Washover, however, is the most common (Hesp and Hyde 1996, Hesp 2002, Davidson-Arnott 2005). While the conditions needed for blowouts to develop are rare, islands such as Padre Island, which are much wider than the average barrier, create an environment suitable for their development.

The increased potential for scarping induced washovers and blowouts led Sallenger (2000) to develop a new model and scale to describe and predict erosion associated with different magnitudes of storm impacts for barrier islands. Sallenger states that storm impact is dependent on the storm's magnitude and on the wave run up associated with the increased wave height caused by storm surge. The ratios of the dune

crest height (D_{high}), dune base height (D_{low}), storm runup (R_{high}), and normal runup (R_{low}) describe the impact potential of a location (Table 1). This model states that if $\frac{R_{high}}{D_{high}} = 0\ to \frac{D_{low}}{D_{high}}$ then a swash regime is present, if $\frac{R_{high}}{D_{high}} = \frac{D_{low}}{D_{high}}\ to\ 1$ then a collision regime is present. In the swash regime, runup and erosion is confined to the foreshore of the beach, while in a collision regime, the runup reaches a height were it collides with the foredune and scarps the base. If runup exceeds the foredune crest height then either an overwash or inundation regime is present, depending on whether only the R_{high} overtops the crest (overwash) or if both the elevation R_{high} and the R_{low} overtops the dune crest (Sallenger 2000).

Table 1- Storm Impact Scale for Barrier Islands Modified from Sallenger 2000.

Range of $\frac{R_{high}}{D_{high}}$ and $\frac{R_{low}}{D_{high}}$	Regimes	Potential Beach Changes
$\frac{R_{high}}{D_{high}} = 0\ to \frac{D_{low}}{D_{high}}$	Swash	• Runup confined to foreshore • Foreshore erodes during storms, sand transported offshore. • Sand is gradually transported back onshore post storm • Little net change
$\frac{R_{high}}{D_{high}} = \frac{D_{low}}{D_{high}}\ to\ 1$	Collision	• Runup collides with foredune base • Sediment eroded from foredune and transported offshore
$\frac{R_{high}}{D_{high}} > 1\ and\ \frac{R_{low}}{D_{high}} < 1$	Overwash	• Runup exceeded dune crest • Sand is transported landward • Net migration of the barrier beach landward
$\frac{R_{high}}{D_{high}} > 1\ and\ \frac{R_{low}}{D_{high}} > 1$	Inundation	• R_{low} exceeds dune crest • Entire beach/foredune continuously subaqueous • Massive net onshore transport

During times of high wave runup, areas of lower elevation can have localized collision and overwash that erodes the foredune creating inlets which leads to the formation of blowouts. The amount of sediment transported landward in these inlets during storms is one of the greatest influences on island transgression. This is because the volume of sand eroded from the beach and foredune and deposited inland during one storm can amount to the same volume of erosion and deposition occurring over months or years between storms (Prince 1958, Hayes 1967, McGowen 1970, Godfrey and Godfrey 1973, Leatherman 1979, Morton and McGowen 1980, Morton and Sallenger 2003, Sallenger 2000, NPS 2010). With the continued rise in sea-level these storm events will have a greater impact on the barrier. This rise in sea-level will increase the height of wave runup, relative to the dune height, causing greater erosion and scarping of the foredune and blowout development. Sediment erosion will then lead to a landward translation of the beach profile (Davidson-Arnott 2005).

Blowouts are depressions formed by erosion of a foredune. In most cases the erosion is caused by scarping of the foredune, due to increased wave runup during storms, or the removal of vegetation through climate change or human activities (Hesp and Hyde 1996, Hesp 2002). These depressions are typically saucer or tough shaped, depending on the amount of vegetation cover, topography and wind. Most blowouts, within the study area are characteristically trough shaped with a longer length than width, a larger opening on the windward end of the blowout, and a more developed deflation basin downwind (Figure 2; Carter et al. 1990, Hesp 2002, Hugenholtz and Wolfe 2009). Removal of vegetation, by scarping or overwash, causes a breach to

develop within the foredune, allowing the sediment to be moved from the backshore of the beach into the dune field (Hesp and Hyde 1996, Hesp 2002). As the coastal winds move sediment toward the entrance to the blowout, wind velocity increases as airflow is focused through a smaller area allowing for more sediment transportation into the dune field, covering any vegetation that is present. This process continues as more sediment is eroded from the foredune, increasing the size of the blowout by creating and enlarging a depositional lobe. Eventually the foredune rebuilds itself and vegetation stabilizes the entrance to the blowout (Mathewson and Cole 1980, Hesp and Hyde 1996, Hesp 2002, Levin 2011). Once this happens, the depositional lobe begins to move away from the beach evolving into a parabolic dune (Carter 1990).

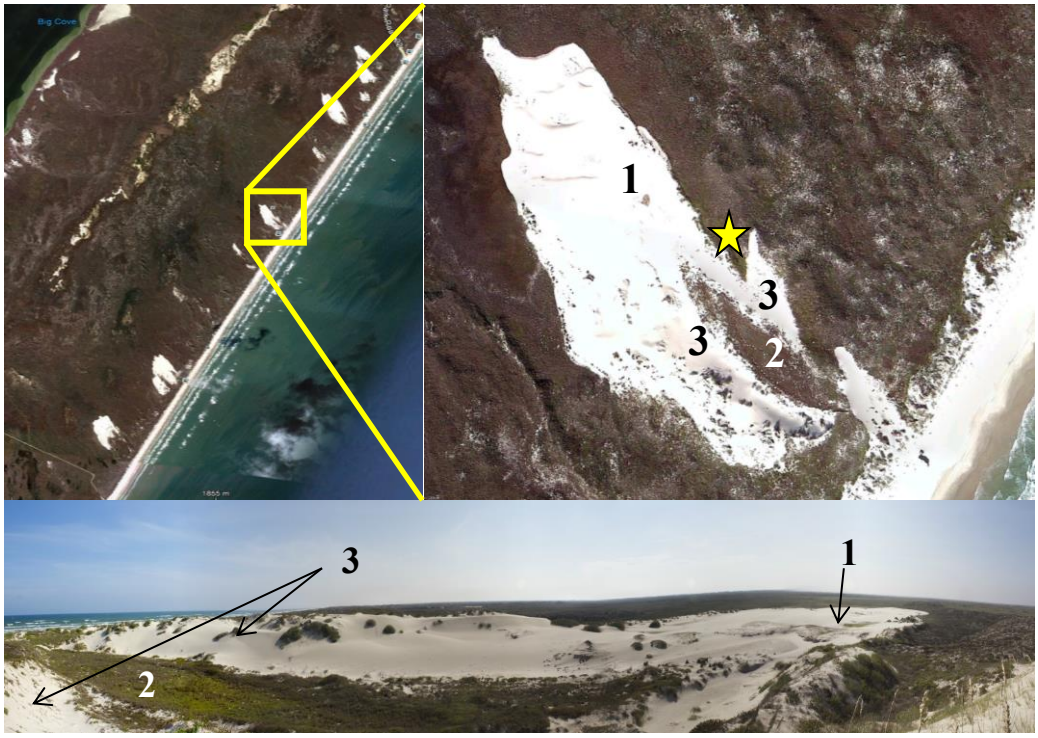

Figure 2 - Trough Blowout Structure: 1) Depositional Lobe, 2) Deflation Basin, 3) Erosional Walls, Star: Vantage Point for Bottom Image.

As previously noted, blowouts tend to become elongated as portions become stabilized by vegetation, creating parabolic dunes from the depositional lobes. Parabolic dunes are characterized by Nield and Baas (2008) as "hairpin or long-walled" with the trailing arms because of the stabilization of vegetation. These dunes remain parabolic as long as the wind stays unidirectional, they have a source of sediment and they remain partially vegetated. If this changes, the blowouts will begin to lose their shape (Tsoar and Blumberg 2002, Dept. of E&R Mgmt. 2012). Original vegetation cover forms on the dune crests and lee slopes of the parabolic dune and as it increases, it slows dune migration across the island. Finally, as the throat of the original blowout closes and vegetation encroaches the parabolic becomes sediment starved and vegetation completely stabilizes the dune (Nield and Baas 2008). If the vegetation does not stabilize the parabolic dune completely or the stabilizing vegetation is removed, the dune will eventually end up as a parabolic dune before transitioning to a sand flat where it becomes dominated by aeolian forcing and not the surrounding topography (Carter et al 1990, Hesp 2002). As it moves into the backbarrier the depositional lobe begins to spread out laterally as it is no longer constrained by island topography (NPS 2010).

Vegetation stabilizes the foredune by extracting the momentum of the winds and sheltering the sand grains (Gares 1992, Hesp and Hyde 1996, Hugenholtz and Wolfe 2009). Specifically, the wind velocity is decreased because of an increase in surface roughness associated with the presence of vegetation, leading to an area of increased deposition and allowing embryo dunes and hummocks to develop (Hesp 2002). These same processes are integral for the foredune reestablishing itself after impact from

extreme storms. However, the frequency and intensity of tropical systems may not allow for a complete rebuilding of the foredune because the initial destruction (reaction time) that a tropical system causes occurs exponentially quicker than the rebuilding of the island (relaxation time; Stone 2004, Houser and Hamilton 2009).

Recovery time, the time it takes for the island to significantly rebuild after a storm event, is typically between 5 – 10 years along the Gulf Coast. In contrast, the average time between tropical storm impacts is 7.1 years (GLO 2005, Houser and Hamilton 2009, Leatherwood 2013). Recovery following storms begins with berm reconstruction and forebeach accretion. Subaerial aggradation of the backshore can begin once the foreshore has recovered. Continued sediment deposition then begins to rebuild the dune structures, however it cannot begin to fully recover until vegetation has reestablished itself and the foredune is stabilized. This process takes much longer than the initial recovery because the vegetation must recover enough to once again trap sediment efficiently enough to force sediment deposition (Morton et al. 1994).

The continued increase in relative sea level complicates the recovery process because island recovery occurs simultaneously with this increase. As sea level rises, wave runup increases in height relative to the dune, causing erosive scarping with both major and minor storms and increasingly removing extensive amounts of vegetation as dunes previously unaffected by runup begin to experience wave impacts. These new impact areas begin to experience wave impacts on a more regular basis, reducing the overall vegetation cover of the foredune and allowing for greater amounts of sediment to

be transported into the backbarrier and a greater potential for blowout formation as the system becomes destabilized (Sallenger 2000, Davidson-Arnott 2005).

Though the reconstruction process is inhibited by the magnitude and frequency of storms, day to day activities also influence the construction and destruction of the foredune and vegetation growth. Vegetation is highly sensitive to climate and anthropogenic influences; it can be easily damaged in coastal environments because of acceleration of airflow over the dune crest, change in climate or vegetation, high velocity wind erosion, or by anthropogenic activities such as grazing or beach traffic (Nield and Bass 2008). Traffic associated with driving on the beach crushes vegetation and seaweed, allowing for an increase in wind velocity and thereby inhibiting deposition at the foredune toe, creating a lower beach profile and increased runup potential (Godfrey and Godfrey 1973, Blum and Jones 1985, Hesp 2002, Houser et al. 2013). An increase in potential runup will subsequently allow for greater scarping of the foredune and potential blowout development so long as it does not exceed the height of the dune and cause washover. As human populations along the coast increase, the combination of human presence, sea level rise, and the potentially increased frequency and magnitude of storms caused by climate change, understanding the development and mechanics of blowouts is increasingly imperative (Oosting and Billings 1942, Davidson-Arnott 2005).

3.1.1 Blowouts at Padre Island National Seashore

Blowouts in Padre Island National Seashore were originally studied by Mathewson and Cole (1980) and Mathewson (1987). In his study, historical aerial photographs from 1937 to 1973 and a geomorphic map based on a 1909 USGS topographic quadrangle sheet were used to map the location of blowouts or "aeolian fans" near Yarborough Pass, ~24 km from the beach access point of Park Road 22. This study concluded that three blowouts were the direct result of hurricane breaches associated with a Hurricane in 1933. By 1938, the area had not revegetated and subsequently, the middle blowout was selected by the State of Texas as the site for Yarborough Pass in order to improve fishing in Laguna Madre. By 1948, the blowout and foredune of the north and south sites of the sites stabilized with vegetation leaving only the active sand sheets of their deflation basins and Yarborough Pass which had refilled in due to sediment supplied by longshore drift but not vegetated. Tropical storms in the 1950's created many new blowouts and that stabilized by 1969.

Due to dredging, the location of Yarborough pass was topographically lower than the surrounding land and continued to act as an active blowout extending from the foredune across the island over 2 kilometers into the backbarrier wind tidal flats. By 1978 the throat of this blowout had almost completely closed and subsequently the depositional lobe continued to migrate downwind and combine with the wind tidal flats. Today this area has completely revegetated. Mathewson (1987) concludes that is impossible to predict the site of the next major foredune breach due to the understanding that blowouts only develop as a result of "hurricanes of significant intensity" and that

"daily processes" to not lead to breaks within the foredune. He also postulated that these "aeolian fans" can only last for ~ 30 years based on the dates of his study (Mathewson and Cole 1980, Mathewson 1987).

The purpose of the present study is to extend the study completed by Mathewson (1980), and help develop a more complete understanding of blowout progression within Padre Island National Seashore. In this study aerial photographs, taken twice a decade since 1969 will be morphometricly analyzed. This data will then be compared to the beach morphology, storm chronology, and climate records to determine how and why the blowouts have developed and evolved over the past 50 years in order to help the park develop management practices that will allow the natural processes to continue to persist with in the National Seashore.

3.2 METHODOLOGY

3.2.1 Aerial Photograph Morphometrics

Aerial photographs provide a historical record of the spatial distribution of blowouts on Padre Island and how they have evolved over time. Aerial photographs and satellite images were acquired from the United States Geological Survey (USGS) and the Padre Island National Seashore (PAIS) using the requirement that they must be taken at least twice a decade since the 1969. By searching with in the study area using Earth Explorer, it was possible to find imagery for the years of 1969, 1974/75 (some frames from the PAIS were missing from 1974), 1979, 1984, 1989, 1993, 1996, 2002, 2008 and 2010. These images were used to track blowouts from their initial conception to their final stabilization by vegetation. Once acquired, the imagery was projected into Universal Transverse Mercator Zone 14N, because this was the projection the used in the 1974 imagery provided by the NPS.

After georefrencing, each consecutive aerial photograph was hand digitized to mark the boundaries of the blowouts. This digitizing was completed using ArcGIS 10.1 and the selections were reinforced by a study comparing the boundaries found by hand with both unsupervised classification (Parallelepiped and Minimum Distance) and supervised classification (IsoData) by using ENVI, an image processing software. These digitized polygons were then used to allow for a comparison based a morphometric analysis. Though not included in the morphometric analysis, blowouts found within the non-driving section were also digitized to analyze potential anthropogenic affects with in

the study area and to determine the differences between the driving and non-driving section.

The morphometrics used in this study are the length, width, area, segmentation, and perimeter in addition to the velocity and direction at which the blowouts move across the island (Table 2). These metrics were calculated within ArcGIS by using the measure tool for length, width, perimeter, and area. The area with individual blowouts in 1969 was sectioned off in order to determine if blowouts reoccurred within the same spatial area cyclically (Figure 3). The sections are labeled A-P with blowout A at the southern extent of the study area working up toward blowout P located at the access road. Study Area 1 (SA1) and 2 (SA2) are also used as labels of two blowouts where a detailed ground-penetrating radar study was conducted (Section 4).

Segmentation is the measure of the number of bare sand area present within each section for each aerial photograph. This was done in order to account for stabilization of the blowouts throughout the study period. To calculate the velocity, and in turn direction of travel for each blowout the centroid point of each segment of a particular blowout was calculated using ArcToolbox. To do this the "Feature to Point" tool was implemented, which locates the centroid of each polygon. From here the mean values of all centroids were found by taking the average X and Y values of the individual centroids using the "Mean Center" tool. This returns one mean location of all segments for a given year. Calculating the angle between subsequent points tells the direction of travel while measuring the distance between points and dividing that by the number of years between

each centroid then determined velocity at which the blowouts have moved across the island over the period of the study.

To develop a greater understanding of the beach morphology, the dune height, max height and dune base were calculated using cross sections that corresponded with the center of the blowout. The elevations barrier island were developed by using a digital elevation model based off 2009 LIDAR data. This LIDAR data was collected for PAIS using the Compact Hydrographic Airborne Rapid Total Survey (CHARTS). The data has a 1 m cell size and by using an inverse distance weighted algorithm the areas between eachh point were populated. To analyze the topography, the lidar was transected every 20 m allong the shoreline of both the driving and non-driving sections. These transects ran from the shoreline to 700 m landward (Houser et al. 2013). This data allows for the dune crest height, base, overall elevation and slope to be calculated allong with cross shore variations in each of these variales to be calculated.

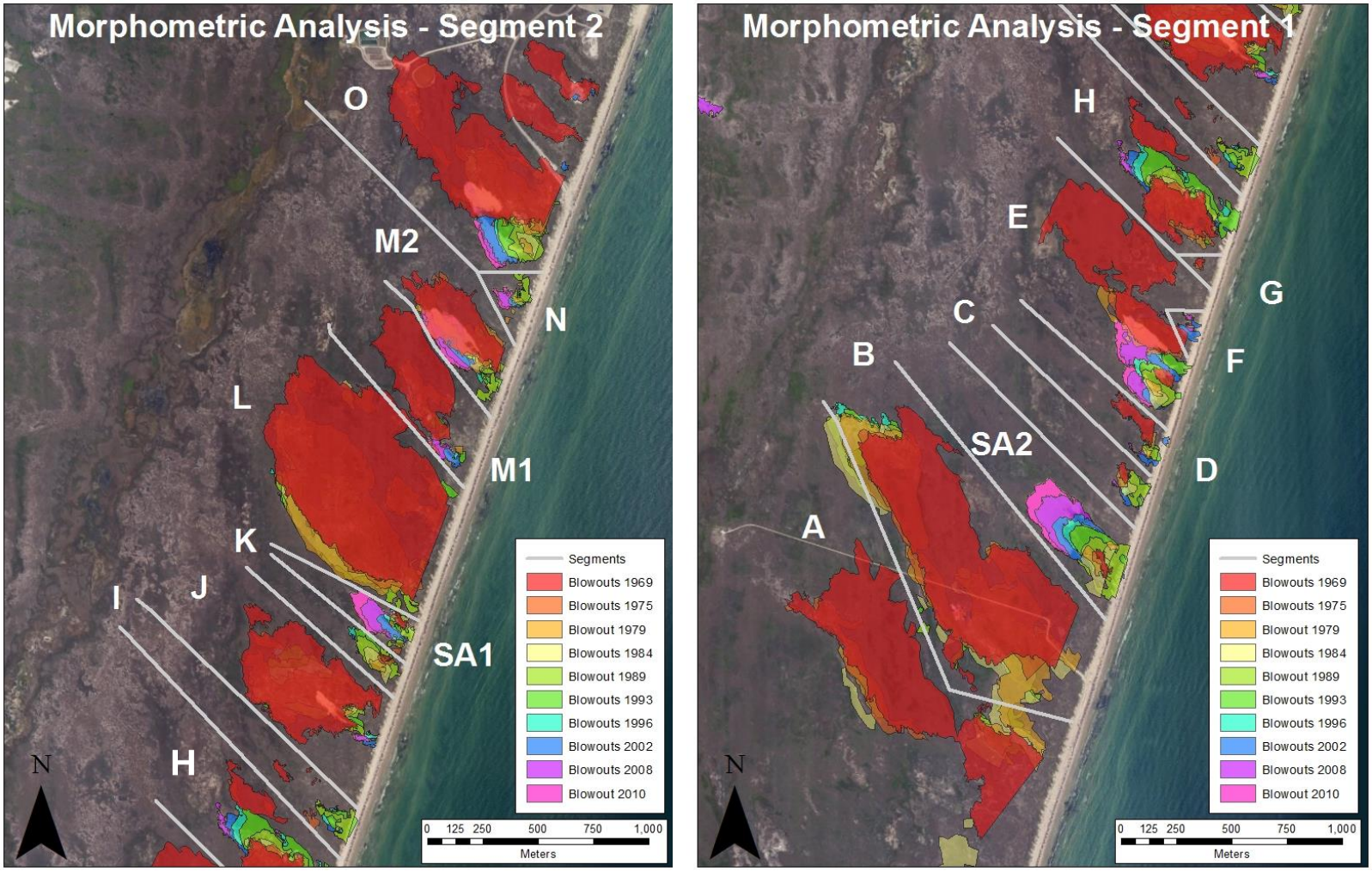

Figure 3- Blowout Sections Within the Study Area

Table 2- Morphometric Analysis Parameters Used for Cluster Analysis

	Description	Visual Representation
Length	Distance between the proximal and distal end of the blowout	
Width	Distance between widest points at dune normal	
Area	The area bare sand for the blowout and depositional lobe including the deflation basin	
Perimeter	The outer edge bare sand for the blowout and depositional lobe including the deflation basin	
Segmentation	The number of bare sand area present within each section for each aerial photograph	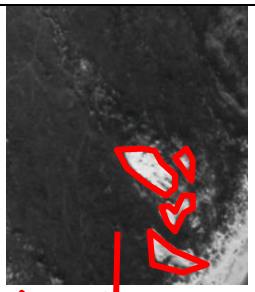 Seg = 4  Seg = 1

3.2.2 Data Analysis

Cluster Analysis

Cluster analysis is used to split variables, in this case the morphometric data, into approximately homogenous groups based on observed values using different algorithms (Scott and Knott 1974, Fraley and Raftery 1998). This process tries to cluster data by minimize within-group variance and maximize between-group variance (Aldenderfer and Blashfield 1984, StatSoft 2013). For this study the variables were joined using tree clustering which joins objects together based on successively larger clusters using a measure of similarity or distance. The distance measured in order to compute distances in this study was based on Euclidean distances. Euclidean distance is computed as:

$$distance(x, y) = \left\{\sum_i (x_i - y_i)^2\right\}^{1/2}$$

The blowout length, width, area, segmentation, perimeter, throat width and velocity as well as the morphology variables of dune height, crest height, dune base, slope, bathymetry at 100 m and the wave runup were all used variables used with in this cluster analysis. This analysis was run using single linkages to create homogenous clusters for both the initial appearance of the blowout and for the current or final extent. Once several blowouts were linked together using Euclidean distances the clusters are then linked together by nearest neighbor amalgamation. The distance between two clusters is then determined by the greatest distance between any two objects in the different clusters (StatSoft 2013). Once these variables are "strung" together the morphometric data was plotted based on these homogenous groups for analysis.

Runup

Stroms have the potential to impact the foredune because of increased wave runup induced by strom surge. Stockdon (2006) found that runup can be calculated for all beaches by :

$$R_2 = 1.1\left(0.35\beta_f(H_0L_0)^{\frac{1}{2}} + \frac{[H_0L_0(0.563\beta_f^2 + 0.004)]^{\frac{1}{2}}}{2}\right)$$

where β_f is the beach slope, H_0 is the deep water wave height and L_0 is the deep water wavelength . The slope of the beach is then calculated by:

$$\beta = \frac{D_b - S_{100}}{100}$$

where D_b is the height of the dune base and S_{100} is the bathymetric elevation 100m offshore. Using this set of parameters wave runup was calculated for each of the transects intersecting the blowouts for a theoretical medium grade storm and normal conditions. Once the wave runup for the specified storm is known it is possible to predict the storm impact on the island by comparing this to the dune crest as described in Sallenger (2000; Table 1).

Temporal Variability

Vegetation, which plays a key role in the blowout stabilization, is affected by changes in the climate of a region. To account for changes in the climate prior to and thorughout the study, percipitation and temperature data from NOAA (2012)'s Global Historical Climatology Network (GHCND) Monthly Summaries were analyzed. This analysis was conduncted inorder to understand delineate changes or trends that could

lead to changes in vegitation cover and extent. The mean temperature (Figure 4a) and precipitation (Figure 4b) were based on data collected monthly by NOAA (2012) from 1945 to the 2012. To idientify trends in both of these data sets a 12 month moving average trendline was incorperrated into each graph. Within the percipitation chart the montly average temperatrues reborted by the National Seashore are also shown. Both data sets were also fit with a second order polynomal trendline to show potential additional trends.

3.2.3 LiDAR

Light Detection and Ranging, or LiDAR, data was employed to calculate the volumetric change of the blowouts within the study area. LiDAR is an active remote sensing platform that uses light pulses to calculate the elevation over a surface. LiDAR is a commonly used method of obtaining data in the field of coastal research. This technology has been used to map bathymetry (Irish and Lillycrop 1999), measure characteristics of dunes (Woolard and Colby 2002, Wolfe and Hugenholtz 2009), analyze morphology (White and Wang 2003, Sallenger et al. 2003, Brock et al. 2004, Houser et al. 2013), and measure response and recovery from extreme storms (Houser et al. 2008, Houser and Hamilton 2009, Stoker et al. 2011)

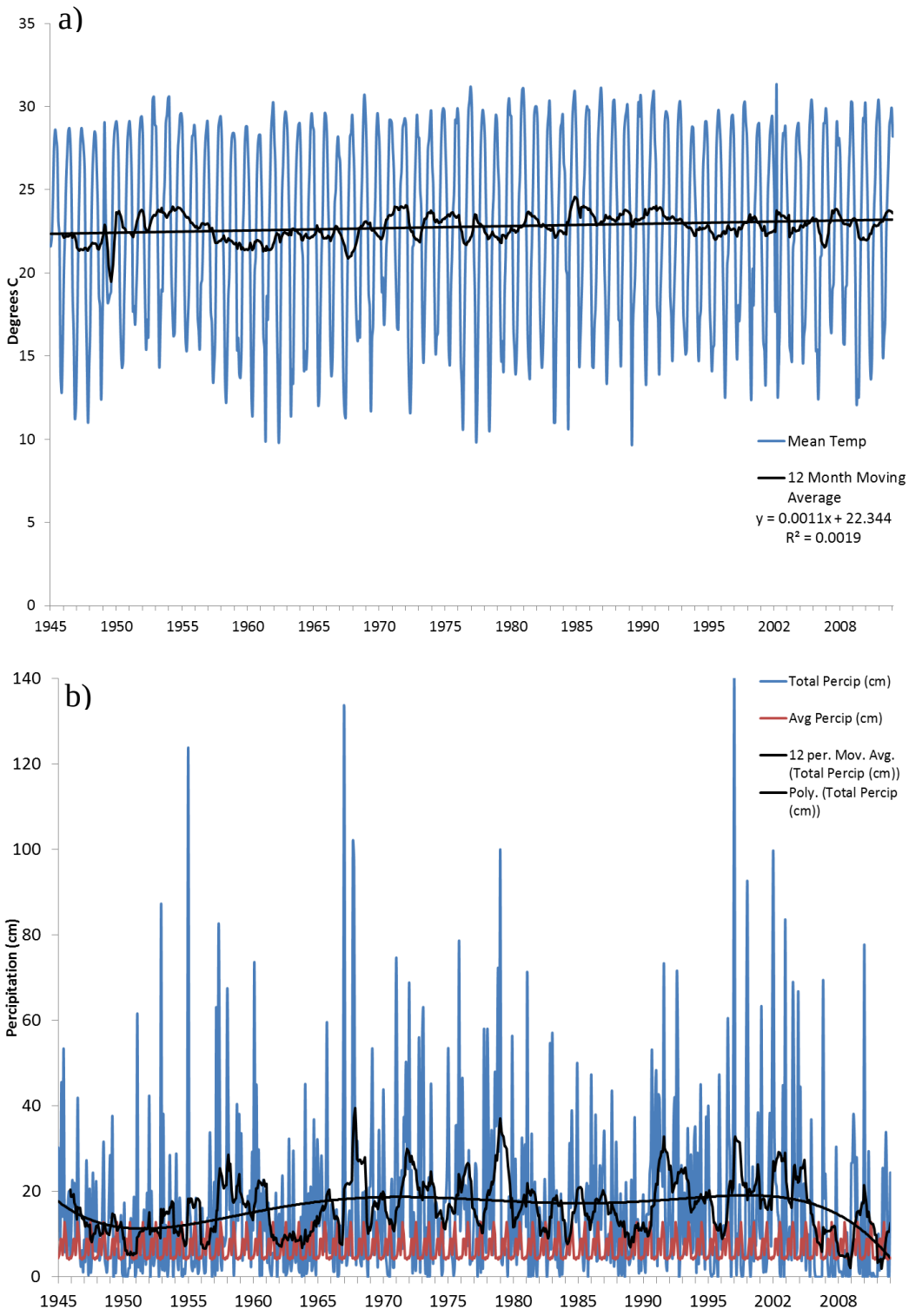

Figure 4 - a) Mean Temperature 1945-2012 and b) Average Monthly Precipitation 1945 – 2012

Over the past decade LiDAR data was by PAIS in 2005 and the US Department of Agriculture (USDA) in 2011, for the extent of Padre Island National Seashore. The 2005 data was collected using NASA's Experimental Advanced Airborne Research LiDAR (EAARL). This is an aircraft mounted pulsed laser ranging system designed to measure ground elevation and coastal topography with a vertical resolution of 15 centimeters and horizontal resolution of 1 m. The USDA data is part of the National Elevation Data set. This dataset has a horizontal resolution of 3m and a vertical resolution of 2.44 meters. Because of the discrepancy of cell size associated with the horizontal resolution differences, the 2005 data was resampled in ArcGIS to match the resolution of the 2011 data.

This LiDAR data provides both the volumetric and spatial extent for blowouts, foredune, and the backbarrier regions of the island with in the study area. Using raster algebra, the difference in elevations found in 2005 and 2011 were calculated. LiDAR data was compared with the newest digitized aerial photography to provide a more detailed geomorphic understanding of the site, while simultaneously denoting areas of erosion and deposition.

3.3 RESULTS

Blowouts, which in aerial photographs historicly covered 20 kilometers of Padre Island National Seashore, are currently only observed within the first fourteen kilometers of drivable beach (Figure 5). Presently blowouts occur approximately every 330 meters along the first 6000 meter stretch extending from Park Road 22. In 1969 blowouts covered the seaward side of the island. These occurred not only with in this stretch but also extended north another eight kilometers into what is now the non-driving portion of the National Seashore. Analysis of aerial photographs from 1969 suggests that this area had the same number and extent of blowouts as the rest of the study area (Figure 6). In April 1969, this section of the seashore was restricted to foot traffic only, and by 1973 the Parks Service already noticed the vegetation line on this section of the beach had increased 21 m seaward (NPS 1973). Since 1973, vegetation has continued to increase causing the majority of blowouts in this section to revegetate leaving only three sand sheets today. One of these patches, close to the beach access point of Park Road 22 is a stabilized reminent of one of the 1969 blowouts. Another blowout, which developed between 2008 and 2010 , is located behind the camp ground in an area of high visitor traffic. The final blowout developed in the mid 1990's potentially when a Category 4 hurricane hit land with in 50 miles of the study site (NOAA 2012). While blowouts can be generated by storms, the limited number in the no driving section compared to the driving section suggests that driving appears to be the primary force behind the continued blowout development.

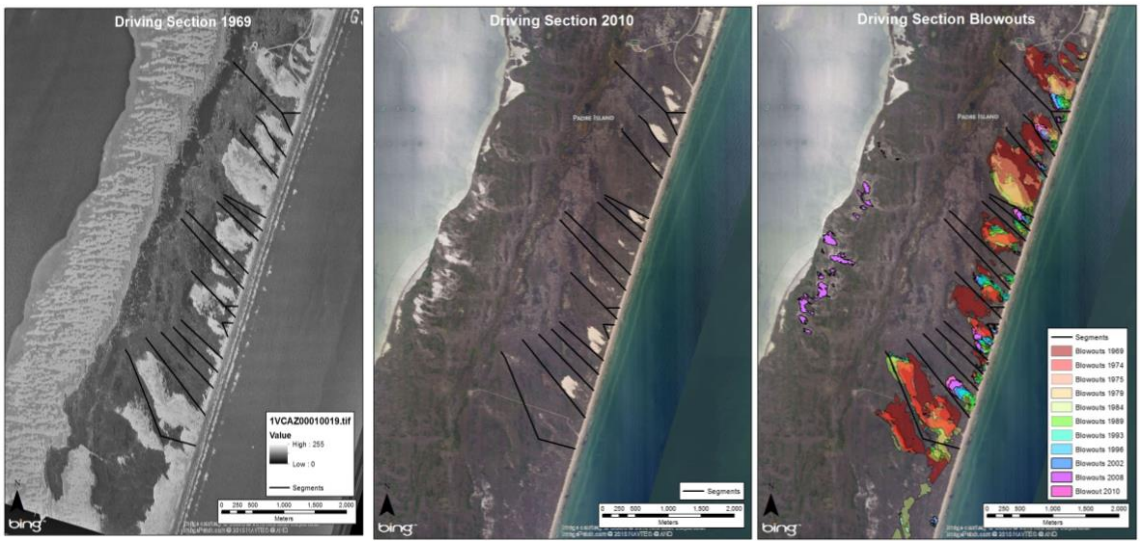

Figure 5- Blowouts on Driving Section of Padre Island National Seashore 1969-2010 and Total Change

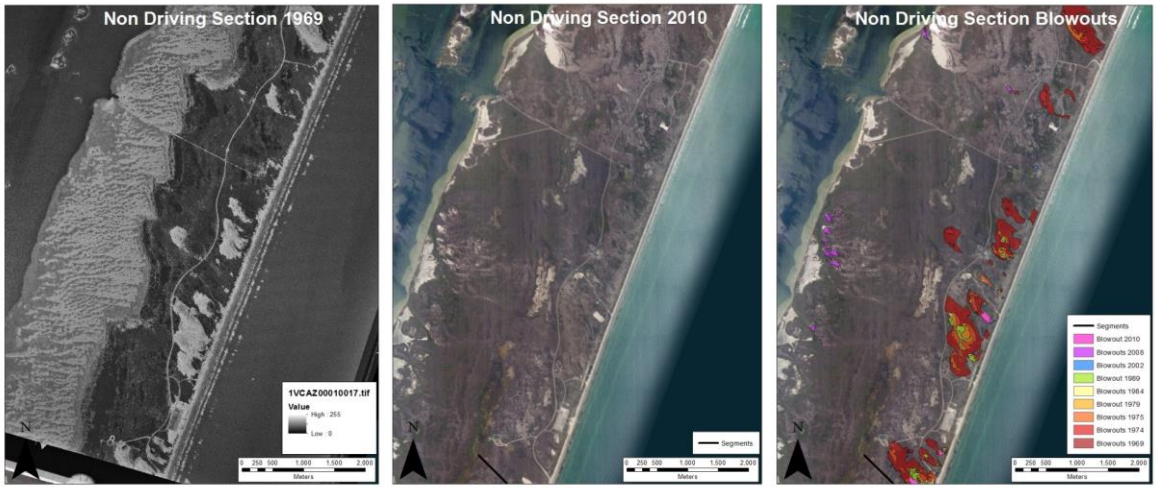

Figure 6- Blowouts on Non-Driving Section of Padre Island National Seashore 1969-2010 and Total Change

3.3.1 Cluster Analysis

A cluster analysis was completed on blowouts with in the driving section to determine what classes are present in the study area initially at the beginning of the study. These classes are based on length, width, area, segmentation, perimeter, velocity, and throat width. This analysis returned two major clustering classifications, which are referred to as Clusters 1 and 2 (Figure 7). Cluster 1 consists of blowouts SA2, C, D, F, G, H, I, K, SA1, and N while Cluster 2 has A, B, E, J, L, M1, M2, and O (Table 3). To compare the results of the morphometric calculations each group was graphed based on its cluster group.

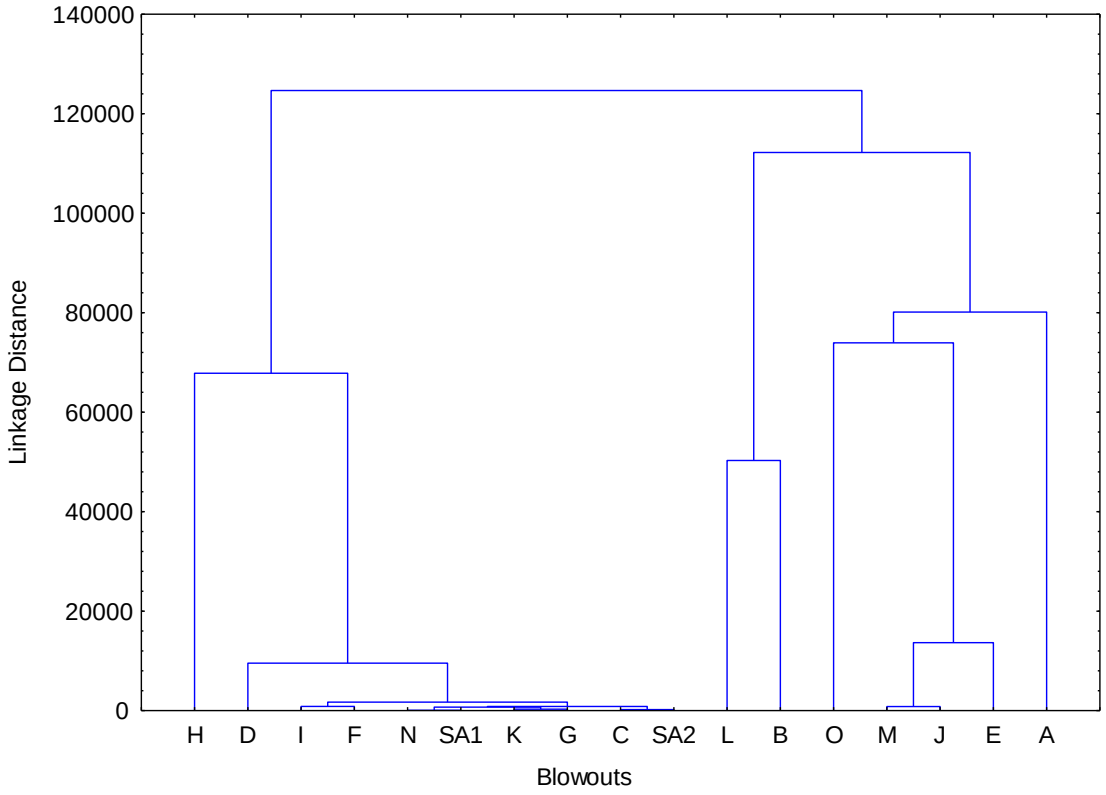

Figure 7- Cluster Analysis Based on Metrics Measured from Aerial Photographs

a)

	Length	Width	Area	Segmentation	Perimeter	Dheight	MaxHeight	Dbase	Avg	Slope	Height/Slope	100m	Dbase/Slope	Velocity	Throat	Distance
SA2	Short	Thin	Small	Few	Smooth	Short	Lowest	High	Below	Steap	Big	Gentle	Flat	Large	Large	Far
C	Short	Thin	Small	Few	Smooth	Short	Lowest	High	Below	Steap	Big	Gentle	Steap	Small	Small	Far
D	Short	Thin	Small	Few	Smooth	Short	Lowest	High	Below	Steap	Big	Gentle	Flat	Large	Large	Far
F	Short	Thin	Small	Many	Smooth	Short	Lowest	Low	Below	Steap	Big	Gentle	Steap	Small	Small	Far
G	Short	Thin	Small	Few	Smooth	Tall	Highest	High	Below	Shallow	Big	Gentle	Flat	Small	Small	Far
H	Long	Wide	Large	Many	Undulated	Short	Lowest	High	Below	Shallow	Small	Abrupt	Flat	Small	Small	Far
I	Short	Thin	Small	Many	Smooth	Tall	Highest	Low	Above	Shallow	Small	Abrupt	Flat	Small	Small	Near
K	Short	Thin	Small	Few	Smooth	Short	Lowest	Low	Below	Steap	Big	Gentle	Steap	Small	Small	Near
SA1	Short	Thin	Small	Few	Smooth	Tall	Highest	Low	Above	Steap	Big	Gentle	Steap	Small	Small	Near
N	Short	Thin	Small	Many	Smooth	Tall	Highest	High	Above	Shallow	Big	Abrupt	Flat	Small	Small	Near
A	Long	Wide	Large	Few	Undulated	Tall	Highest	Low	Above	Shallow	Small	Abrupt	Steap	Large	Large	Far
B	Long	Wide	Large	Few	Undulated	Tall	Highest	Low	Above	Shallow	Small	Abrupt	Steap	Large	Large	Far
E	Long	Wide	Large	Many	Undulated	Short	Lowest	Low	Above	Steap	Small	Gentle	Steap	Large	Large	Far
J	Long	Wide	Large	Few	Undulated	Tall	Highest	High	Above	Shallow	Small	Abrupt	Flat	Large	Large	Near
L	Long	Wide	Large	Few	Undulated	Short	Lowest	High	Below	Steap	Small	Gentle	Flat	Large	Large	Near
M1	Long	Wide	Large	Few	Undulated	Short	Lowest	Low	Below	Shallow	Small	Abrupt	Steap	Small	Small	Near
M2	Long	Wide	Large	Few	Undulated	Tall	Highest	Low	Above	Steap	Big	Abrupt	Steap	Large	Large	Near
O	Long	Wide	Large	Few	Undulated	Tall	Highest	High	Above	Shallow	Small	Abrupt	Flat	Large	Large	Near

b)

	Length	Width	Area	Segmentation	Perimeter	Dheight	MaxHeight	Dbase	Avg	Slope	Height/Slope	100m	Dbase/Slopw	Velocity	Throat	Distance
SA2	Long	Wide	Large	Many	Undulated	Tall	Highest	High	Above	Steap	Big	Abrupt	Steap	Fast	Large	Far
C	Short	Wide	Large	Few	Undulated	Short	Lowest	High	Below	Steap	Big	Gentle	Flat	Slow	Small	Far
D	Short	Thin	Small	Many	Smooth	Short	Lowest	High	Below	Steap	Small	Gentle	Flat	Slow	Small	Far
F	Short	Thin	Small	Few	Smooth	Short	Lowest	High	Below	Steap	Small	Gentle	Flat	Slow	Small	Far
G	Short	Thin	Small	Many	Smooth	Tall	Highest	Low	Above	Steap	Small	Gentle	Flat	Slow	Small	Far
H	Long	Thin	Small	Few	Smooth	Tall	Highest	High	Above	Steap	Small	Gentle	Flat	Slow	Small	Far
I	Short	Wide	Large	Many	Undulated	Short	Lowest	Low	Below	Shallow	Big	Abrupt	Steap	Fast	Small	Far
K	Long	Thin	Small	Few	Smooth	Short	Lowest	Low	Below	Shallow	Big	Abrupt	Steap	Fast	Small	Near
SA1	Long	Thin	Small	Few	Smooth	Short	Lowest	Low	Below	Steap	Big	Gentle	Flat	Slow	Small	Near
N	Short	Wide	Large	Few	Undulated	Tall	Highest	High	Above	Steap	Small	Gentle	Flat	Slow	Large	Near
A	Long	Thin	Small	Few	Smooth	Short	Lowest	Low	Below	Steap	Big	Abrupt	Steap	Slow	Small	Near
B	Short	Wide	Large	Few	Undulated	Tall	Lowest	Low	Above	Shallow	Big	Abrupt	Steap	Fast	Large	Far
E	Long	Thin	Small	Many	Undulated	Tall	Lowest	Low	Above	Shallow	Big	Abrupt	Steap	Fast	Small	Far
J	Long	Wide	Large	Few	Undulated	Short	Highest	Low	Below	Steap	Small	Gentle	Flat	Fast	Large	Far
L	Short	Thin	Large	Few	Undulated	Tall	Highest	High	Above	Shallow	Small	Abrupt	Steap	Slow	Small	Near
M1	Short	Thin	Small	Few	Smooth	Short	Highest	High	Above	Steap	Small	Gentle	Flat	Fast	Small	Near
M2	Long	Wide	Large	Few	Smooth	Tall	Highest	Low	Below	Shallow	Small	Abrupt	Steap	Fast	Small	Near
O	Long	Wide	Large	Few	Undulated	Short	Lowest	Low	Below	Shallow	Big	Abrupt	Steap	Fast	Small	Near

Table 3- Classification Groups and Parameters a) Initial Parameters in 1969 b) Final Parameters in 2010

Length

The length of each blowout was measured and recorded for all years that the blowout was present in the aerial imagery (Figure 8). The figures are split based on which group the blowouts are clustered into. Cluster 1 contains smaller blowouts with a maximum length of 600 m, with the average length of blowouts in Cluster 1 measuring less than 200 m. All blowouts within Cluster 1 maintain roughly the same size throughout the duration of the study period. This is in stark contrast to Cluster 2 where the length of all blowouts was greater than 600 m at the beginning of the study period. However, by 1979 all but one experienced a sharp drop in length, which continued until 1996 when all but L began to expand again. At present, five of the eight are still expanding and are still above the average length for Cluster 1.

Width

The blowout width of both groups (Figure 9) is similar to the reported data for length but with a distinct separation between groups in 1969. One blowout, H, does not follow the same trend as the rest of its group. This blowout was originally approximately 200 m wider than all of the others however through vegetative restabilization it joins the average width of its group by 1974. For the majority of the study period, trends in width are very similar to the trends length. Cluster 1 stays relatively stable throughout the entire duration while Cluster 2 experiences a sharp drop between 1969 and 1979 before becoming more consistent. Over the past few years, length and width characters of Cluster 2, because not as many blowouts are currently widening compared to ones that are lengthening.

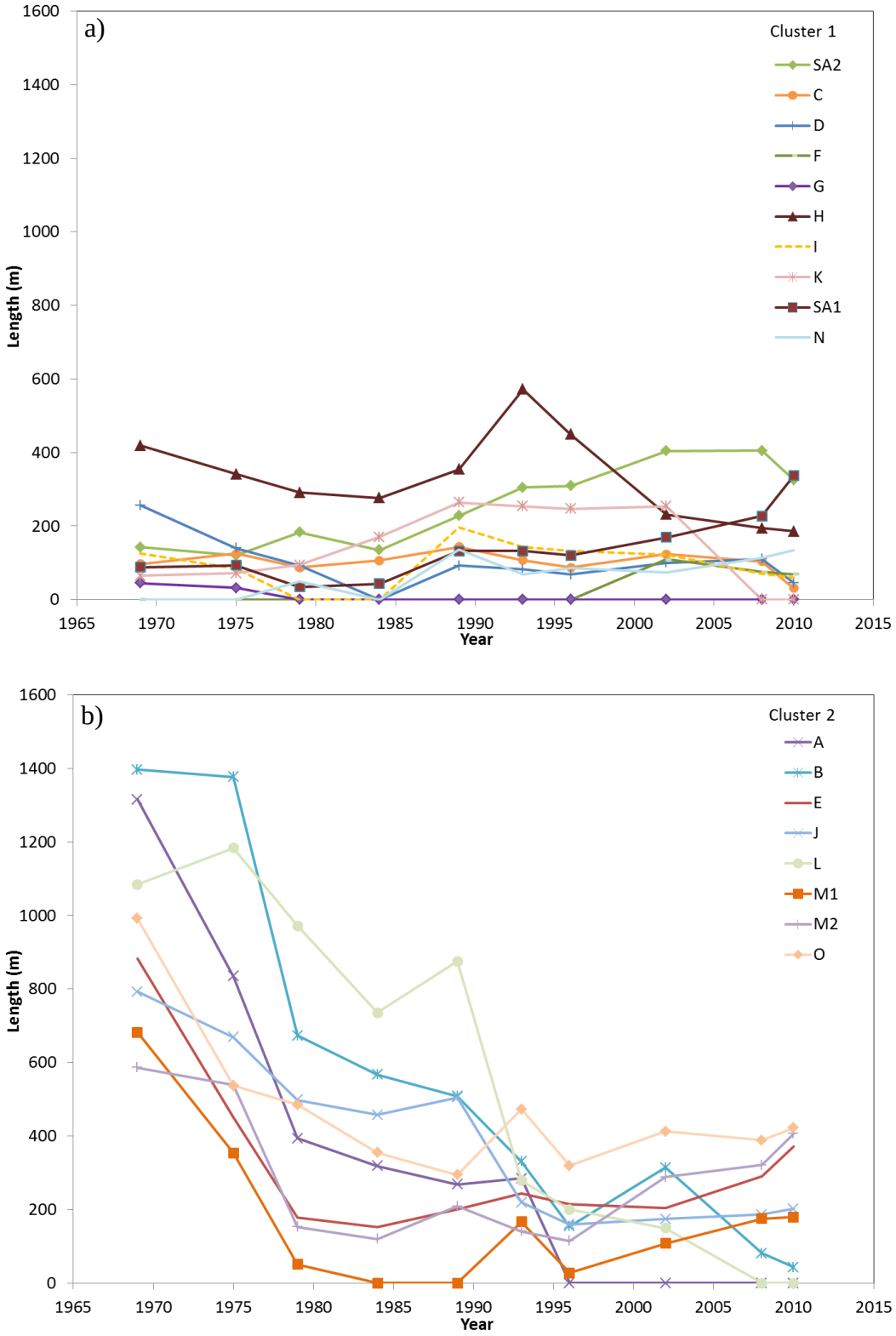

Figure 8- Length of Blowouts Measured in Aerial Imagery from 1969- 2010

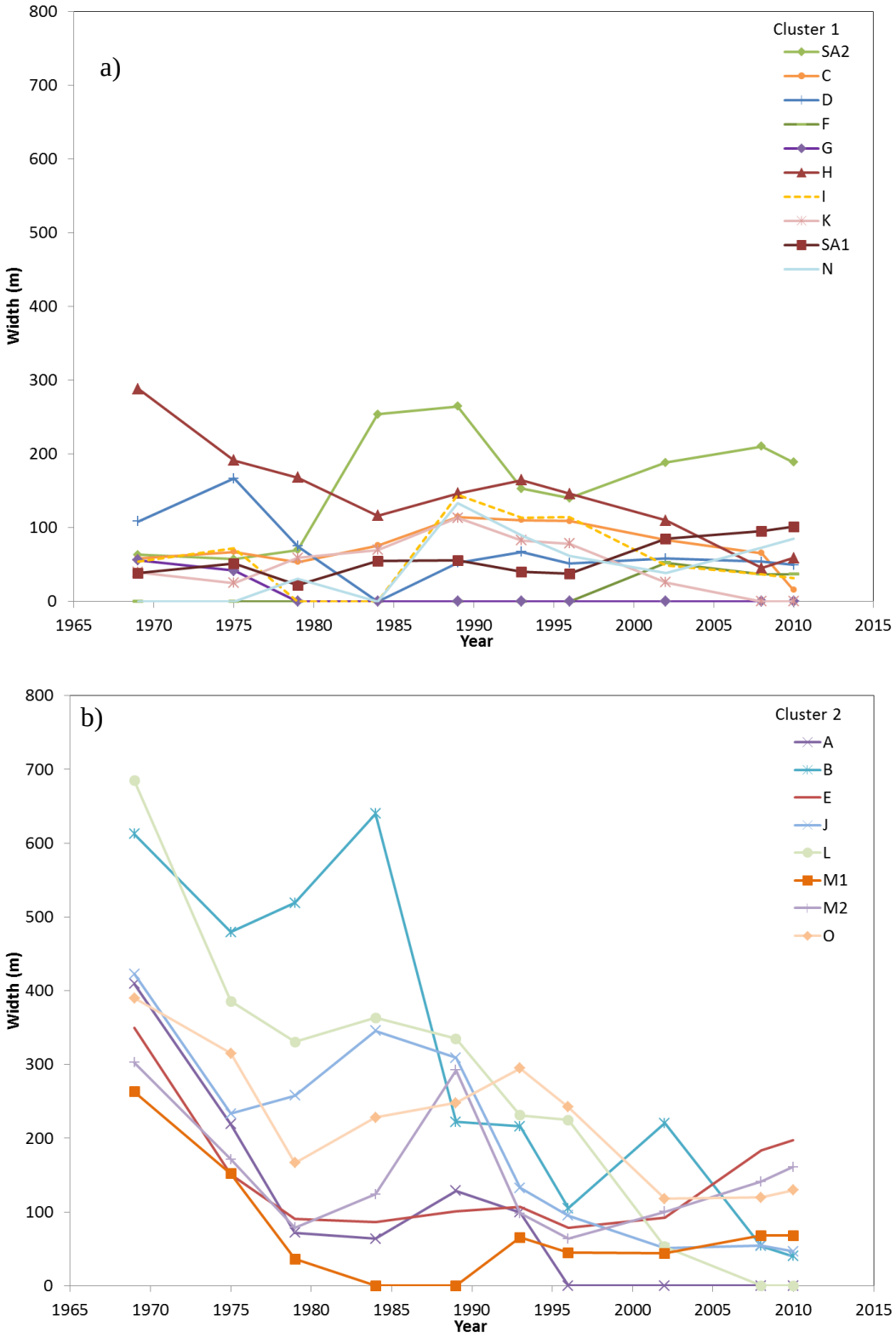

Figure 9- Width of Blowouts Measured in Aerial Imagery from 1969- 2010

Area

As expected when length and width trends are similar, changes in area (Figure 10) over time parallel the length and with trends. Similar to its changes in width, blowout H begins as an outlier from Cluster 1, however, by 1984 it joins both the average and trend within the group but only for that year before growing again until 1993 when it begins to stabilize once again. Beginning in 1979 SA2 also strays from the cluster growing in since until 1993 before leveling out. In 1996 and SA1 begin to increase at greater rates than other blowouts in this group and surpasses H in between 2002 and 2008. In Cluster 2 behaves in the same manner as previously discussed. Increases in area are observed in blowouts E, O and M2 at the end of the study.

Segmentation

Segmentation (Figure 11) differs from the overall trends previously observed, because there are no major differences between Cluster 1 and 2. With the exception of I, all blowouts began with only a few patches of open sand. Throughout the study period, vegetation regrew and the blowouts began to stabilize. With stabilization, the number of segments grew as vegetation encroached upon the open sand. Eventually only a few patches of sand that have not stabilized will be left. This is what was found at the end of the study. Blowouts A, G, K, and L completely stabilized leaving no areas of open sand while for consecutive photographs Blowouts D, I, and M1 stabilized before reactivating.

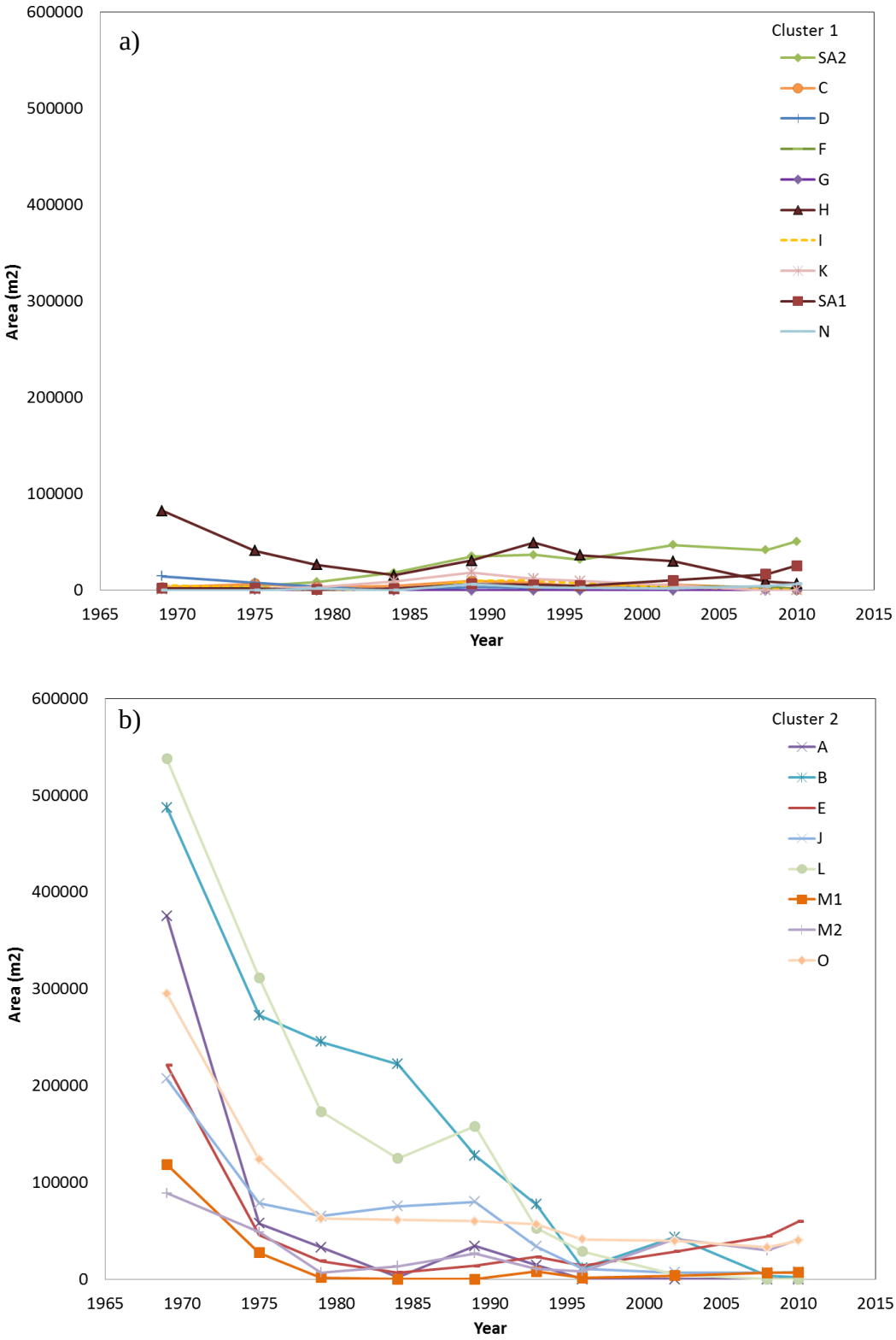

Figure 10- Area of Blowouts Measured in Aerial Imagery from 1969- 2010

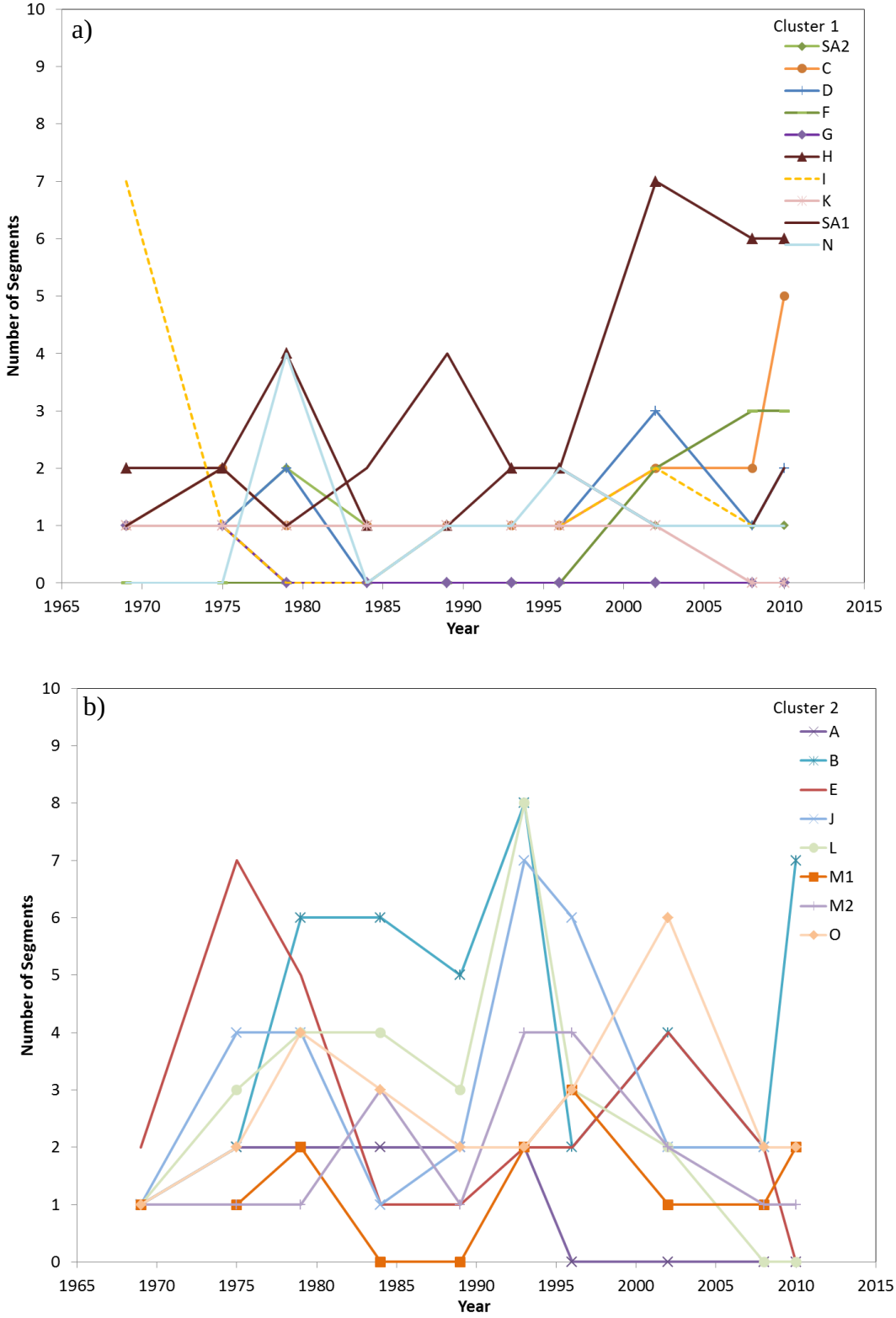

Figure 11- Segmentation of Blowouts Measured in Aerial Imagery from 1969- 2010

Perimeter

Similar morphometric trends exist when analyzing perimeter (Figure 12), because the average perimeter of Cluster 2 blowouts are much larger than Cluster 1. Blowout H is once again the outlier with in Cluster 1 because it has the largest perimeter until it is surpassed by SA2 in 2010. The rest of Cluster 1 maintains a small perimeter, congruent with the area measurements discussed above, and on average is less than 1,000 meters. Perimeter calculations for Cluster 2 differ from most of the other morphometrics because all blowouts within the group experience a major drop from their initial calculated perimeter. However, the perimeter of two blowouts, M2 and O, remains steady while blowout L increases. Though blowout B does suffer a slight decrease in size, it increases to have the largest perimeter within the entire study. Over the period of study, blowout perimeter decreased until 2002 when there was an overall increase in perimeter. The differences in perimeter are highly dependent on how and where vegetation is reestablished in the blowout.

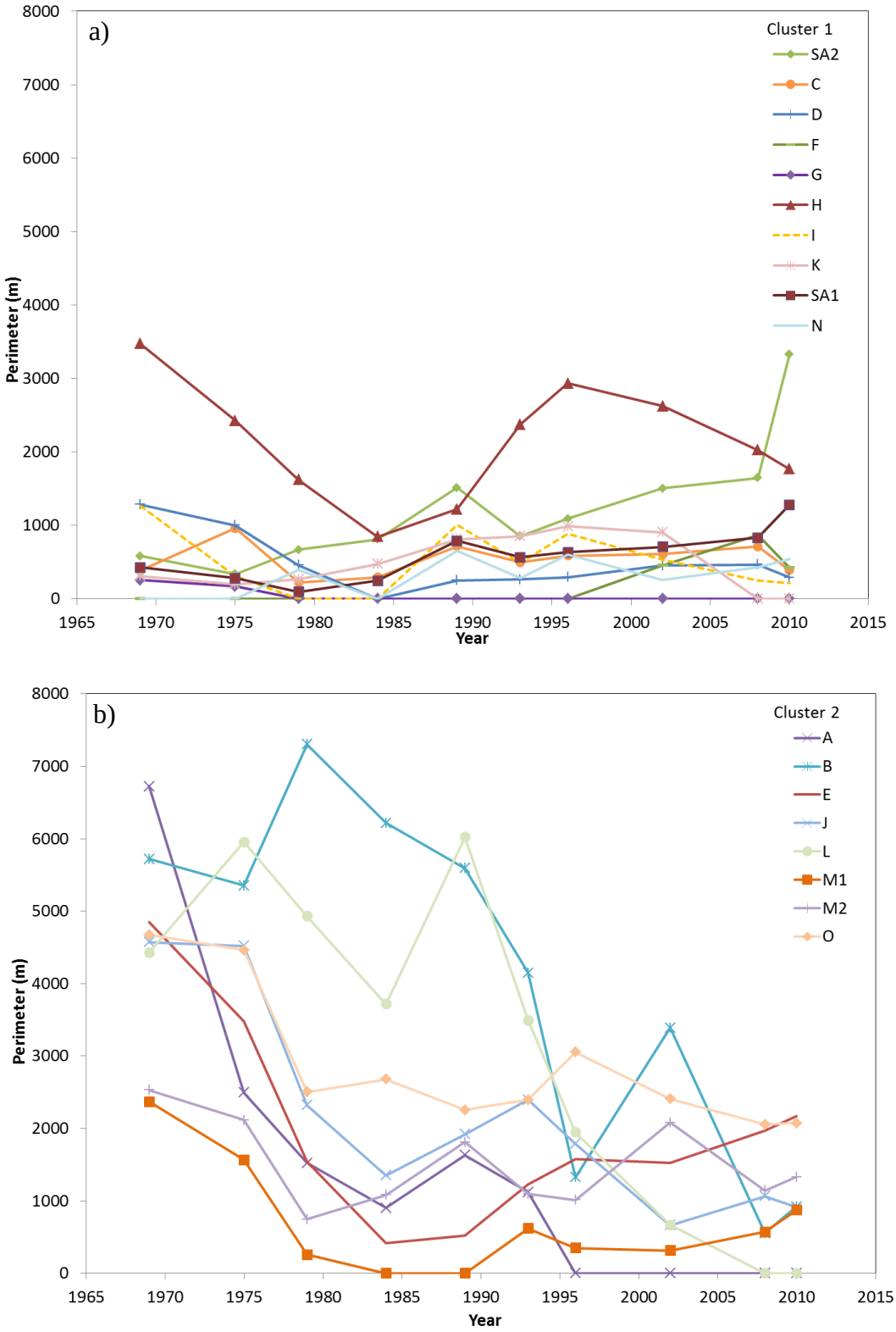

Figure 12- Perimeter of Blowouts Measured in Aerial Imagery from 1969- 2010

Throat Width

Unlike the other metrics previously discussed, increases in throat width (Figure 13) appears to be dependent on with larger intensity and more frequent storms impacting the study area. Distinctive increases in throat width occur in 1974, 1984, 1989 and 1993. Between the measurements before and the dates mentioned above, there was at least two hurricane intensity storms and between two and seven tropical systems that impacted within 200 miles of our study area (Figure 14). The largest spike in throat width occurs in 1984 when four major storms, including two storms that made landfall as category 3 hurricanes and seven tropical systems impacted the area (NOAA 2012). Through visual examination of the aerial photographs however, it seems that most of the blowouts developed their current shape and pattern of movement between 1984 and 1989 during a relatively quiet period with in 370 km of the study site with only two category 1 storms striking land in near Galveston in 1989. A tropical depression did make landfall in 1986 at the northern end of the non-driving section (NOAA 2012), however, due to the lack of major storms impacting the area the foredune was able to begin recovery as vegetation recolonized.

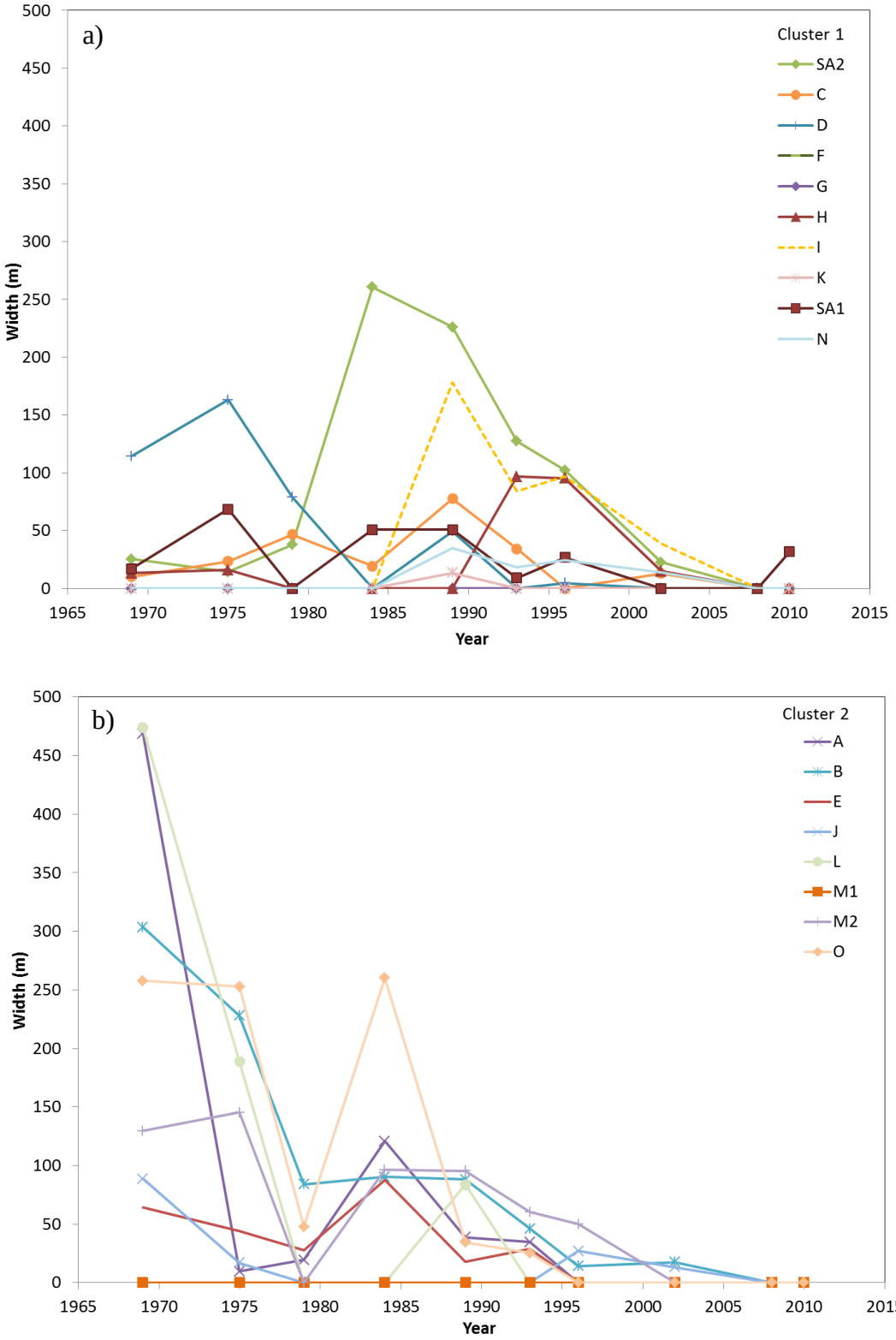

Figure 13- Throat Width of Blowouts Measured in Aerial Imagery from 1969- 2010

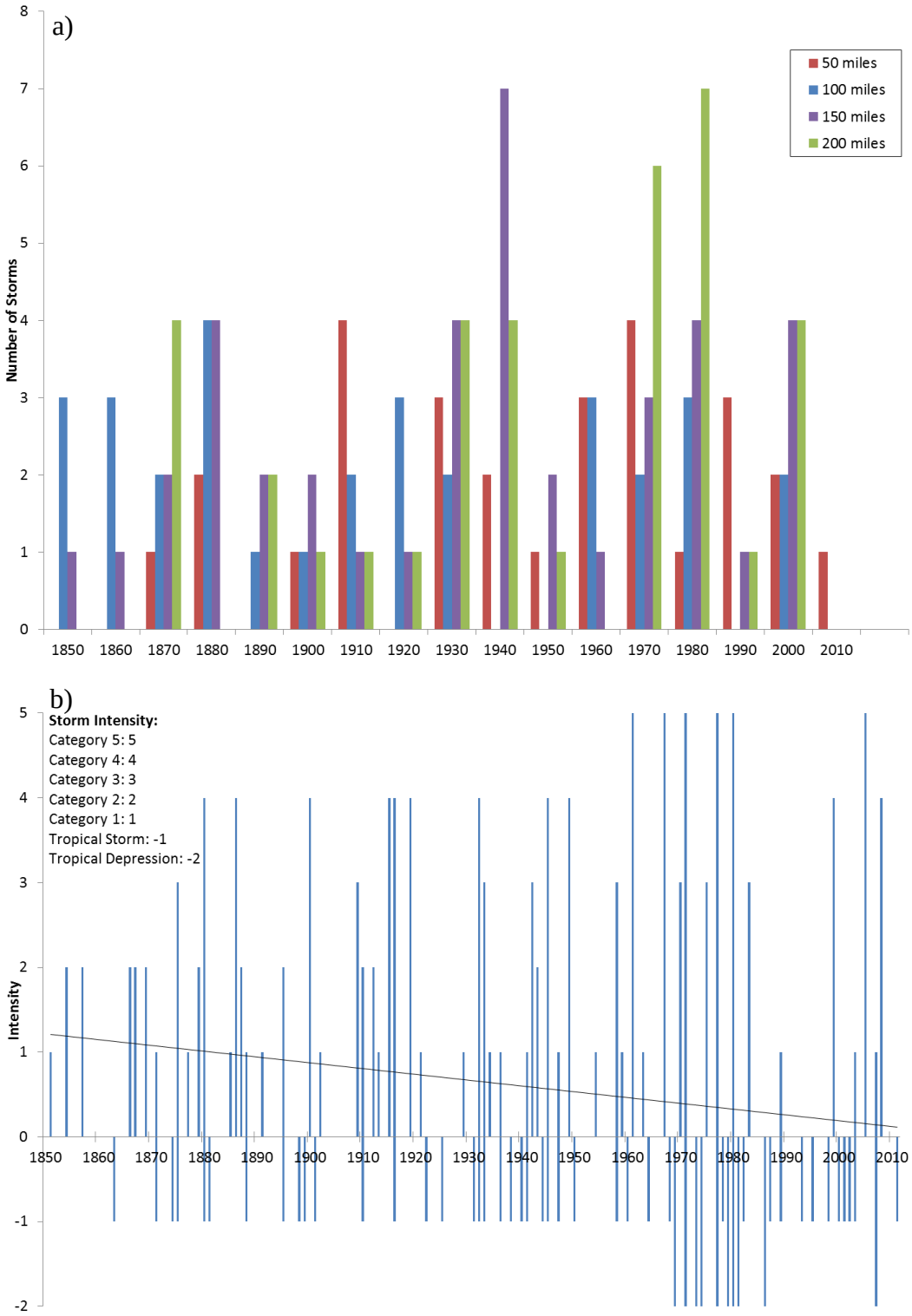

Figure 14- Frequency (a) and Intensity (b) of Tropical Systems within 200 Miles of Study Area

3.3.2 Foredune Height and Beach Elevation

Across each transect for each blowout the following parameters were calculated from the 2009 LiDAR: the bathymetric slope, crest height, dune base, maximum height, and beach slope for the area in front of each blowout (Figure 14, Table 4). The average crest height for all transects is 4.3 m. The maximum height is the difference between the crest height and dune base (Sallenger 2000). The average maximum height is 3.3 m. Dune height and crest height exhibit an overall decrease in value from north to south, but with variance. There is an above average height dune approximately every 1300 m and an area of lower than average elevation (trough) every 1100 m along the driving section of the beach. All blowouts within the study area overlap one of these troughs. This is due to focused wind and water velocities during storms as well as an amplified potential of the lower dunes to be overtopped with increasing wave height. While the dune height and crest height are variable at a regular interval the dune base is consistently elevated 1m above sea level. The slope of the beach between the dune toe and 100m offshore isobath is also intermittent, with areas of flatter and steeper beach face. Roughly every 3000 m, there is a steeper section of beach while in between these spikes is an area of flatter terrain.

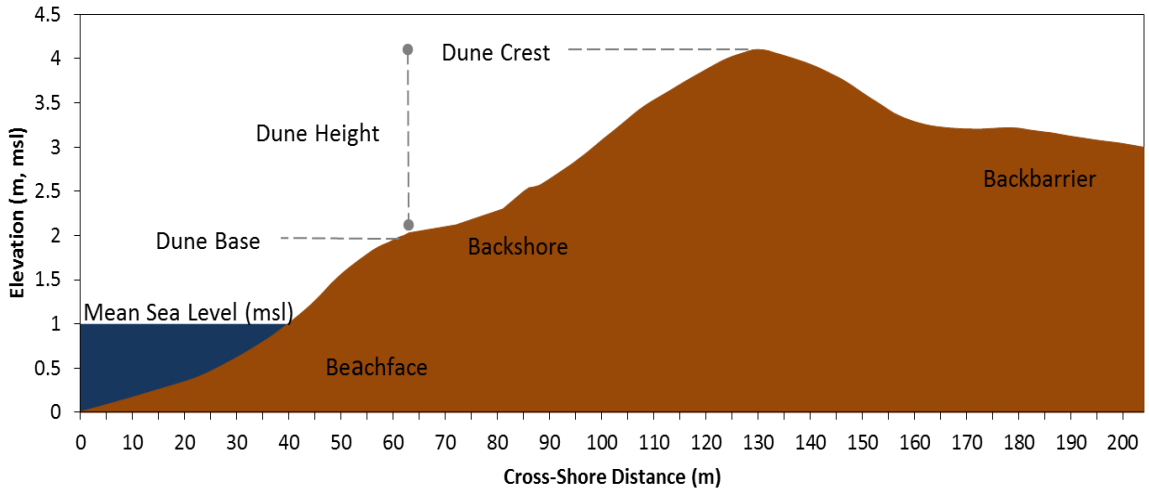

Figure 15- Average Beach Profile for Padre Island National Seashore- Driving Section

Table 4- Foredune Height and Beach Elevation for Each Blowout in the Driving Section

Cluster 1	SA2	C	D	F	G	H	I	K	SA1	N
SOUTH	5120	4720	4480	3960	3660	3500	3160	2360	2180	640
Dune Height	2.25	1.92	3.20	5.25	4.37	5.44	4.00	1.59	4.39	4.82
Maximum Height	3.00	3.65	4.19	6.15	5.64	6.46	5.68	2.14	6.17	5.34
Dune Base	0.75	1.73	0.99	0.89	1.27	1.02	1.68	0.55	1.78	0.52
Bathymetry										
500 Meters	-3.71	-3.95	-3.99	-3.74	-3.74	-3.95	-3.62	-3.69	-3.65	-3.93
100 Meters	-3.04	-3.27	-3.29	-3.27	-3.04	-2.82	-2.47	-3.24	-3.33	-2.84
Slope	-0.0017	-0.0017	-0.0018	-0.0012	-0.0018	-0.0028	-0.0029	-0.0011	-0.0008	-0.0027

Cluster 2	A	B	E	J	L	M1	M2	O
SOUTH	6320	5520	4220	2580	1800	1340	920	180
Dune Height	3.69	2.02	2.79	1.11	2.10	5.72	3.54	5.24
Maximum Height	4.53	2.33	3.47	1.99	2.86	6.56	4.49	5.70
Dune Base	0.84	0.31	0.68	0.88	0.76	0.84	0.95	0.46
Bathymetry								
500 Meters	-4.02	-3.71	-3.95	-3.76	-3.78	-3.82	-3.73	-3.66
100 Meters	-2.92	-2.91	-3.40	-3.03	-3.24	-2.92	-2.91	-2.70
Slope	-0.0027	-0.0020	-0.0014	-0.0018	-0.0013	-0.0022	-0.0021	-0.0024

To find potential areas of weakness in the foredune, the wave runup for a 95th percentile storm was compared to the average wave height reported by PAIS (NPS 2010). For the 95th percentile storm a deep water wave height of 2.5 m and a wave period of 8 s were used to calculate the wave runup using Stockdon's (2006) equation. For normal conditions with a wave height of .75 m the average wave runup on the island is .46 m. The average runup for a 95th percentile storm, however, is 0.84 meters. On average for this section of PAIS the dune base elevation is 0.92m and the crest elevation is 4.48 m. The ratio of the runup to crest height for this storm and typical daily conditions is calculated for the study site in Figure 16.When this data is plotted in conjunction with the average blowout location for the study period it shows that the blowouts form at localized topographic lows in the foredune (Figure 17) which correlates to low points in the ratio of runup to crest height. This is because at areas where there an increased potential for erosion and scarping of dunes with lower height, compared to ones of higher elevation. However if the dune is to low it will just experience overwash and not experience scarping. To account for spatial variability of the blowout during the study error bars are associated with each blowout. These error bars show each blowouts farthest extent alongshore, left end of error bar, as well as the point where the blowout was closest to the beach access of Park Road 22, right end of error bar, with the center point being the average location.

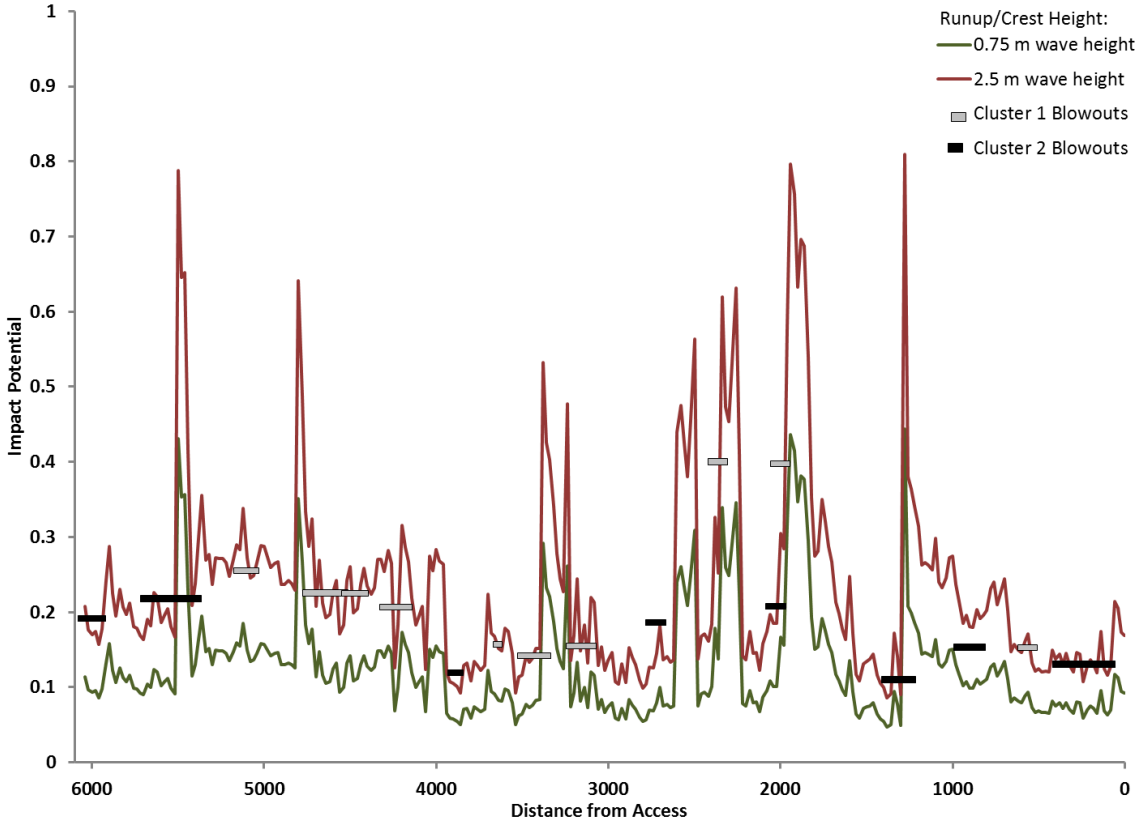

Figure 16- Storm Impact Potential for Average Wave Height Compared to the 95th Percentile Storm on the Driving Section of PAIS

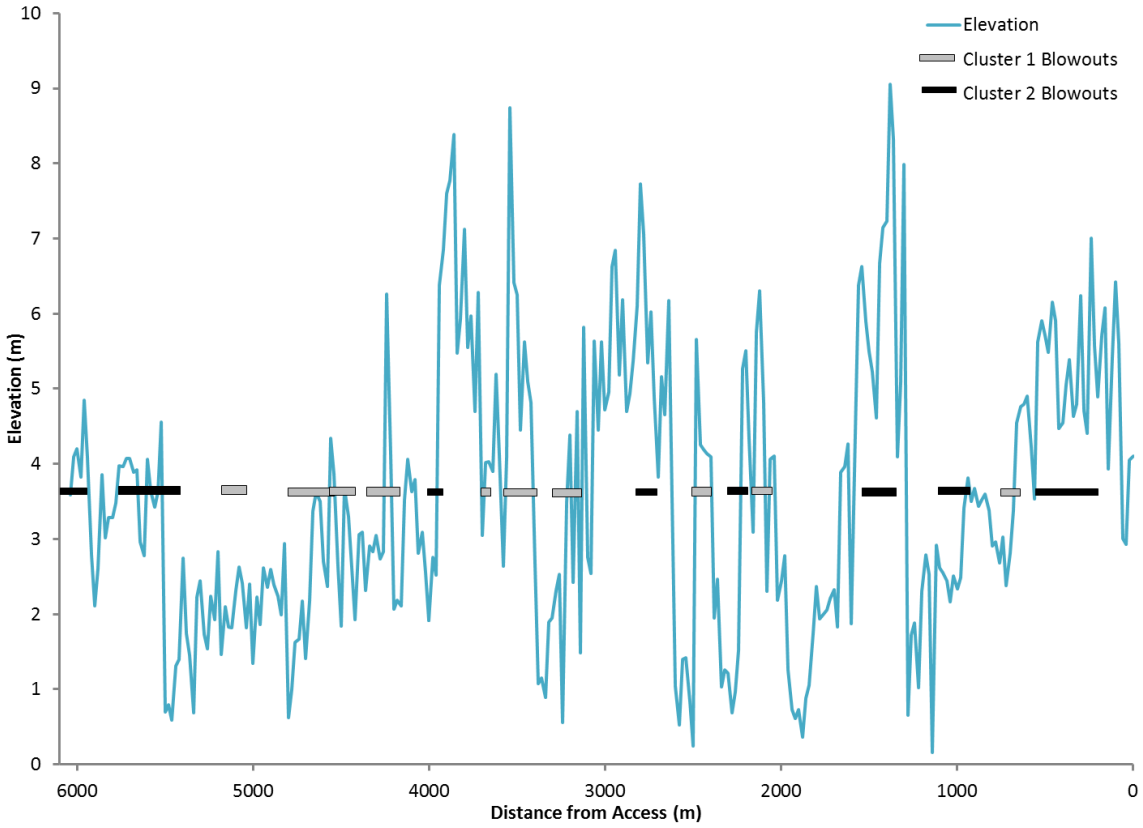

Figure 17- Foredune Elevation of the Driving Section of PAIS

3.3.3 Erosion and Deposition

To provide an understanding on where erosion and deposition are occurring within the study area, LiDAR data from 2011 was subtracted from data acquired over the same site in 2005 (Figure 18 and 19). The resulting raster provides the location and volumetric differences in the foredune, dune field and backbarrier. The study area has two main dune lines that are continuously present along the beach. The second dune line has a greater width and elevation then the foredune and is where most of the blowouts currently occur, unless they are still connected to the backshore. After subtraction, it is

possible to see the internal changes of the blowout, which is something the other metrics could not illustrate. There is little erosion in the foredune, with localized pockets of 2 m^3 of deposition, but the backbarrier regions that were free of blowouts had no net change. For Cluster 2, the most extensive erosion, 5.6 m^3, was found at blowout O, the closest blowout to the access road, but the average erosion for the cluster was between 1 and 2 m^3. The erosion occurred mainly at areas of higher elevation adjacent to the low center of the blowout where restabilization is occurring. The maximum erosion in Cluster 1 is 5.4 m^3 found in blowout E and SA1 while average erosion ranged between 2 and 3 m^3 and is occurring to the NW, W and SW of the blowouts where the larger dunes began to flatten out into parabolic sand sheets, as observed in the 2005 data. Based off the volumes of erosion and deposition reported for the study area between 2005 and 2011, the mean volume of sediment transported was calculated to be -0.17 m^3, for the entire study area, suggesting that more erosion has occurred than deposition, which in turn suggests that this section of the island experienced erosion between 2005 and 2011.

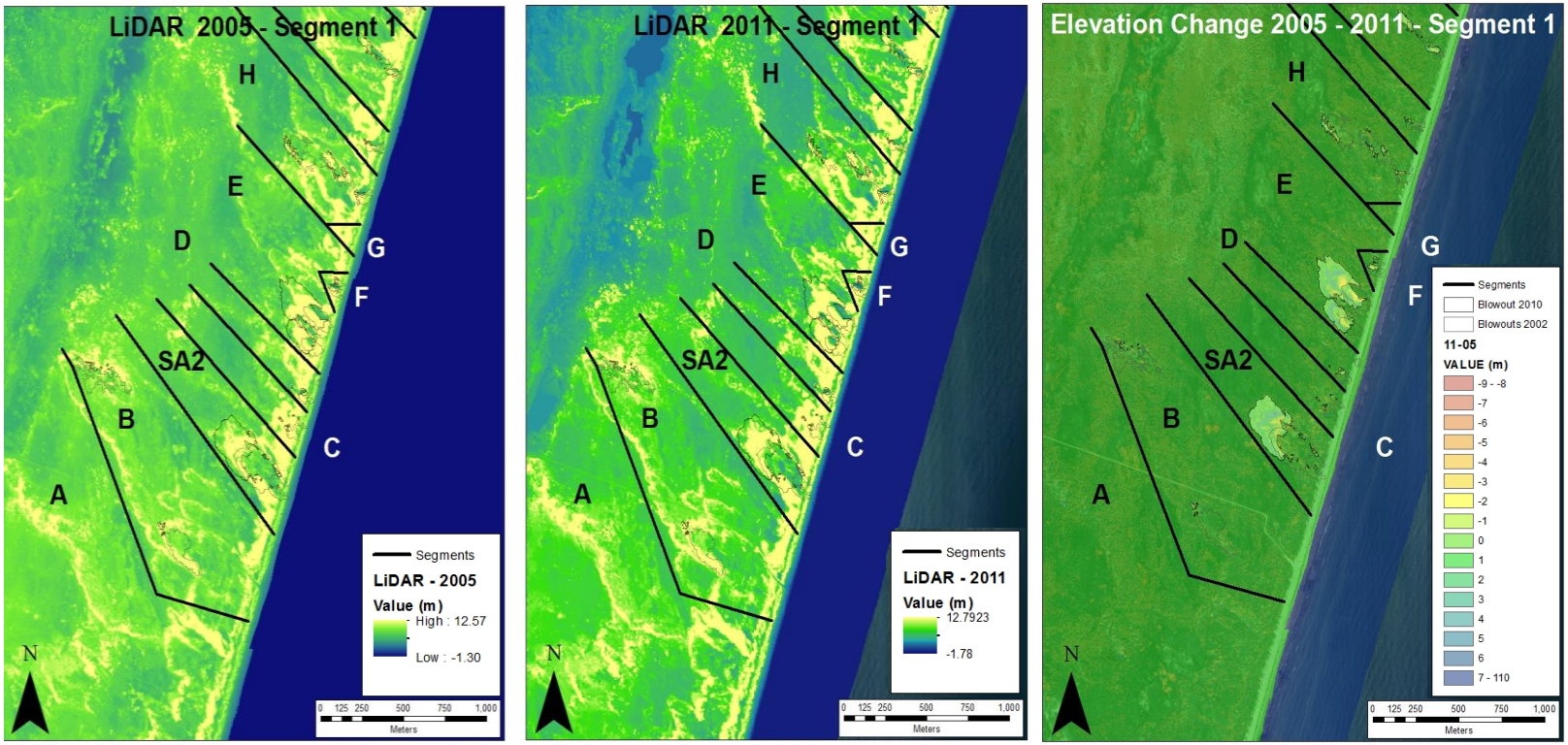

Figure 18- LiDAR Segment 1; 2005, 2011 and Change Between 2005 and 2011.

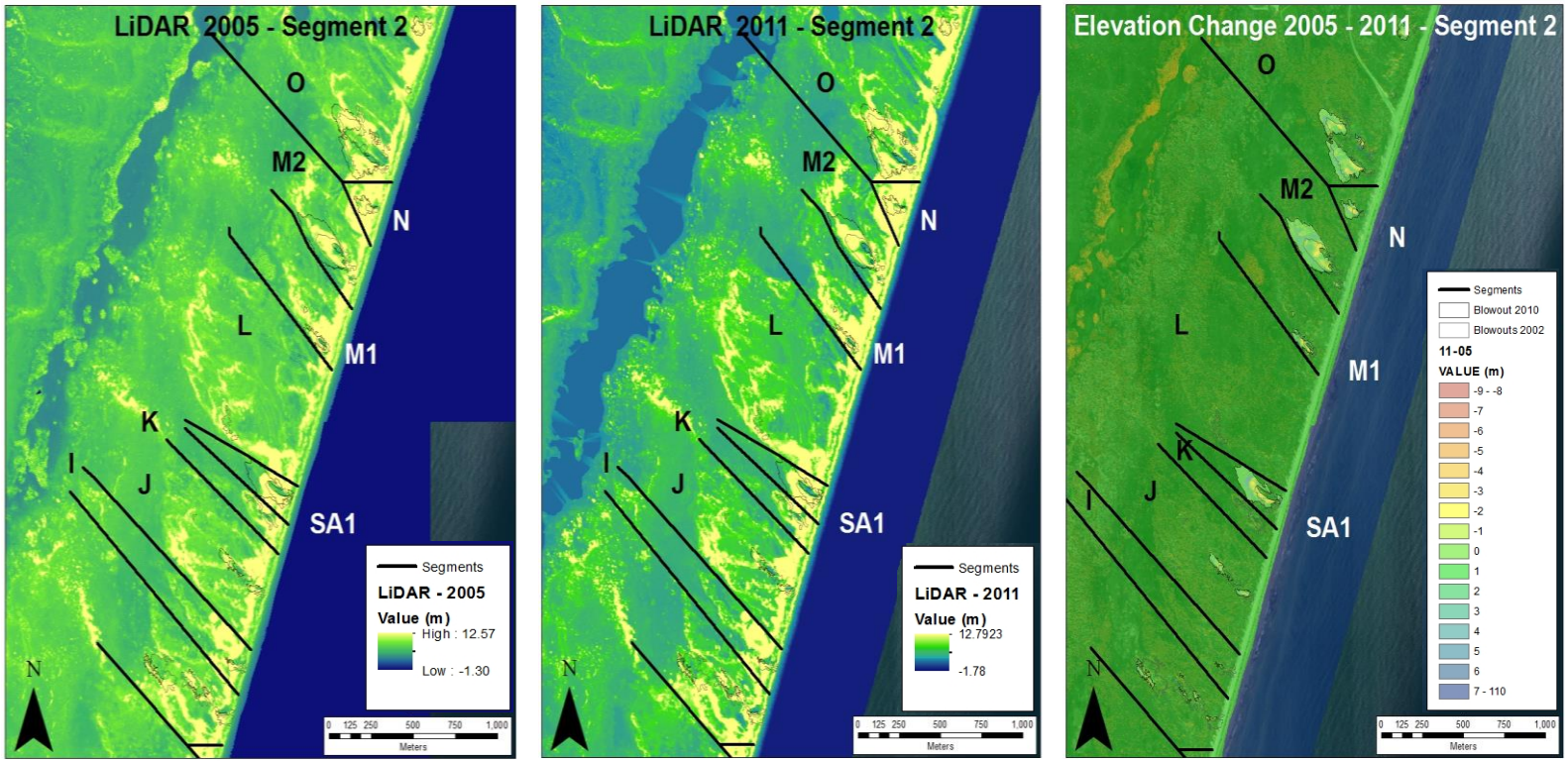

Figure 19- LiDAR Segment 2; 2005, 2011 and Change Between 2005 and 2011

3.4 DISCUSSION

A combination of beach morphology, wave runup, and anthropogenic effects help with the conception of blowouts at PAIS while the same variables coupled with aeolian processes shape the internal structure and evolution of each individual blowout. Though blowouts at PAIS were previously studied by Mathewson (1980), technological advancements coupled with an extended temporal scale allows for a more in-depth study of the blowouts with in Padre Island National Seashore, which has led to a greater understanding of the development and evolution of these features. The runup potential provides an understanding of how these areas are easily prone to scarping during storms that can lead to the formation of new blowouts or the extension of current ones. These blowout prone areas coincide with areas of the beach that lack hummocks and an incipient foredune due to vehicular traffic pulverizing vegetation and seaweed leading to an overall flattening of the backshore. This driving section is the location of the vast majority of dune blowouts located on the island and therefore leads to management implications when the National Seashore management is trying to continue its goal to "*save and preserve, for purposes of public recreation, benefit, and inspiration, a portion of the diminishing seashore of the United States that remains undeveloped...*" Though blowouts are caused by natural processes, within the driving section of PAIS they continue to be developed by human influences and therefore this section is not being preserved as a natural environment based on PAIS initial directive.

Cluster analysis reveals that the blowouts within the driving section of Padre Island National Seashore can be grouped into two distinct Clusters. On average blowouts

in Cluster 1 are shorter, wider, have a smaller area with a smaller perimeter and had less segments then those blowouts found in Cluster 2. These same blowouts were also associated with a shorter dune height because of a lower crest height and a higher dune base, while Cluster 2 has a taller dune and lower base elevation. Due to the lower overall dune height of Cluster 1 there is a greater potential for overwash with increased wave runup, however, because Cluster 2 dunes have higher average elevations they are more likely to experience collision with increased runup and more scarping. Cluster 2 also has a flatter beach profile, creating the potential of increased runup, with a more abrupt offshore bathymetry versus a steep shore face with a gentler offshore bathymetry present in Cluster 1. Finally these Cluster 1 blowouts were typically farther from the access road and consisted of a smaller throat when attached to the backshore, leading to a slower velocity than blowouts found in Cluster 2 (Table 3).

When comparing the initial cluster analysis of the earliest blowouts to the morphometrics associated with blowouts present at the end of the study there are some discrepancies suggesting there could potentially be a shift from two groups to four throughout the study. When taking into account these new groupings, blowouts H and M2 would become their own group as well as blowouts B and L because they are the end members of their original group. This is because their morphometrics are either larger or smaller than where they are presently grouped causing them to be outliers. H is currently the largest blowouts in Cluster 1 in respect to the length, width, area, and perimeter while M2 in Cluster 2 holds the smallest value for all of those same variables. Both M2 and H have very similar values in these variables, which is, why they could be grouped

together. In contrast, B and L are currently located in the same group but they are at the higher end of the spectrum within Cluster 2. Although both are not the longest or have the greatest perimeter, they are both the widest and contain the largest area within their current group. This shift from two clusters to four clusters could be in part based on the lack of beach morphology data from 1969, however, this change in cluster helps explain the pattern of Cluster 2 where the blowouts all start out large and then decrease to close to the size of Cluster 1 before beginning to regain size. Cluster 2 currently has some blowouts that have stabilized in growth or completely revegetated which would lead to a change in clustering based on the change in the variables used for cluster analysis.

Understanding where the greatest potential for foredune breaching occurs is important because previous studies suggest that potential breaks are where future blowouts may form. Their movement, not overwash, is a mechanism controlling the landward migration of some barrier islands (Godfrey and Godfrey 1973, Sallenger 2009). This re-stabilization of the foredune can also be seen when looking at the storm impact regimes shown in Sallenger (2000). Depending on the relationship between the wave run up to dune crest and the dune base to dune crest it is possible to identify the affect of increased wave runup on the island. Padre is currently dominated by a swash and collision regime during storms up to the 95^{th} percentile. However if the storm has a wave height of a storm of above 3.7 m with an 8 s period or if there is an increase in the wave period while the wave height stays steady at 2.5 m then the islands response shifts from collision to overwash.

An increase in sea level rise would subsequently increase storm runup in both major and minor storms. A storms impact depends on the dune crest and base elevations relative to the storm surge height and if there is a rise in sea-level there is an increased runup associated with storms (Sallenger 2000). This increase in runup will intensify scarping leading the foredunes to erode more often and easily as aeolian transport dominates the steapened feature moving sand into the backbarrier (Davidson-Arnott 2005). Additionally Padre may move from a swash and collision regime into one dominated by collision and overwash if there is an increase in sea level. Though collision and overwash will move the island landward in response to the rise in sea level it wil also lead to a flattening of the beach profile by removing sediment from the beach and foredune. This removal of sediment will lower the average dune height and decrease the beach slope subsequently increasing the potential for overwash and inundation.

This swash and collision regime is found in both the driving and non-driving sections of the National Seashore. However, within the non-driving section the dune base and crest elevation is higher and therefore there is less potential for scarping to induce blowout development (Houser et al. 2013). North of the northern barricade, where driving is once again allowed, the foedune base and crest elevation once again decreases and blowouts can once again be seen. Compared to the driving sectoin, the non-driving portion has only 800 m less of foredue that is in the collision regime, which is only 13 % of the entire non-driving section of PAIS. Due to only this small area being different and the fact that there are no natural blowouts remaining in the non-driving section anthropogenic forcing must lead to the foredune being lower and therefor more

suceptable to blowout development in the driving section. Even if it is not a direct cause of erosion, the ability to drive on the beach impacts the foredune height and therefor the islands ability to withstand strom impact.

At the inception of the park, cows from the King Ranch and Dunn Ranch freely roamed the park, over-grazing much of the island (Weise and White 1980). This over-grazing, coupled with a drought in the late 1940's and 1950's, left much of the island with large expanses of barren sand. After the cows were removed and precipitation increased, vegetation began to develop and cover much of the backbarrier section of the island (Weise and White 1980, Prouty and Prouty 1989). As the vegetation increased however, so did the number of visitors that began to visit the park. Annually the park service tallys the number of vistiors that enter the National Seashre through its main gates (Figure 6). These visitors are a combinitation of beachgoers, fishermen and representatives of Oil and Gas compainies with holdings inside the park boundaries (NPS 2012). While the exact number of visitors who exercise their right to drive on the beach within the Seashore is not calculated, the majority of visitors that do drive stay with in the first few miles of the access road (Houser et al. 2013). Many studies conducted within the National Seashore show that the vegitation type and extent found within the driving section of the beach is signaficantly different then what is found in the nondriving section (Blum and Jones 1985). The expanse and differing vegetation types provides a stabilizing anchor to the foredune by diminishing the erosive velosity of the wind and limiting erosion. Houser et al. (2013) also found that driving led to a change in the beach profile because vehicles destroyed vegitation and seaweed in the backshore

leading to decreased foredune stability, eliminating a the primary mechanism that traps sediment before its transport to the lee side of the foredune. Without vegitation to trap sediment, embryo dunes cannot form, consequently no new foredune develops causing the beach profile to flatten. With this flattening comes an increased in the potential for both normal wave heights and storm waves to scarp the base of the dunes because of larger runup. Scarping in turn leads to a removal of vegitation causing a weak point in the foredune that can develop into a break creating an environment suitable for the formation of blowouts.

Within the first 8000 m of the drivable beach, the flattened beach morphology controls the continued development of blowouts. This flattening is due to a crest height difference of 0.61 m and a 0.59 m dune base elevation difference between the driving and non-driving section (Houser et al. 2013). Currently active blowouts are only located where the dunes are below the average height of dunes for this study area. Each of these locations also lacks hummocks and vegetation, which, if present, indicate a stabilized foredune toe. In other locations, where the foredune is above average height, the blowouts behind them are completely revegetated. The revegetated blowouts are also located farther from areas of anthropogenic influence than the active blowouts. This is due to the fact that there is less driving the farther from Park Road 22 that you travel because a 4x4 vehicle is needed to traverse the island past the 5 mile marker. Because there is less anthropogenic influences at the southern end of the study area there is less pulverized vegetation and a more natural beach profile. As a result, blowouts A and B have completely revegetated. Restabilization begins to occur at 4800 m from the access

road; here the ratio of crest height to beach slope are both higher than average, indicating a decreased potential for scarping in storm events. The National Seashore contains only one active blowout, near the 30 mile marker, farther south than 5500 m from Park Road 22. Beyond this point, the extreme rise and fall of crest height and maximum height diminishes as the foredune becomes a completely redeveloped linear feature.

Blowouts in the section of beach barred from vehicular traffic completely revegetated within 20 years of the area being blockaded with an all but one throat closing with in the first 4 years. However, areas that experience the driving on the beach have not revegetated in the same timely manner. Of the blowouts in the driving section, only four blowouts have completely revegetated during the 40 year study period without reactivating at some point in the study. On average the blowouts that did revegetated took over 28 years though throat closure occurred in just over 10 year. Blowouts that did at one point completely stabilize only to be reinitiated took 14 years to completely revegetated, with a throat closure rate of 10.5 years, before redeveloping. Even the ten blowouts that never completely revegetated experienced throat closure. However, these blowouts took seven more years than the others on average to close. The drastic difference between the two sections of beach must be attributed to the anthropogenic forcing caused by driving leading to a flattened beach profile and the removal of vegetation as that is the only causation factor that differs between the two sites.

The lack of vegetation is due to the changed morphometric environment. This is a conflict for National Park Service because it contradicts a portion of their main goal. In the 1973 Master Plan, three management objectives were set up 1) serve the visitor, 2)

preserve the resource and 3) administer the area. The potential for future vehicular impact to affect the island as a resource was already an issue in this Master Plan and it stated "Vehicle traffic may build to such an extent in the future that management will prohibit vehicles completely or permit them only on a reservation basis" (National Park Service 1973, p. 19).

Though there is no perfect plan for helping "eliminate the adverse influences of man" (NPS 1974, p13), the decrease in dune base, due to beach driving, allows for increasing runup and scarping in a medium intensity storm. Driving "disrupts the landared excange of sediment between the beach and dune, which ultimately affects the responseof the island to elevated storm surge" (Houser et al. 2013, p 42). Because of this scarping will be worsened when the same area is affected by tropical storms and hurricanes especially with the continued rise in sea level. This is subsequently intensified by the decrease in the sediment budget feeding the foredunes. Less sediment creates a slower recovery time after more intense storms leaving less vegetation cover stabilizing the dune during normal island conditions leading to greater erosion as sediment is transported landward (Davidson-Arnott 2005). This provides a potential management problem for PAIS as they continue to "*save and preserve, for purposes of public recreation, benefit, and inspiration, a portion of the diminishing seashore of the United States that remains undeveloped..."* (Weise and White 1980).

3.5 CONCLUSIONS

The following conclusions were drawn from this study:

1. Different scales of wave runup determine the size of blowouts and their evolution. When the ratio of wave runup to wave crest high is low, there is increased potential scarping which leads to erosion.
2. Blowouts form in areas where wave runup causes sand to migrate from the backshore to the backbarrier part of the island. On the National Seashore, active blowouts occur where vehicle traffic and anthropogenic influences are high. Vehicle traffic affects this area by crushing vegetation and compacting the beach sediment, causing a lower beach profile.
3. In areas that have blowouts but no vehicle traffic, blowouts completely restabilized within 20 years and most of their throats closed within 4 years. In areas of high vehicle traffic, only 30 percent of the blowouts stabilized, taking an average of 10 years for throats to close and a total of 29 to completely restabilize. The decreased slope profile due to vehicle traffic also allows for greater wave runup. This increased runup leads to longer beach recovery time between storms and allows for more foredune erosion and blowout development.

4. AN IN-DEPTH GROUND-PENETRATING RADAR ASSESSMENT OF AEOLIAN BLOWOUTS ON PADRE ISLAND NATIONAL SEASHORE

4.1 INTRODUCTION

Blowouts are depressions formed by erosion of a foredune that are typically saucer or tough shaped, depending on vegetation extent, topography, and wind. Removal of vegetation by scarping or overwash causes a breach to develop within the dune line (Hesp and Hyde 1996, Hesp 2002). Sediment is then removed from the beach and foredune as wind is accelerated through the breach and transported into the backbarrier. Sediment covers and abrades vegetation initially present until eventually the foredune rebuilds itself and vegetation stabilizes the entrance to the blowout. Before the foredune completely rebuilds the sediment eroded from the blowout spreads out in the back barrier covering this vegetation (Mathewson and Cole 1980, Hesp and Hyde 1996, Hesp 2002, Levin 2011). Sediment is moving within the blowout as long as aeolian processes are acting upon it, however, it is difficult to capture all this movement when looking at historical aerial images of a study area because these photographs are static two dimensional snapshots of specific times within the blowouts life. In order to understand the subsurface extent of the blowout and volume of sand moving within the system, ground penetrating radar can be used as a secondary remote sensing platform to image the area.

Ground Penetrating Radar (GPR) has become a very useful technique to study the internal stratigraphy of dunes without actively disturbing an area. (Havholm et al.

2004, Neal 2004) and GPR is now used extensively in the study of coastal geology (*Neal,* 2004). Sedimentary analysis of barrier islands relies on sequence stratigraphy as the primary interpretive tool. Prior to the use of GPR the only way study the stratigraphy of these systems were to find outcrops, which are rare on barrier islands, or dig trenches and collect cores. These invasive techniques disrupt the integrity and placement of the deposited sediments (Neal and Roberts 2001, Jol and Bristrow 2003) and in the case of blowout may actually cause it to develop. With the use of a non-invasive technique like GPR, interpretations are based on the identification of radar surfaces facies contained within the sections with the assumption that bedding structures cause reflections that can be recognized in radar sections and that reflection errors are identified, ignored or removed during data processing (Everett 2013).

This technique has been successfully used to determine extent, internal structures, thickness and stratigraphy in coastal and aeolian environments (Leatherman 1987, Harari 1996, Bristow et al. 2007, Hugenholtz 2008, Weymer et al. in press) with Neal and Roberts (2001) and González-Villanueva (2011) using GPR to study blowout structure, fluvial and deltaic (Haeni 1991, Gawthorpe et al. 1993, Woodward 2003), glacial (Fisher et al. 2005, Jol et al. 1996, Cassidy et al. 2003), and lacustrine depositions (Haeni 1996, Moorman and Michael 1997, Smith et al. 2003). As noted GPR can be used in all of these different fields to understand the subsurface stratigraphy without disrupting the sediment and also to locate and evaluate hazards (Jol and Bristrow 2003).

It is possible to link stratigraphic signatures to specific depositional environments because seismic and GPR reflections parallel the bedding surfaces. Though the ability to

recognize bedding planes and cross-stratification with in a survey help point researchers in the direction of the correct depositional environment these features are do not definitively categorize environments as the same structures may be visible in multiple environments (Jol and Bristow 2003). An example of this is hummocky cross bedding which can be found in both arid aeolian and coastal environments. Due to their radar reflection facies are described based on (1) shape, (2) dip, (3) relationship between and (4) continuity of the reflections (Neal 2004). Common facies used in radar stratigraphy based on the work of Mitchum et al. (1977) and Neal (2004) and relevant to reflectors found within the study site is shown in Table 5 and 6.

Table 5- Terminology to Define and Describe Radar Surfaces Modified in Part from Mitchum Et Al. (1977) and Neal (2004)

Radar Surfaces		
Upper Boundary	Erosional Truncation	
	Toplap	
Lower Boundary	Downlap	
	Concordant	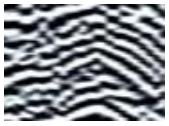

Table 6- Terminology to Define and Describe Radar Facies Modified in Part from Mitchum Et Al. (1977) and Neal (2004)

Radar Facies		
Reflection Shape	Planar	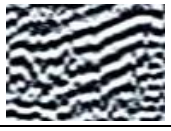
	Concave	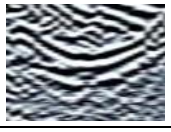
	Convex	
Reflection Dip	Horizontal	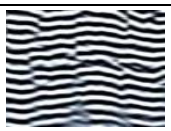
	Dipping	
Relationship Between Reflectors	Parallel	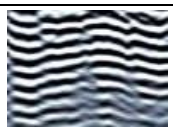
	Subparallel	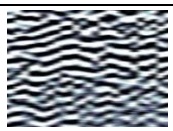
	Chaotic	
Reflection Continuity	Continuous	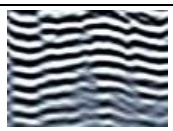
	Moderately Continuous	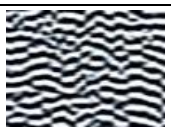
	Discontinuous	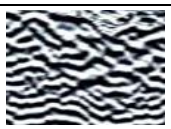

GPR uses changes in electromagnetic energy propagation to detect changes in dielectric properties between different layers of sediment (Harari 1996, Neal and Roberts 2001). These dielectric properties, also known as Relative Dielectric Permittivity (RDP), are calculated by using the ratio of a materials electrical permittivity to the permittivity of a vacuum (Conyers and Goldman 1997). Water content of subsurface materials defines the velocity and changes in the dielectric signature due to the location of the water table and lithological boundaries as well as changes in composition, orientation, packing and grain shape of the sediment (Neal and Robert 2001, Everett 2013). There is a tradeoff between the resolution of data and the depth at which stratigraphy can be resolved because of an increased attenuation of the electromagnetic signal at increased depth. To correct for this decrease, a smaller frequency GPR can be used to gain insight into structures that are deeper. Higher frequency units will resolve shallow features at a greater level of accuracy because of the conductivity of water particles however will not penetrate as deep (Neal and Roberts 2001, Everett 2013).

The GPR unit uses a control unit that sends a pulse and either one or two antennas to measure the delay between the time a pulse was transmitted and its arrival. If one antenna is used the survey is completed in monostatic mode, while if two are used the survey is done in bistatic mode (Neal and Roberts 2001). The transmitting antenna sends a pulse of electromagnetic energy into the subsurface, where it is reflected by changes in dielectric properties and then the receiving antenna detects the reflected electromagnetic waves when they reach the surface. The time delay between the transmitting antenna sending the pulse and the receiving antenna receiving the return

pulse is proportional to the depth of the subsurface feature that reflects the wave (Harari 1996). The returned signal, also called two way travel time, is measured in nanoseconds (10^{-9} s) in ground-penetrating radar and the velocity can then be converted into meters when the dielectric constant for the material is known (Sensors & Software 1999, Neal and Roberts 2001).

Ground-Penetrating radar has recently been used extensively to study blowouts, washovers and sand dunes both in coastal regions (Bailey and Bristow 2000, McGourty and Wilson 2000, Botha et al. 2003, Claudino-Sales et al. 2008), and in continental interiors (Harari 1996, Stokes and Swinehart 1997, Hugenholtz 2008). Bailey and Bristow (2000) used GPR image the internal structure of coastal dunes in Wales without disrupting their study sites. In this study they found GPR to be a useful technique to resolve cross-stratification, cut and fill troughs and bounding surfaces to gain understanding an understanding of different periods of growth and destruction within the system. Ground-penetrating radar was also found, by McGourty and Wilson (2000), to resolve gravel ridges, blown sand deposits, truncated reflectors caused by erosion and the location of the water table on the northern coast of Northern Ireland. They were successfully able to resolve depositional and erosional facies and areas where soil developed (GPR used in association with coring). Dipping reflectors were also inferred as a former dune ridge that was subsequently eroded and overwash refilled with deposited sediment. Botha et al. (2003) used GPR this technique to determine whether limbs of parabolic sand dunes on the Maputaland coastal plain in South Africa were simple or complex features. Their subsurface images showed complex internal structures

with cross-bed forests, shallow troughs and stacked aeolian sands showing buried historic dune topography. In both cases the authors were able to elucidate stratigraphic relationships in the radar facies and surfaces to determine vertical accretion rates and understand the periodicity of dune remobilization. GPR can also be used in conjunction with optically stimulated luminescence (Stokes and Swinehart 1997, Bristow et al. 2007), storm deposits or depositional surfaces (Aagaard et al. 2007), and aerial photographs (Neal and Roberts 2001, Gonzalez-Villanueva et al 2011) to date activation ages of subsurface structures.

In this study ground-penetrating radar surveys will be conducted at two sites within Padre Island National Seashore. These surveys were then analyzed to identify the radar surfaces and radar facies. LiDAR data and the digitized blowout extents were then compared with the GPR analysis. This comparison allows for the digitized GPR transects which show the history of the blowout in three dimensions to be referenced to surficial two dimensional exposures found in aerial photographs. This then allows for a greater insight into the processes that create the subsurface structures and developmental phases that the blowout moves through over time.

4.2 METHODOLOGY

4.2.1 Ground-Penetrating Radar

A PulseEKKO 100 was used in this study to conduct a common offset survey based on the Bailey and Bristow (2000) and Neal and Roberts (2001) methods, GPR surveys were conducted at two blowout formations on the Island (Figure 20) using a 200 MHz antenna with a step size of 0.4 meters and the antennae separated by 0.5 meters. Study Site 1 (SA1) is a blowout stabilized by vegetation that contains a parabolic depositional sand sheet that is migrating across the backbarrier. Study Site 2 (SA2) is a blowout still attached to the backshore. Spatially, the surveys were collected along the average direction of travel and across the width for each blowout. To preserve correct step size throughout the survey a survey grid was laid out at each site before the surveys were conducted using survey tape marked every 0.4 meters.

To account for the topography changes across transects, a Total Station survey was conducted using a Topcon GTS. These surveys used the same grid system and an elevation point was taken every 0.4-1 meters depending on the severity of elevation change along the transect. The grids were also shot in using a Garmin handheld GPS in order to place the transects spatially within a GIS, however their elevation could not be used because of the large margin of vertical error when it comes to this type of unit. After collection, the data was downloaded and, due to survey direction and order, if needed transposed to align the start and end points of the elevation profiles and the GPR.

Figure 20- Study Site 1 (SA1) and Study Site 2 (SA2) Where Ground-Penetrating Radar Surveys Were Conducted

Within Transect 1 and Transect 3 at Site 1 and Transect 3 at Site 2, there are multiple areas containing errors. These areas show parabolic structures radiating down past the extent of where the rest of the signal dies out. The error was caused because of the proximity of the transmitter and receiver to the computer collecting the data. The computer causes interference between the transmitter and receiver when it is in close vicinity however there is not a set distance between the two and with the vegetation cover present along many transects the fiber optic cables connecting the two get tangled

and snagged with extended distance. Due to inclement weather on the final two days of the study, a transect down the length of Site 2 was unable to be acquired.

Before interpretation, the collected data must first be post processed. To process the surveys the data must be corrected using trace editing and migration, dewow, background subtraction, AGC gain and shifting the topography of the profile. The first step completed in data processing was to remove redundant traces or fill gaps created by collection error. Trace editing is a tool that makes it possible to remove traces that are replicated or contain errors and then replace traces with data that has been interpolated from adjacent reflectors (Everett 2013). After the traces are edited they must then be migrated to assure that the traces are located correctly in the spatial plane. Migration ensures the returned energy is located in one position so that the depth of dipping strata is not underestimated because of how the radar wave emitted returns a parabolic signal (Van Kempen and Sahli 1999, Jol and Bristow 2003, Neal 2004).

Applying high-pass filters are the next step in data processing. "Wow" is a low frequency deviation in the electromagnetic field that leads to a variation in the baseline amplitude. By applying a "dewow" filter it is possible to correct this deviation and attenuate the low frequency to produce a baseline amplitude of zero (Neal 2004, Everett 2013). The second high-pass filter applied to the collected data is a background subtraction filter used to remove noise and increase weaker signals (Sensors and Software 1999). The weaker signals are increased by reducing high amplitude ground clutter by subtracting the adjacent average amplitudes (Everett 2013). These two

processing techniques aid in interpretation by weakening low frequency noise acquired during data collection.

In addition to background subtraction, the application of automatic gain control (AGC) also helps weaker signals. AGC is inversely proportional to signal strength and therefore equalizes all amplitudes in the trace. This is done by estimating the difference between the average in specific period of time and the amplitude of the entire trace. As gain control can amplify both noise and reflectors, different combinations of window size and gain were considered before application of these parameters were finalized (Jol and Bristow 2003, Neal 2004, Everett 2013).

Once all processing techniques were implemented, a final topography shift was performed to correct for elevation changes over the transect. Though migration rectifies the dip angle of strata in areas of steep topography, this does not fix all dip discrepancies. On sloped surfaces the GPR antenna has a horizontal factor which increases the value of recorded dip and misaligns reflections. By correcting for topography after migration these dips and traces are reoriented into the correct positions (Neal 2004, Everett 2013). In this study the elevations recorded by the Total Station Survey were normalized using LiDAR data collected in 2011, discussed below, to accurately place the deflation basin, the surveys lowest point, at its correct location above mean sea level and give the radar reflectors the correct spatial location in the subsurface.

4.2.2 Aerial Photography and LiDAR

While the GPR displays the subsurface features it is also important to understand how these features are expressed on the surface over time. To do this aerial imagery collected in 1969, 1974/75, 1979, 1984, 1989, 1993, 1996, 2002, 2008 and 2010 was acquired for the two study sites. These images were all georefrenced using Universal Transverse Mercator Zone 14N and the blowouts and active sand features were digitized (See section 3 for further details).

Light Detection and Ranging (LiDAR), an active remote sensing platform, data was employed to show areas of erosion and deposition within the study area. LiDAR data that was collected by PAIS in 2005 and the U.S. Department of Agriculture (USDA) in 2011was used via raster algebra to find the difference in elevation between the two dates. The 2005 data was collected using NASA's Experimental Advanced Airborne Research LiDAR (EAARL). This is an aircraft mounted pulsed laser ranging system designed to measure ground elevation and coastal topography with a vertical resolution of 15 centimeters and horizontal resolution of 1 m. The USDA data is part of the National Elevation Data set. This dataset has a horizontal resolution of 3m and a vertical resolution of 2.44 meters. Because of the discrepancy of cell size associated with the horizontal resolution differences, the 2005 data was resampled in ArcGIS to match the resolution of the 2011 data (See section 3 for further details).

4.3 RESULTS

4.3.1 Study Site 1 (SA1)

Since 1969, there have been active blowouts in this study area (Figure 21, Table 7). Within this site there are five different phases that the blowout progress through during the study due to changes in erosion and deposition patterns. A phase is marked by changes in erosion or deposition that occur within the blowout and can be seen in the aerial photographs. These phases can then be correlated to radar surfaces found in the GPR surveys. Together these depict the three dimensional evolution of the blowout by showing the volume of sediment associated with changes in erosion or deposition due to either scarping or the vegetation stabilizing the blowout. The blowout inhabited the same location in 1969 and 1974 (Phase 1) with little vegetation or expansion until it revegetated prior to acquiring the 1979 images. In 1979 (Phase 2) a smaller blowout was located in the current vegetated center before stabilizing by the mid 1980's. In 1984 (Phase 3) the original blowout reactivated in the same location as the 1969 blowout. Between 1984 and 1989 a new foredune began to develop as vegetation reestablished seaward causing sand to deposit in front of the historic foredune. By 1989 the blowout enlarged once again filling the area from the current foredune back to where the termination point of the blowout in the 1970's. After 1989 (Phase 4) the blowout progressed towards its current location. In 1993 and 1996 the blowout stayed roughly the same size but moved inland behind the foredune. In 2002 (Phase 5), the blowout once again broke through the foredune and expanded in width. Since then, the foredune has reestablished and a depositional lobe began forming at the terminus of the blowout.

Table 7- Study Site 1 (SA1) Phases Derived from Aerial Photographs

	Years	Environment	Photograph
Phase 1	1969- 1974	• Intitial blowout • Remains relatively unchangeing until stailization after 1974 • Throat attached to backbeach	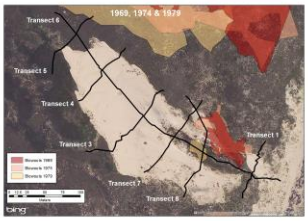
Phase 2	1979	• New blowout initiates pre-1979 • Dettached to backbeach • Revegetated post-1979	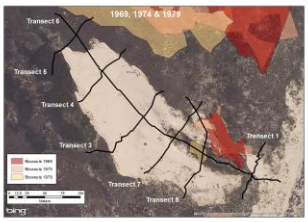
Phase 3	1984	• Blowout initiiates post-1979 • Attached to backbeach in a wide scarped area	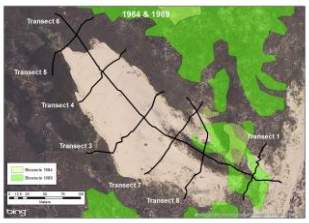
Phase 4	1989-1996	• New foredune develops seaward of historic foredune • Throat stays attached to beach though new foredune • Foredune restablishes by 1996	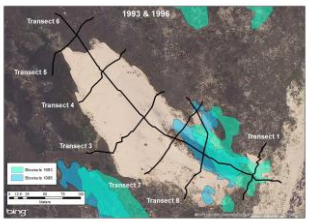
Phase 5	1999-2012	• Hurricane Brett (1999) restablishes blowout throat • Blowout expands to current location • Foredune almost completely restablished in 2012	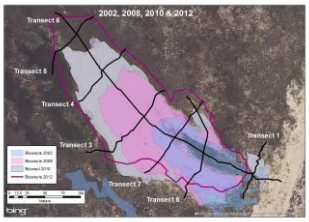

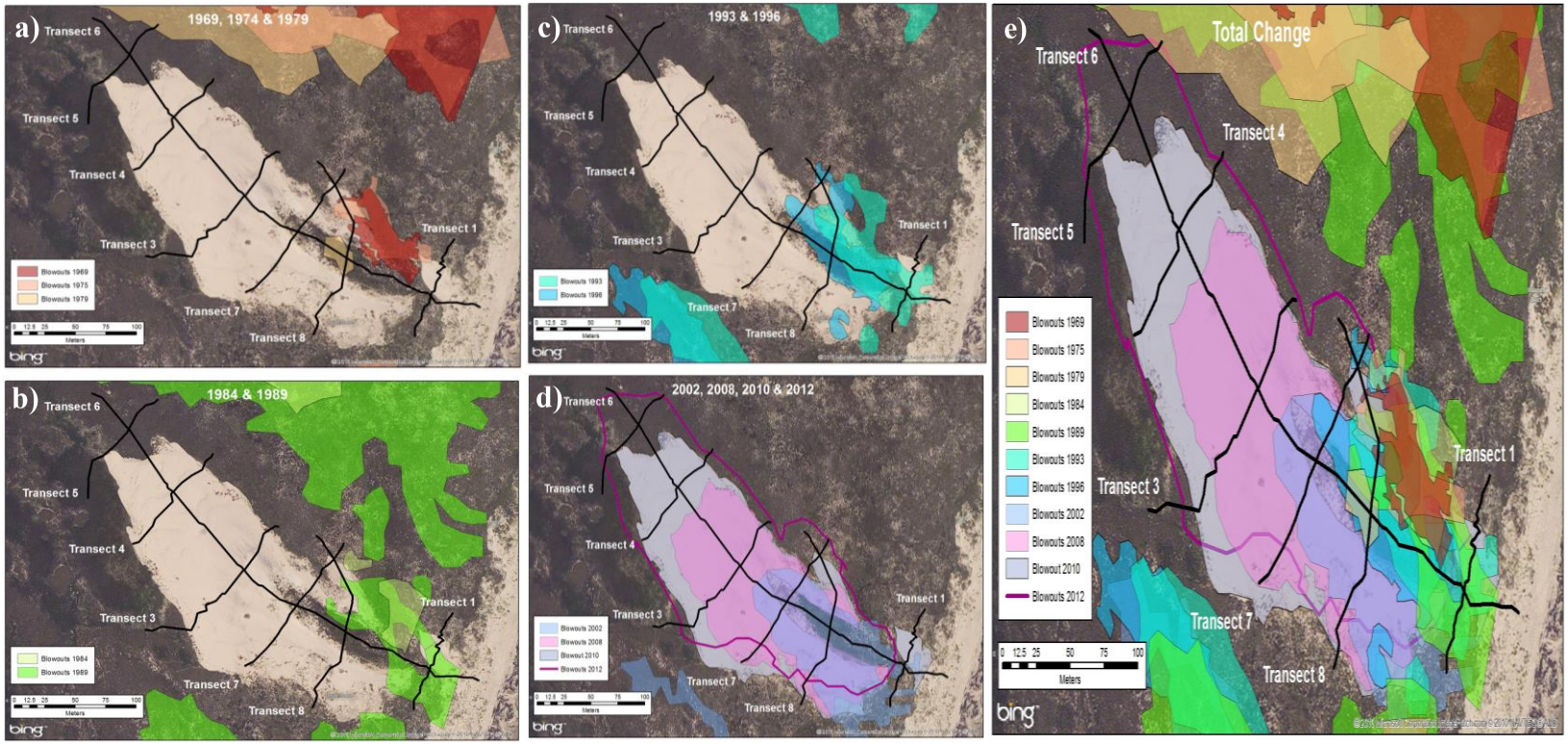

Figure 21- Blowout Evolution of Study Site 1 (SA1): a) 1969-1979, b) 1984-1989, c) 1993-1996, d) 2002-2010, and e) Total Change Throughout Study

Using LIDAR data collected in the past decade it is possible to discern where current erosion and deposition is occurring in the first blowout (Figure 22). In the vegetated center of the blowout there was no major erosion or deposition between 2005 and 2011 due to the vegetation stabilizing this region slowing the winds momentum and protecting the sand from aeolian processes (Phase 5). Erosion appeared to be occurring around the center of the blowout with most sediment loss occurring on the steep slopes of the southwestern flank and near Transect 3 where the end of the blowout connects to the depositional lobe. The sediment that was removed from these areas was deposited on both the lee side of the western dune and between Transect 3 and 4 in the depositional lobe. The sediment transport trends this direction throughout the entire study period when aeolian processes were acting upon to the active sand due to the primary wind direction with in the National Seashore and the topographic forcing associated with the dunes. There was a minimal amount of erosion at the historic neck and Transect 1, due to vegetation cover, while there is patchy deposition occurring along the foredune. Transect 4 and 5 remained at equilibrium or had a small amount of sediment deposited. The depositional lobe is in equilibrium because this area is in the flat backbarrier and is no longer associated with topographic forcing of the wind so the velocity is less and this area is continuously supplied with sand being eroded from the blowout as the lobe spreads out. This data does not contain the data for erosion and deposition between 2010 and present, the continuation of Phase 5< where there should be a net deposition between Transect 4 and the current extent of the blowout that was surveyed in the fall of 2012.

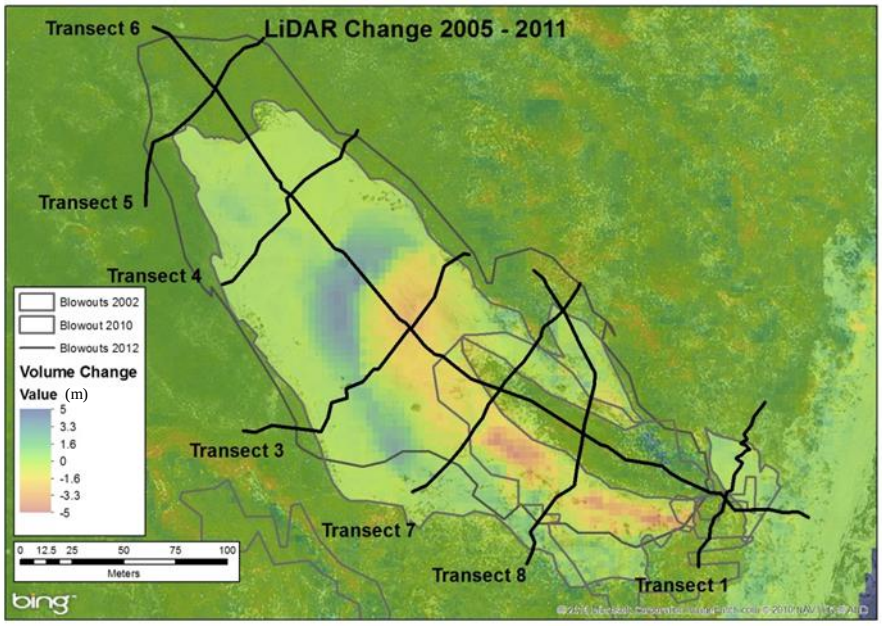

Figure 22- LiDAR of Study Area 1; Volume Change Between 2005 and 2011.

Over 1,020 meters of GPR data was collected from seven different transects at Site 1. To develop an understanding for the entire subsurface structure, transects were evenly spaced within the blowout. Transect 1 cuts through the historic entrance of the blowout to find infill structures that have developed as the foredune was re-established. Transect 3 was completed at the end of the blowout where parabolic sand sheet begins. Transect 4 and 5 are evenly spaced near the terminus of the parabolic. Transect 6 began at the far terminus of the sand sheet and traveled down the center of the blowout and into the foredune. To obtain an in depth understanding of the blowout itself Transects 7 and 8 were positioned between Transect 1 and 3. These two transects extend up and over the 8-10 meter dunes flanking the blowout. Transect 2 is not shown at this study site because Transect 8 was collected as an extension of the original transect. Except for Transect 6, all transects began at the western edge and moved east.

Sedimentary relics and phases can be seen with in each study site within the ground-penetrating radar data (Figure 23). These features are referred to as radar surfaces, radar packages, and radar facies. Facies are the sedimentary bedding and structures within the profile and describe general the shape, dip and continuity of deposition. Radar packages show continuous strata that form in the sediment record and are bounded by radar surfaces. Radar surfaces are formed by unconformities and depositional breaks with in the sediment record (Baker and Jol 2007). These surfaces show phases with in the blowout associated with changes in erosion and deposition patterns, typically due to storm runup, and can be seen in surface expressions within the historical aerial photography.

Transect 1 contains mostly flat strata with two potential surfaces. The first surface is found at about -8 meters (Pre-Phase 1) while the second surface is found closer to 0 meters (Phase 5) and contains downward dipping beds around 40 meters from the beginning of the transect. The upper surface is associated with oblique chaotic reflections showing erosional truncation due to foredune erosion, while the lower reflections show concordant laterally continuous parallel to subparallel reflectors. These lower reflectors, associated with foredune building and deposition, continue in the subsurface until around 8m where another radar boundary is present. This boundary, though close to the maximum depth of penetration and difficult to resolve, shows convex reflections with erosional truncations associated with the historic scouring a foredune in much earlier than the start of this study.

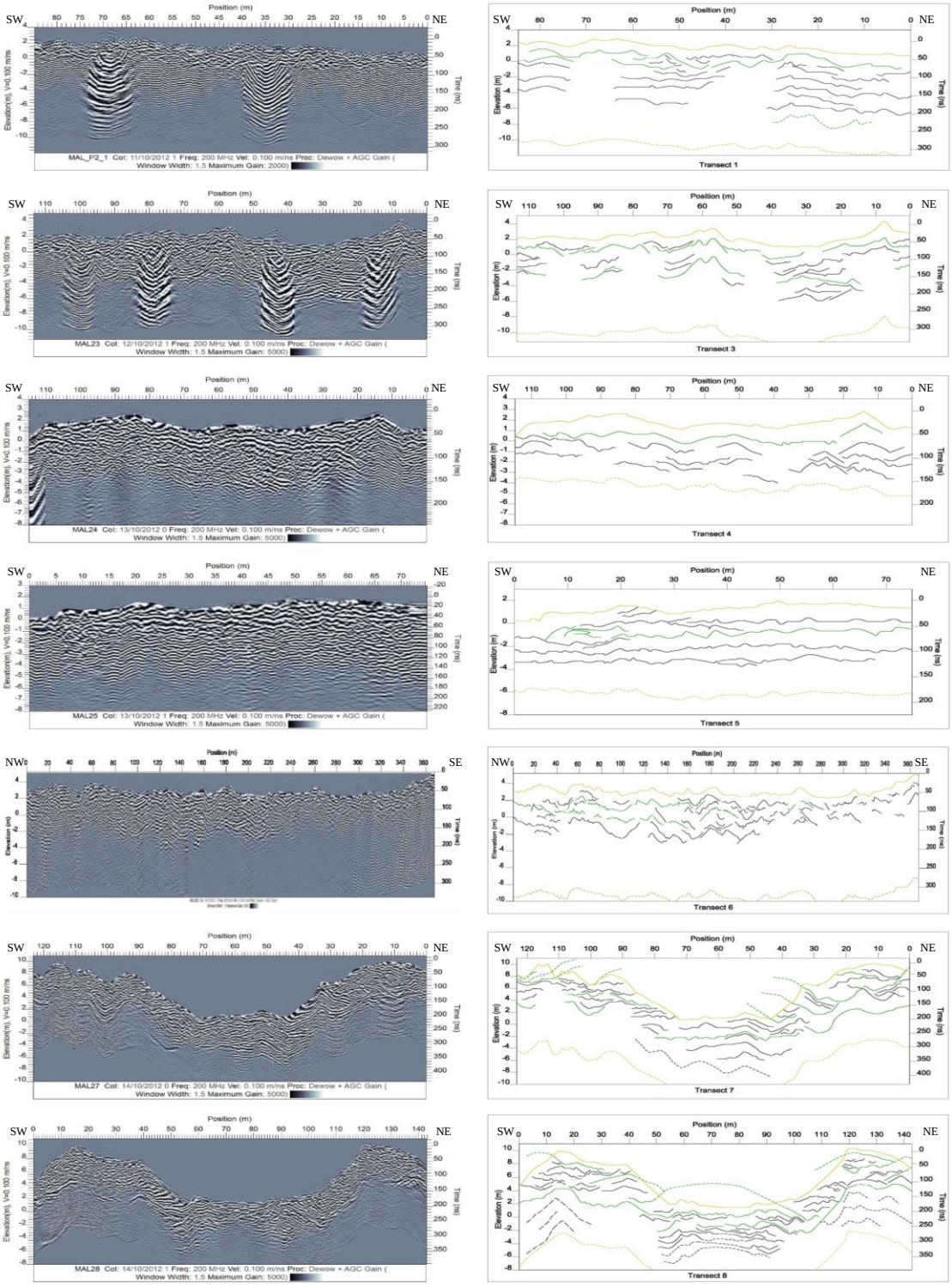

Figure 23- GPR Transects for Study Area 1 (SA1) with Radar Surfaces Shown in Green and Radar Facies Shown in Black with Inferred Features Dotted. A More Detailed Image of Each Transect Found in Appendix 1.

Transects 7 and 8 run parallel to each other on the southwestern end of the transects and cross the deflation basin before going up and over the 10-meter tall secondary line of dunes until the transects cross at their eastern terminus. These transects have multiple surfaces where erosional facies can be seen as sand was removed from the blowout and it expanded. Above the deflation basin there are multiple sinuous subparallel and oblique reflectors, associated with Phases 1 through 5, that show sediment was eroded and deposited as the dune migrated from northeast to southwest. Areas below the deflation basin are mainly horizontally deposited with a few concave structures, below -2 m, associated with Phase 1, historic scouring and historic blowout locations up until the mid-1970's. Beginning with Phase 2, as the blowout increased in size towards the west toplap and downlap can be seen on either side of the deflation basin associated with erosional truncation of facies as the blowout cut through the original dune structure. An area can be seen in Transect 8where the dip angle of the lowest facies boundary is comparable to the current slope of the eastern erosional wall. This is most likely associated with scarping and erosion of the blowout after revegetation post 1979 and redeveloping towards the east before 1984. Around 1993, the deflation basin begins to form through Transect 7. Its expansion can be seen by the dotted surfaces extending into the current deflation basin, between 2 m and 8 m, in both Transect 7 and Transect 8. These facies were truncated as the sediment was removed from the deflation basin and deposited in the depositional lobe towards the southwest.

Transect 3, which is across the edge of the current deflation basin, has two surfaces that can be interpreted although the facies in these packages are much more

complex than Transect 1. The upper section of facies seen at 0 m is associated with morphologic changes 2002 -present (Phase 5), consists of both concave and convex reflection configurations roughly sub parallel to each other with erosional truncation and toplap associated with aeolian processes acting on the unvegetated surface as the foredune rebuilt. The truncation and concave and convex reflections occur due to the deflation basin being eroded in the early 2000s and that sediment being deposited on the western edge of the basin. Below this surface are a set of laterally discontinuous reflectors as well as crosscutting reflections with low to moderate dips. This can be interpreted as historically vegetated dune deposits associated with Phase 1 and 2 found in the 1969-1983 aerial photographs (Figure 20). This section is bounded by another layer of chaotic, concave and convex reflectors that are subparallel to oblique showing an environment dominated by aeolian processes allowing sand sheets and mounds (dunes) to develop which can be found below -2 m. This lowest section represents a period before 1969 when the island was dominated by active sand sheets (Mathewson 1980) and there were active dune fields with minimal vegetation previous to Phase 1.

Transect 4 and 5 only have one sub aerial bounding surface. Between this surface found at 0.5 m and the aerial expression there are thick layers of laterally discontinuous reflectors showing both toplap and erosional truncation showing the depositional lobe of the blowout as it extends into the backbarrier. Based on the aerial photographs in Figure 20, this package is associated with Phase 5, the most recent expansion of the blowout as the foredune recovered. Below 0.5 m however, subparallel laterally continuous

horizontal reflectors with slight concavity or convexity dominate associated with aeolian deposits in the flat backbarrier before 1969 and the start of Phase 1.

Through the center of the blowout (Transect 6) it is possible to see the sloping stratigraphy of previous termination points of the blowout from 0-200 m and above 2 m depth, but it is not possible to see distinct boundaries between 200 m and 360 m at depth due to extensive erosion with in the deflation basin. This transect is dominated by oblique chaotic structures due to the direction of data collection. The end of the deflation basin can be seen around 180m where there is an increase in surface topography as you move out on the depositional lobe towards 0m. Reflectors in this area are much more continuous but equally as chaotic from extensive deposition. This is to be expected because as the depositional lobe expands landward the lobe acts more like a sand sheet in the middle with downlap occurring at the end of the lobe continuously farther inland as it expands.

4.3.2 Study Site 2 (SA2)

The second study area, Site 2 (Table 8), is a blowout that has been stabilized by vegetation but still contains an active sand sheet where sediment was originally deposited. Based on the aerial photos this blowout develops through four different phases of evolution. The blowout at this site developed before 1969 (Phase 1) and was roughly the same size and in the same position for the decade after the first photo was taken with the foredune situated farther inland then its currently location (Figure 24). Pre-1984 (Phase 2), however, the blowout extended in width and the neck enlarged

extensively. Between 1984 and 1989 the current foredune began building seaward of the historic foredune. As this new foredune began stabilizing with vegetation the blowout continued growing in size establishing a neck though the new foredune. This neck stayed established into the 1990's as the blowout lengthened pushing farther inland. By 2002 (Phase 3), the foredune ridge finally began reestablishing its presence and the blowout began to stabilize with vegetation in the center. Between 2002 and 2008 rapid vegetation stabilized the majority of the former blowout and most of the active sand was contained in the depositional lobe at the end of the blowout. Currently the blowout is completely stabilized (Phase 4), with the exception of a few small patches of active sand on dune crests.

Due to vegetation cover stabilizing the sand there was minimal erosion and deposition found when comparing the 2005 data to 2010 (Figure 25). In areas where there are still active patches of sand with in the vegetation there is erosion. Typically the areas of erosion are found at a higher elevation and on the windward slope of the dune. The material eroded from these areas is deposited on the lee slope of these higher elevation areas. Between where the blowout ended in 2002 (Phase 3) and where the active sand sheet was located in 2010 (Phase 4), there is extensive erosion, with deposition occurring at the areas to the west of the erosion, due to the average wind direction on Padre Island. The foredune in front of the vegetated blowout is contains steady deposition between 2005 and 2011 which has helped protect the area and enhanced vegetation recovery.

Table 8- Study Site 2 (SA2) Phases Derived From Aerial Photographs

	Years	Environment	Photograph
Phase 1	1969- 1979	• Blowout develops pre- 1969 • Remains stable during period • Throat attatched to the backshore however some detachment beginning in 1979	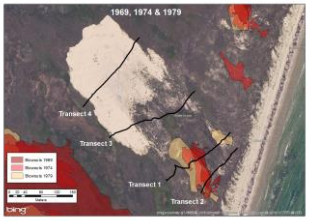
Phase 2	1984-1996	• Blowout extends in width s • Throat becomes widelyscarped unvegetated area • New foredune developes seaward of historic foredune • Blowout expands in length Foredune reestablished by 1996	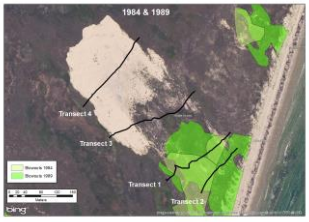 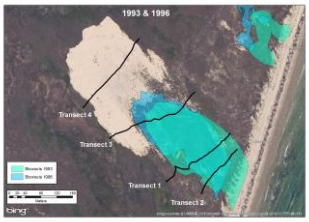
Phase 3	1999-2008	• Hurricane Bret (1999) creats at least 2 small throats • Foredune recovers • Blowout expands in both length and width	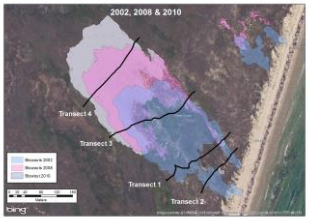
Phase 4	2010-2012	• Foreduen completley restablishe • Blowout completely revetated • Only deposional lobe active	

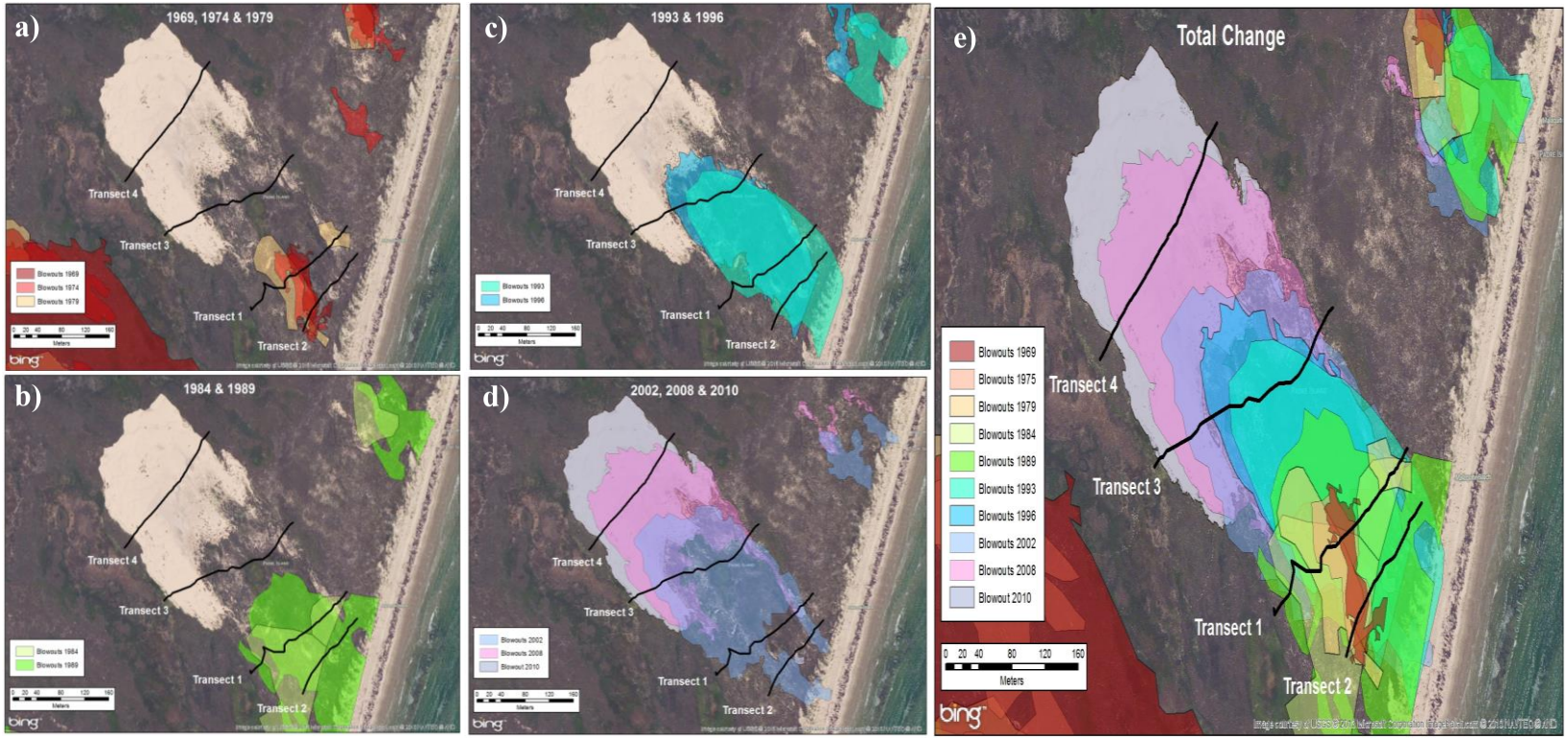

Figure 24- Blowout Evolution of Study Site 2 (SA2) a) 1969-1979, b) 1984-1989, c) 1993-1996, d) 2002-2010, and e) Total Change Throughout Study

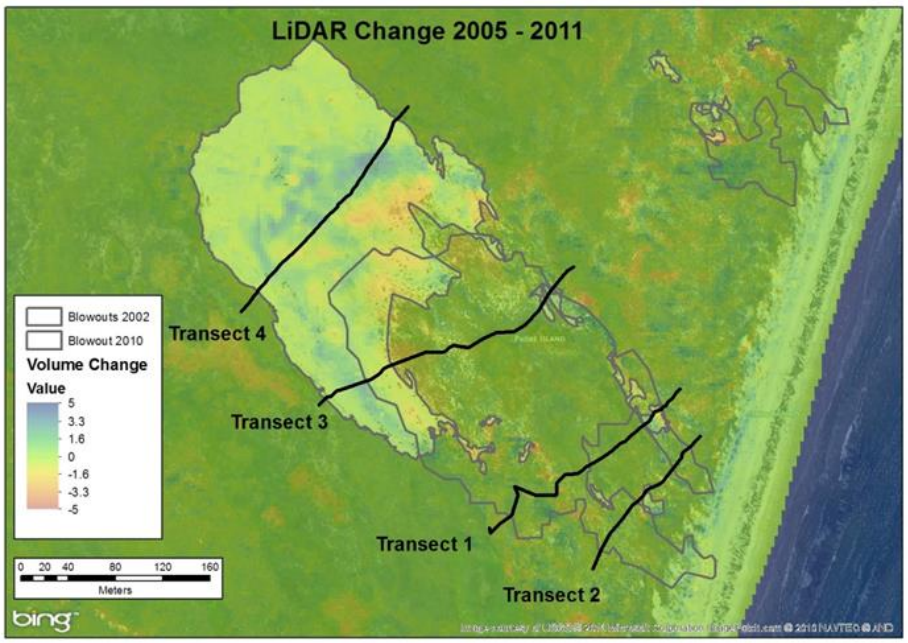

Figure 25- Volume Change at SA2 Between 2005 and 2011

At this blowout, which has stabilized with vegetation, 715 meters of GPR was collected in four different transects. Transect 1 traversed the vegetated center of the blowout, extending from a flat area in the west, over the western dune, and ending in a flat between dunes on the eastern side of the blowout. Transect 2 was completed through the vegetated historic neck of the blowout between the former foredune and the current foredune. The transition area between the vegetated blowout and the current sand sheet is surveyed by Transect 3. On the western side of this transect there are still active aeolian processes acting on the open sand, while the eastern portion has stabilized by vegetation. The last survey completed in this site is across the active sand sheet.

The GPR (Figure 26) surveys recorded sedimentary structures at a maximum depth of about 4 m before the signal to noise ratio is to great to resolve structures. In the

first two surveys, which show the blowout arms, deflation basin, and neck of the previously active blowout, multiple boundary layers can be seen as sediment was extensively eroded and deposited here from 1984 until revegetation in 2002.

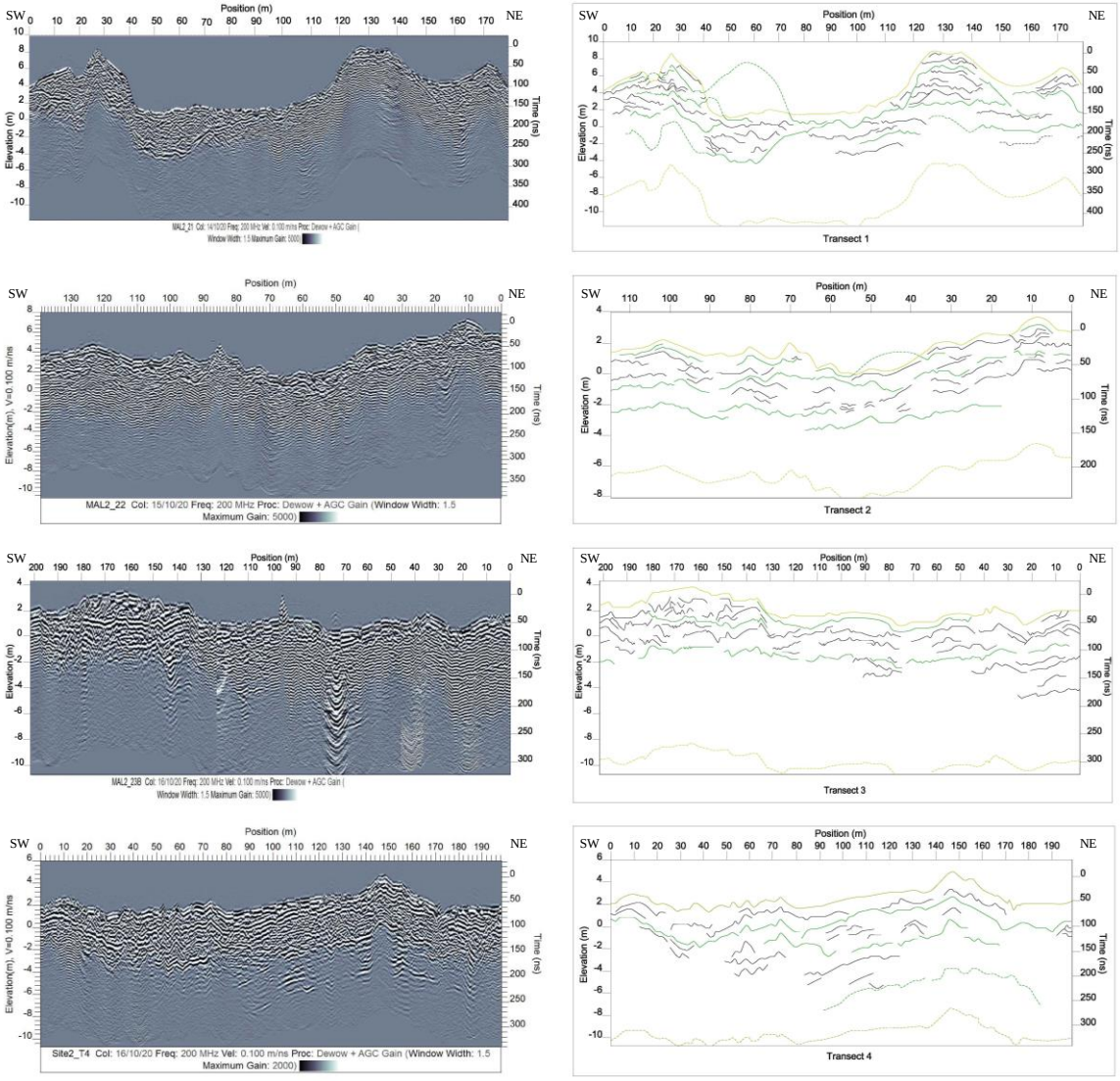

Figure 26- GPR Transects for Study Area 2 (SA2) with Radar Surfaces Shown in Green and Radar Facies Shown in Black with Inferred Features Dotted. A More Detailed Image of Each Transect Found in Appendix 2

The neck of the blowout was imaged with Transect 2 and contains roughly three radar surfaces. The top layer, which is less than a meter thick, is comprised of continuously parallel reflectors that formed when vegetation began to anchor the sediment in place and is associated with Phase 4. Below Phase 4 is Phase 3, a package of laterally discontinuous chaotic reflectors formed as aeolian processes dominated the blowout while it was still active and sediment was actively being moved from the backshore but the foredune was being rebuilt seen at a depth of around -1 m. Around 80 m there is a sharp rise in topography associated with an area of the neck that revegetated more quickly than the adjacent areas allowing for greater deposition from the backshore due to vegetation slowing the wind and forcing sand grains to fall out of entrainment. Around -2.5 m in depth, there is the start of another radar package of facies. This area consists of parallel reflectors that are mainly continuous with a few laterally discontinuous crosscutting reflectors. These reflectors represent a period before 1969 (Phase 1), when aeolian sand sheets with small foredunes and patchy vegetation dominated the island (Weise and White 1980). Convex facies are associated with areas of vegetation cover allowing for greater deposition then vegetation free areas.

Transect 1, which cuts across the former blowouts arms and through the deflation basin, is the most complex transect at this site. In the subsurface it is possible to see sediment is moving from the east to the west as well as where dune structures previously inhabited. This is shown by toplap truncation reflectors on the northeast side of the blowout, between the elevations of 2 m and 7m, where the deflation basin cuts through the dune and downlap truncation on the southwestern side of the deflation basin. The

dunes associated with the blowout arms are one of the last areas of the actual blowout to revegetate and extend areas of higher elevation in the surface during Phase 3. Below the deflation basin is a highly reflective concave reflector boundary, reaching down to almost -4 m, where reflections below are parallel and laterally continuous and above is chaotically laterally discontinuous. This feature is an initial blowout or overwash channel that has been subsequently refilled with sediment between Phase 1 and 3.

The survey (Transect 3) which is across the transition zone contains mostly horizontal layers of strata. This transect is associated with two stratigraphic packages. The top package contains the currently active and recently revegetated deposits of the historic deflation basin before the blowout revegetated (Phase 3 and 4). On the southwestern side of the transect are more chaotic reflectors that formed as the depositional lobe moved in that direction. Below the reflection surface at a depth of 1 m, surface are thinner parallel laterally continuous beds of the former flat backbarrier deposited before and during Phase 1.

Transect 4 contains cross bedded sands that were deposited as the sand was transported from the blowout into the depositional lobe during the mid-2000's as shown in Figure 23 (Phase 3). The current sand sheet contains mounds of active sand upwards of 10 meters past Transect 4, though these high areas were not surveyed. In the subsurface are three sedimentary packages associated with this transect. The topmost consisting of about 1m of thick reflectors are the current aeolian driven deposits of the top layers of the migrating depositional lobe. Below this package is a grouping of thinner laterally discontinuous cross-cutting reflectors, between 1 m and -2 m in depth, that are associated with the original migrating of the depositional lobe and this goes to the base of the currently active sand sheet. The lowest reflectors, around a depth of -5 m though difficult to resolve due to the signal to noise ratio at this depth, is the original subparallel and parallel reflectors of the former flat backbarrier prior to Phase 3.

4.4 DISCUSSION

The understanding of the evolution of blowouts has not been extensively studied in the past especially along the Gulf Coast. Due to advances in technology aerial photography, ground-penetrating radar, and LIDAR can now be used to describe the evolution of each blowout in respect to the morphology, aerial extent, subsurface structure and volume of sediment transport. When the three remote sensing techniques are combined together a more complete picture of how each blowout grows and evolves. My findings parallels findings by Stokes and Swinehart (1997), Bailey and Bristow (2000), McGourty and Wilson (2000), Aagaard et al. (2007) and Hugenholtz (2008) in that I was able to accurately locate radar surfaces, packages and facies associated with blowout evolution.

Before the park was established, the overgrazing of cows in addition to a drought in the late 1940's and 1950's, left much of the island with large active sand sheets (Weise and White 1980). This is shown in many of the GPR transects as the lowest radar package with parallel horizontally continuous reflectors. In the 1960's the drought began to subside and the park was established, leading to the removal of large herds of cattle. These two variables allowed vegetation to redevelop and cover much of the backbarrier section of the island (Weise and White 1980, Prouty and Prouty 1989). As vegetation moved back in, the stabilized dune structures developed on the island acting as a defense against storm washover. Between 1940 and 1968, 13 hurricane strength storms and 11 tropical systems passed within 320 kilometers of the study site. This included Hurricane Carla, a Category 4 storm when it made landfall in 1961less then 150

km from PAIS inducing a 3.3 m storm surge on the island (NOAA 2012). These storms increased wave runup on the island, Hurricane Carla's runup alone was greater than the average dune base for the island. This along with the frequency of storm impacts near the National Seashore may have initiated blowouts present at PAIS in the 1969 aerial imagery.

Phase 1 (Table 7 and 8) initiated at both sites with the re-colonization of vegetation on the foredune as it began to recover after it was impacted by a major storm. At SA2 it lasted until 1983 while during the same time span SA1 experienced 2 phases. Phase 1 lasted from 1969 until 1973 and then entered its Phase 2 from 1974 until 1983. At both sites these periods were associated with minimal expansion of the blowout structures however there were changes in the neck locations due to storms as seen in the first image of Figures 20 and 23.

The 1984 imagery shows the start of Phase 3 (SA1) and Phase 2(SA2) with a dramatic change in size and shape of blowouts possibly related to a series of strong storms in the early 1980s (Category 5 storm followed by a Category 2 storm in 1980 and a Category 3 and Category 1 storm in 1983). After 1984 there were no hurricanes to impact the area until after the 1989 image was acquired in February of 1989. Because of the reduced frequency of storms during the early 1980s, vegetation removed from scarping induced by previous hurricanes was able to recover. During this time a new foredune developed seaward of the original foredune as vegetation recovered slowing the wind velocity and forcing sediment deposition. Despite the vegetation regrowth, the blowouts remain active as the throats prevent the foredune from establishing in front of

the blowouts. This regrowth in vegetation initiated phase 4 at study site 1. Here the neck size and shape present in 1989 continued into the 1993 imagery. The neck at Site 2 stays open and extends seaward, however, the blowout continues in Phase 2 until 2000 as the blowout experiences a drastic growth in length while remaining the same width.

A Category 4 storm in 1999 passed within 80 kilometers of the study sites and reactivated the necks of both blowouts. Erosion at Site 1 was much more extensive with the active blowout expanding on the aerial imagery. By 2002, the neck at SA1 was over 100 meters wide, whereas revegetation at Site 2 left only one 40 meter and one 20 meter break in the foredune visible in the aerial imagery. Both of these breaks are preserved as phases in the stratigraphic record at a depth of roughly 1m. Both foredunes recovered between 2002 and 2008 with a large volume of sand being transported from the actual blowout into a parabolic sand sheet. At both sites, the lowest phase in Transect 3, is attributed to this growth. The parabolic depositional lobe increased in size in 2008 with sediment being deposited over the vegetation at Transect 4, shown by the chaotic reflections above a more parallel set of reflections, creating the first phase in both GPR transects.

A reactivation of the blowout necks in 2002 eroded away all deposited stratigraphy preserved in Transect 1 of Site 1. This erosion of the foredune caused the start of Phase 5 at the site which continues until present with the imagery showing the blowout expanding towards the west. The reactivation occurred due to increased wave runup associated with a storm or multiple storms between 1996 and 2002. When the wave runup increases, the foredune is scarped, removing vegetation and allowing more

sediment to infiltrate the backbarrier. The neck and width of the blowouts located at both sites stayed the same between 1993 and 1996 though deposition can be seen in the GPR transects as mostly flat lying reflections due to sediment continuously funneling from the backbeach into the blowout. This leads to the length of the blowouts at both sites extending, even as the necks and foredune began to revegetate. Once it is no longer constrained by the topography as it reaches the flat backbarrier, the parabolic depositional lobe spreads out as a flat sand sheet and no longer has a distinct parabolic morphology.

Phase 5 can be looked at more in-depth then the other due to the LIDAR survey present during this time. These surveys help show how the sand is moving within the blowouts boarders on the surface. A comparison between 2005 and 2011 data shows that erosion is occurring at the end of the deflation basin and that sediment is being deposited into the depositional lobe in east to west fashion. Areas containing the steepest slopes on the windward side of the blowout show stratigraphy that is not continuous. These breaks in the stratigraphic record, seen as the subsurface toplap and downlap structures found in Transect 7 and 8, are where sediment has been eroded as the deflation basin grew in both width and depth. This eroded sediment can be found on the top and leeward side of the dune in both the LIDAR and GPR data.

SA2 also enters a new phase in 2002, Phase 3. At this site the blowout begins to vegetate until the physical blowout was completely stabilized between 2008 and 2010. As the blowout stabilizes the depositional lobe begins to migrate across the backbarrier stretching out the secondary dune into trailing arms. These arms slowly begin to vegetate

starting with the seaward margin first and moving into the backbarrier as the foredune reestablishes completely between 2002 and 2008. In 2010 due to the complete revegetation of the blowout structure this site enters Phase 5. Phase 3 and 4 can be further studied due to the LIDAR surveys taken between the two periods. These surveys show that the subsurface expression of the blowout moving from east to west is what is occurring on the surface. The cross bedded structure of found in the GPR record at this site is due to the amount of sediment deposited between these seven years. In some places over 5 meters of deposition occurred between 2005 and 2011 at a rate of .83 m/year, all of which are preserved in the stratigraphic record as climbing layers. At this site, sediment is being transported from the seaward side of the depositional lobe into its interior however now that the lobe is no longer attached to a sediment source, the dune, and no longer constrained by the blowout walls it may begin to spread out and become more parabolic

The coupling of ground penetrating radar with LIDAR and aerial photography has provided insight into how two blowouts within Padre Island National seashore have developed and evolved over the past 43 years. This data shows that both blowouts with in the study area go through cyclic phases that are associated with initiation due to increased wave runup, an external control, and recovery between storm events, an internal control. When there is a long period between storms the foredune can recover and the blowout begins to stabilize. However when there are frequent or high magnitude storms the foredune never has the time to redevelop protecting the backbarrier vegetation from being covered by sand and a blowout developing. When only surficial extents are known it is impossible to completely understand the cyclic nature of blowout development at PAIS. The internal structures found through completed GPR surveys help put together a greater understanding of how other blowouts in this region have developed and evolved over an extended period. This understanding in turn helps PAIS management assess their physical resources, ecosystems and develop plans of action for management issues in order to continue to "*save and preserve, for purposes of public recreation, benefit, and inspiration, a portion of the diminishing seashore of the United States that remains undeveloped..."* (NPS 1973, Weise and White 1980).

4.5 CONCLUSIONS

The following conclusions were drawn from this study:

1. Ground-penetrating radar successfully conveyed subsurface stratigraphy and structures associated with evolution phases that are found within the blowouts in Padre Island National Seashore.
2. Study Site 1 contains 5 phases over the course of the study showing revegetation of the initial blowout, reactivation due to wave scarping during storms, reestablishment of the foredune, more scarping due to storms and finally the beginnings of the foredune once again rebuilding.
3. Study Site 2 contains 4 phases starting with a small blowout that extends in size as its foredune is removed through wave scarping and the deflation basin and depositional lobe expands into the backbarrier. The foredune then rebuilds cutting off the wind and sediment allowing the blowout to revegetate until now when the only active sand is the depositional lobe moving into the backbarrier.
4. The radar surfaces and facies lend to an understanding of the conditions under which the sediment is deposited. Parallel horizontal reflections are associated with active aeolian processes and can be interpreted as active sand sheets and the historic backbarrier. Concave reflectors are linked with blowout necks and deflation basins as well as localized erosion while convex reflectors show deposition. Depending on the sequence of the facies with in the radar surfaces the historical morphology of the blowouts is known at individual locations.

5. CONCLUSION

Beach driving within Padre Island National Seashore provides induces an environment in which blowouts are more likely to develop. In areas that have blowouts but no vehicle traffic, blowouts completely stabilized while areas of high vehicle traffic less than one third of the blowouts have stabilized. Driving decreased the slope profile due to compaction and seaweed pulverization allowing for greater wave runup. This increased runup creates a longer beach recovery time between storms allowing for more foredune erosion and blowout development.

Ground penetrating radar surfaces and facies lend an understanding of the conditions under which the sediment is deposited. Parallel horizontal reflections are associated with active aeolian processes and can be interpreted as active sand sheets and the historic backbarrier. Concave reflectors are linked with blowout necks and deflation basins as well as localized erosion while convex reflectors show deposition. Depending on the sequence of the facies with in the radar surfaces the historical morphology of the blowouts is known at individual locations. GPR coupled with aerial photographs and LiDAR allow a three dimensional dynamic understanding of sediment movement within each study site. This understanding can then be projected out for the entire island to help the National Parks Service accurately manage the National Seashore.

REFERENCES

Aagaard, T., J .Orford and A.S. Murray (2007), Environmental Controls On Coastal Dune Formation; Skallingen Spit, Denmark. Geomorphology, 83, 18.

Aldenderfer, M. S., and R. K. Blashfield (1984), Cluster Analysis Sage Publications, Beverly Hills, California

Bailey, S., and C. S. Bristow (2000), Structure Of Coastal Dunes: Observations From Ground Penetrating Radar (GPR) Surveys, SPIE, 4084, 660-665.

Baker, G. S. and H. M. Jol. (2007) Stratigraphic Analyses Using GPR. Geological Society Of America, Boulder, Colorado.

Bate, G., and M. Ferguson (1996), Blowouts In Coastal Foredunes, Landscape And Urban Planning, 34(3), 215-224.

Blum, M., and J. R. Jones (1985), Variation In Vegetation Density And Foredune Complexity At North Padre Island, Texas, Texas Journal of Science, 37, 63-73.

Botha, G. A., C. S. Bristow, N. Porat, G. Duller, S. J. Armitage, H. M. Roberts, B. M. Clarke, M. W. Kota and P. Schoeman (2003), Evidence For Dune Reactivation From GPR Profiles On The Maputaland Coastal Plain, South Africa. Geological Society, London, Special Publications, 211, 29-46.

Brezina, D. N. (2005), Soil Survey Of Padre Island National Seashore, Texas, Special Report. Natural Resources Conservation Service. US Department of Interior.

Bristow, C. S., G. A. T. Duller and N. Lancaster (2007), Age And Dynamics Of Linear Dunes In The Namib Desert. Geology, 35, 555-558.

Brock, J. C., W.B. Karbill, and A. H. Sallenger, (2004), Barrier Island Morphodynamic Classification Based On LiDAR Metrics For North Assateague Island, Maryland, Journal Of Coastal Research, 20(2), 489-509.

Carter, R.W.G., K.F. Nordstrom, and N.P. Psuty (1990), The study of coastal dunes. In K.F. Nordstrom, N.P. Psuty, and R.W.G. Carter, eds. Coastal Dunes: Processes and Morphology. London: John Wiley &

Sons, pp. 1-14. Claudino-Sales, V., P. Wang and M. H. Horwitz (2008), Factors Controlling The Survival Of Coastal Dunes During Multiple Hurricane Impacts In 2004 And 2005: Santa Rosa Barrier Island, Florida. Geomorphology, 95, 295-315.

Cowles, H. C. (1898), The Ecological Relations Of The Vegetation On The Sand Dunes Of Lake Michigan. The University Of Chicago Press, Chicago.

Davidson-Arnott, R. G. D. (2005), Conceptual Model Of The Effects Of Sea Level Rise On Sandy Coasts, Journal Of Coastal Research, 21(6), 1166-1172.

Department Of Environment and Resource Management (Dept. of E&R Mgmt) The Formation And Function Of Coastal Dunes. Web. 24 April 2012. <http://www.derm.qld.gov.au/register/p00080aa.pdf>

Dickenson, K., HL Berryhill and CW Holmes (1972), Criteria For Recognizing Ancient Barrier Coastlines, In Recognition Of Ancient Sedimentary Environments, Edited By J. K. Rigby, Society Of Economic Paleontologists And Mineralogists. Tulsa, Oklahoma.

Fraley, C., and A. E. Raftery (1998), How Many Clusters? Which Clustering Method? Answers Via Model-Based Cluster Analysis, The Computer Journal, 41(8), 578-588.

Gares, P. A. (1992), Topographic Changes Associated With Coastal Dune Blowouts At Island Beach State Park, New Jersey, Earth Surface Processes And Landforms, 17(6), 589-604.

Gares, P.A. and K.F. Nordstrom (1988), The origin of dune swale blowouts at Island Beach, New Jersey, Geographical Review, 78, 194-204.

Garrison, J. R., J. Williams, S. Potter Miller, E. T. Weber, G. Mcmechan, and X. Zeng (2010), Ground-Penetrating Radar Study Of North Padre Island: Implications For Barrier Island Internal Architecture, Model For Growth Of Progradational Microtidal Barrier Islands, And Gulf Of Mexico Sea Level Cyclicity, Journal Of Sedimentary Research, 80(4), 303-319.

Gibeaut, J. C., T. Hepner, R. Waldinger, A. Gutierrez, J. R. Gutierrez, T. A. Tremblay, R. Smyth, and L. Xu (2001), Changes In Gulf Shoreline Position, Mustang, And North Padre Islands, Texas, Bureau Of Economic Geology, Austin.

Godfrey, P. J., and M. M. Godfrey (1973), Comparison Of Ecological And Geomorphic Interactions Between Altered And Unaltered Barrier Island Systems In North Carolina, Coastal Geomorphology, SUNY-Binghamton, Publications in Geomorphology, 239-258.

González-Villanueva, R., S. Costas, H. Duarte, M. Pérez-Arlucea and I. Alejo (2011), Blowout evolution in a coastal dune: using GPR, aerial imagery and core records.

Journal of Coastal Research, SI 64 (Proceedings of the 11th International Coastal Symposium), 278 – 282. Szczecin, Poland, ISSN 0749-0208

Harari, Z. (1996), Ground-Penetrating Radar (GPR) For Imaging Stratigraphic Features And Groundwater In Sand Dunes, Journal Of Applied Geophysics, 36(1), 43-52.

Havholm, K. G., D. V. Ames, G. R. Whittecar, B. A. Wenell, S. R. Riggs, H. M. Jol, G. W. Berger, and M. A. Holmes (2004), Stratigraphy Of Back-Barrier Coastal Dunes, Northern North Carolina And Southern Virginia, Journal Of Coastal Research, 980-999.

Hayes, M. O. (1967), Hurricanes As Geological Agents: Case Studies Of Hurricanes Carla, 1961, And Cindy, 1963. University of Texas Bureau of Economic Geology, Report of Investigations No. 61.

Hesp, P. (2002), Foredunes And Blowouts: Initiation, Geomorphology And Dynamics, Geomorphology, 48(1–3), 245-268.

Hesp, P. A., and R. Hyde (1996), Flow Dynamics And Geomorphology Of A Trough Blowout, Sedimentology, 43(3), 505-525.

Houser, C., C. Hapke, and S. Hamilton (2008), Controls On Coastal Dune Morphology, Shoreline Erosion And Barrier Island Response To Extreme Storms, Geomorphology, 100, 17.

Houser, C., B. Labude, L. Haider, and B. Weymer (2013), Impacts Of Driving On The Beach: Case Studies From Assateague Island And Padre Island National Seashores, Ocean & Coastal Management. , 71, 33-45

Houser, C. A. and S. Hamilton (2009), Sensitivity Of Post-Hurricane Beach And Dune Recovery To Event Frequency, Earth Surface Processes And Landforms, 34, 15.

Hoyt, J. H. (1967), Barrier Island Formation, Geological Society Of America Bulletin, 78(9), 1125-1136.

Hugenholtz, C. H., and S. A. Wolfe (2009), Form–Flow Interactions Of An Aeolian Saucer Blowout, Earth Surface Processes And Landforms, 34(7), 919-928.

Hugenholtz, C. H., S. A. Wolfe, and B. J. Moorman (2008), Effects Of Sand Supply On The Morphodynamics And Stratigraphy Of Active Parabolic Dunes, Bigstick Sand Hills, Southwestern Saskatchewan Geological Survey Of Canada Contribution 20060654, Canadian Journal Of Earth Sciences, 45(3), 321-335.

Irish, J. L., and W. J. Lillycrop (1999), Scanning Laser Mapping Of The Coastal Zone: The SHOALS System, ISPRS Journal Of Photogrammetry And Remote Sensing, 54(2-3), 123-129.

Jol, H. M. and C. S. Bristow (2003), GPR In Sediments: Advice On Data Collection, Basic Processing And Interpretation, A Good Practice Guide. Geological Society, London, Special Publications, 211, 9-27.

Jungerius, P. D., A. J. T. Verheggen, and A. J. Wiggers (1981), The Development Of Blowouts In ‘De Blink’, A Coastal Dune Area Near Noordwijkerhout, The Netherlands, Earth Surface Processes And Landforms, 6(3-4), 375-396.

Leatherman, S. P. (1979), Barrier Dune Systems: A Reassessment, Sedimentary Geology, 24(1–2), 1-16.

Leatherwood, Art. Padre Island, Handbook Of Texas Online. The Texas State Historical Association. Web. February 28, 2013. <http://Www.Tshaonline.Org/Handbook/Online/Articles/Rrp01>

Levin, N. (2011), Climate-Driven Changes In Tropical Cyclone Intensity Shape Dune Activity On Earth's Largest Sand Island, Geomorphology, 125(1), 239-252.

Mathewson, C., and W. Cole (1980), Geomorphic Processes And Land Use Planning, South Texas Barrier Islands, Applied Geomorphology 16.

Mathewson, C. C. (1987), Aeolian Processes—A Long-Term Coastal Sediment Transport Mechanism, Coastal Sediments '87, 1, 222-235.

Mcgourty, J. and P. Wilson (2000), Investigating The Internal Structure Of Holocene Coastal Sand Dunes Using Ground-Penetrating Radar: Example From The North Coast Of Northern Ireland. 14-19.

Mcgowen, J., C. Groat, L. Brown Jr, W. Fisher and A. Scott (1970), Effects Of Hurricane Celia, A Focus On Environmental Geologic Problems Of The Texas Coastal Zone. University Of Texas At Austin, Bureau Of Economic Geology.

Morton, R. A. (1977), Historical shoreline changes and their causes, Texas Gulf Coast. Gulf Coast Association of Geological Societies Transactions, 27, 352–364. Transactions Of The Gulf Coast Association Of Geological Societies, 27, 13.

Morton, R. A. and J. McGowen (1980), Modern depositional environments of the Texas coast. Austin, Tex: Bureau of Economic Geology, University of Texas at Austin.

Morton, R. A., J. G. Paine and J. C. Gibeaut (1994), Stages And Durations Of Post-Storm Beach Recovery, Southeastern Texas Coast, U.S.A. Journal Of Coastal Research, 10, 884-908.

Morton, R. A., and A. H. Sallenger Jr (2003), Morphological Impacts Of Extreme Storms On Sandy Beaches And Barriers, Journal Of Coastal Research, 560-573.

National Park Service (NPS) (1973), Padre Island National Seashore Master Plan. U.S. Department Of The Interior.

National Park Service (NPS) (2010), Padre Island National Seashore Geologic Resources Inventory Report. Natural Resource Report NPS/NRPC/GRD/NRR—2010/246. National Park Service, Ft. Collins, Colorado.

National Park Service (NPS) (2012), Beach Vehicle Environmental Assessment Finding Of No Significant Impact, 56, Corpus Christi, Texas

National Oceanic and Atmospheric Administration (NOAA). Historical Hurricane Tracks. Web. 18 September 2012. <http://www.csc.noaa.gov/hurricanes/>.

Neal, A. (2004), Ground-Penetrating Radar And Its Use In Sedimentology: Principles, Problems And Progress. Earth-Science Reviews, 66, 261-330.

Neal, A., and C. L. Roberts (2001), Internal Structure Of A Trough Blowout, Determined From Migrated Ground-Penetrating Radar Profiles, Sedimentology, 48(4), 791-810.

Nield, J. M., and A. C. W. Baas (2008), The Influence Of Different Environmental And Climatic Conditions On Vegetated Aeolian Dune Landscape Development And Response, Global And Planetary Change, 64(1–2), 76-92.

Oosting, H. J., and W. D. Billings (1942), Factors Effecting Vegetational Zonation On Coastal Dunes, Ecology, 23(2), 131-142.

Otvos, E. G. (1970), Development And Migration Of Barrier Islands, Northern Gulf Of Mexico, Geological Society Of America Bulletin, 81(1), 241-246.

Prouty, J. S., and D.B. Prouty (1989), Historical Back-Barrier Shoreline Changes, Padre Island National Seashore, Texas, Transactions - Gulf Coast Association Of Geological Societies, 39, 9.

Psuty, N. P. (1992), Spatial variation in coastal foredune development, in: Carter, R.W.G. et al. (Ed.) (1992). Coastal dunes: geomorphology, ecology and management for conservation: Proceedings of the 3rd European Dune Congress Galway, Ireland, 17-21 June 1992. pp. 3-13

Sallenger, A. H. Jr. (2000), Storm Impact Scale For Barrier Islands, Journal Of Coastal Research, 16(3), 890-895.

Sallenger, A. H. Jr., Et Al. (2003), Evaluation Of Airborne Topographic LiDAR For Quantifying Beach Changes, Journal Of Coastal Research, 19(1), 125-133.

Scott, A. J., and M. Knott (1974), A Cluster Analysis Method For Grouping Means In The Analysis Of Variance, Biometrics, 30(3), 507-512.

Sensors & Software, Inc. (1999), Practical Processing Of GPR Data. 18. Mississauga.

Smith, D. G., C. J. Simpson, H. M. Jol, R. A. Meyers, and D. R. Currey (2003), GPR Stratigraphy Used To Infer Transgressive Deposition Of Spits And A Barrier, Lake Bonneville, Stockton, Utah, USA, Geological Society, London, Special Publications, 211(1), 79-86.

Statsoft, Inc. (2013). Electronic Statistics Textbook. Tulsa, OK: Statsoft. Web. Accessed 17 April 2013. <http://www.statsoft.com/textbook/>

Stockdon, H. F., R. A. Holman, P. A. Howd and A. H. Sallenger Jr (2006) Empirical Parameterization Of Setup, Swash, And Runup. Coastal Engineering, 53, 573-588.

Stoker, J. M., D. P. Turnipseed, and K. V. Wilson (2011), Using Regional Scale Pre- And Post-Hurricane Katrina Lidar For Monitoring And Modeling, In Recent Hurricane Research-Climate, Dynamics, And Societal Impacts, Edited By A. Lupo And Of, Pp. 575-592, Intech, Vukovar, Croatia.

Stokes, S. And J. B. Swinehart. 1997. Middle- And Late-Holocene Dune Reactivation In The Nebraska Sand Hills, USA.

Texas General Land Office (GLO) (2005), The Dune Protection And Improvement Manual For The Texas Gulf Coast. Web. 24 February 2013. <http://coastal.tamug.edu/am/CapturedWebSites/GLO_Coastal_Dune_Manual/index.html>

Tsoar, H., and D. G. Blumberg (2002), Formation Of Parabolic Dunes From Barchan And Transverse Dunes Along Israel's Mediterranean Coast, Earth Surface Processes And Landforms, 27(11), 1147-1161.

Weise, B. R., and W. A. White (1980), Padre Island National Seashore: A Guide To The Geology, Natural Environments, And History Of A Texas Barrier Island, Edited, Bureau Of Economic Geology, Austin.

White, S. A., and Y. Wang (2003), Utilizing Dems Derived From LIDAR Data To Analyze Morphologic Change In The North Carolina Coastline, Remote Sensing Of Environment, 85(1), 39-47.

Wolfe, S. A., and C. H. Hugenholtz (2009), Barchan Dunes Stabilized Under Recent Climate Warming On The Northern Great Plains, Geology, 37(11), 1039-1042.

Woolard, J. W., and J. D. Colby (2002), Spatial Characterization, Resolution, And Volumetric Change Of Coastal Dunes Using Airborne LIDAR: Cape Hatteras, North Carolina, Geomorphology, 48(1–3), 269-287.

APPENDIX 1. STUDY SITE 1 GPR PROFILES

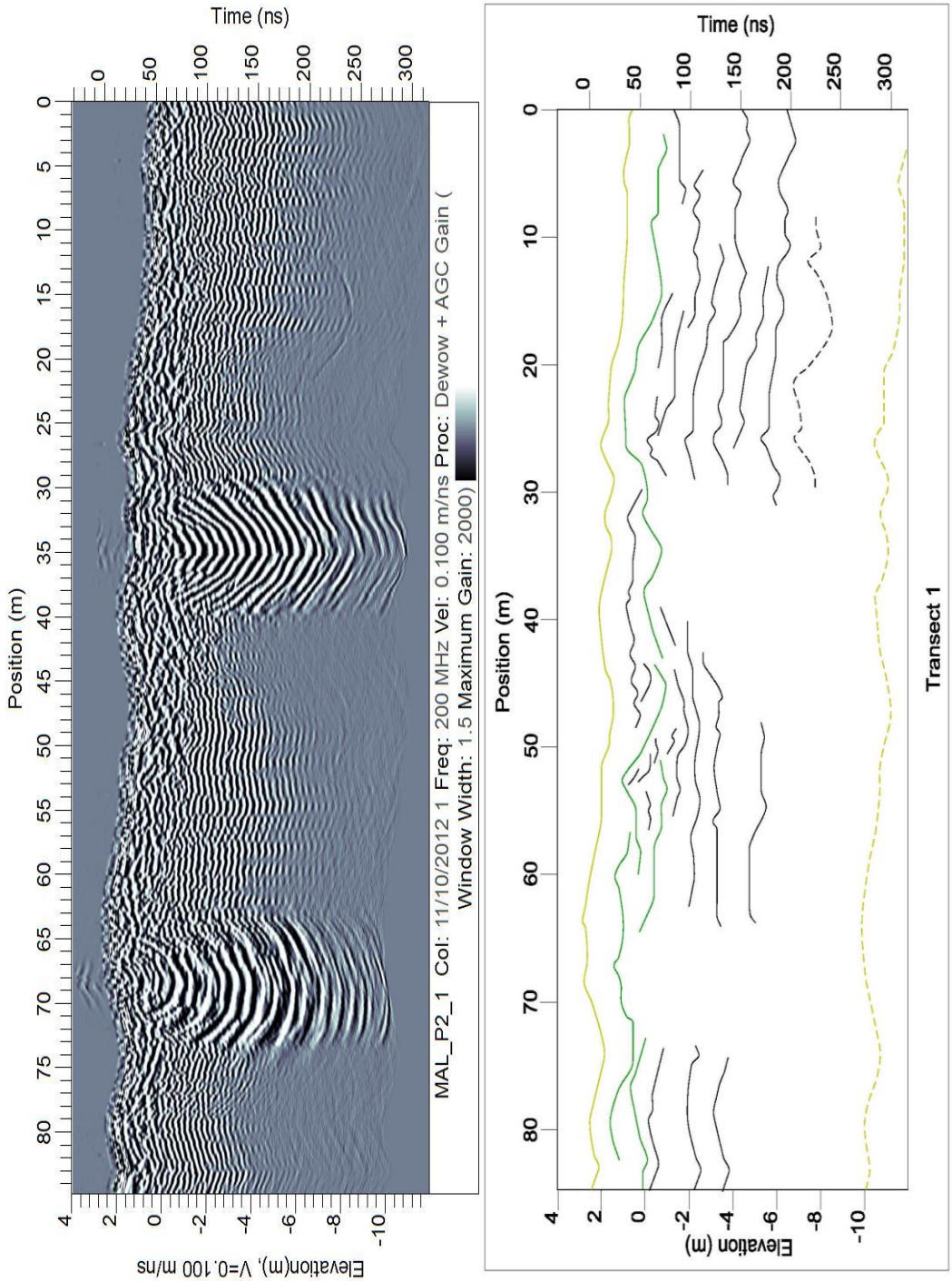

Transect 1

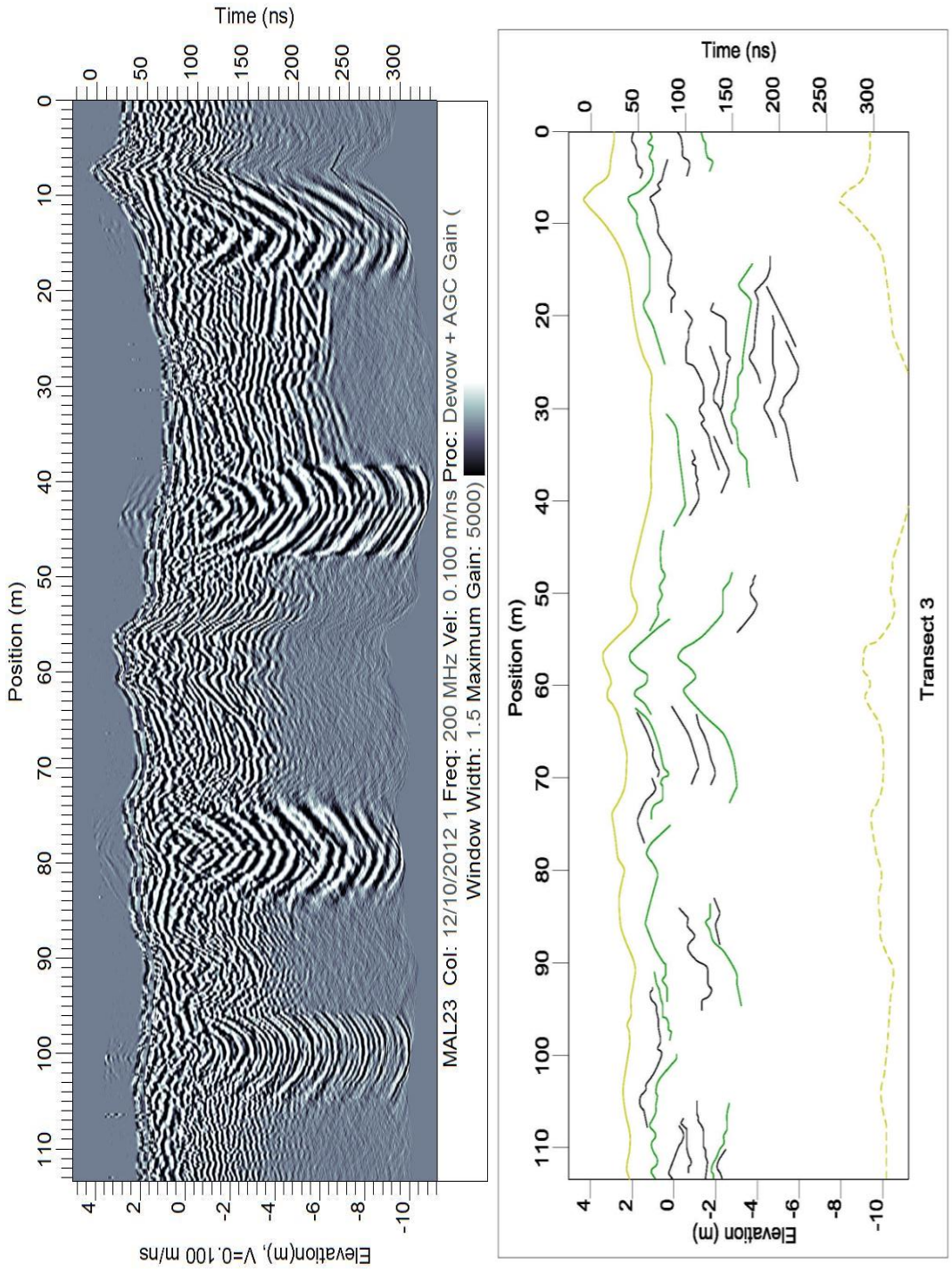
Time (ns)
Position (m)
Elevation(m), V=0.100 m/ns
MAL23 Col: 12/10/2012 1 Freq: 200 MHz Vel: 0.100 m/ns Proc: Dewow + AGC Gain (
Window Width: 1.5 Maximum Gain: 5000)
Time (ns)
Position (m)
Elevation (m)
Transect 3

Transect 3

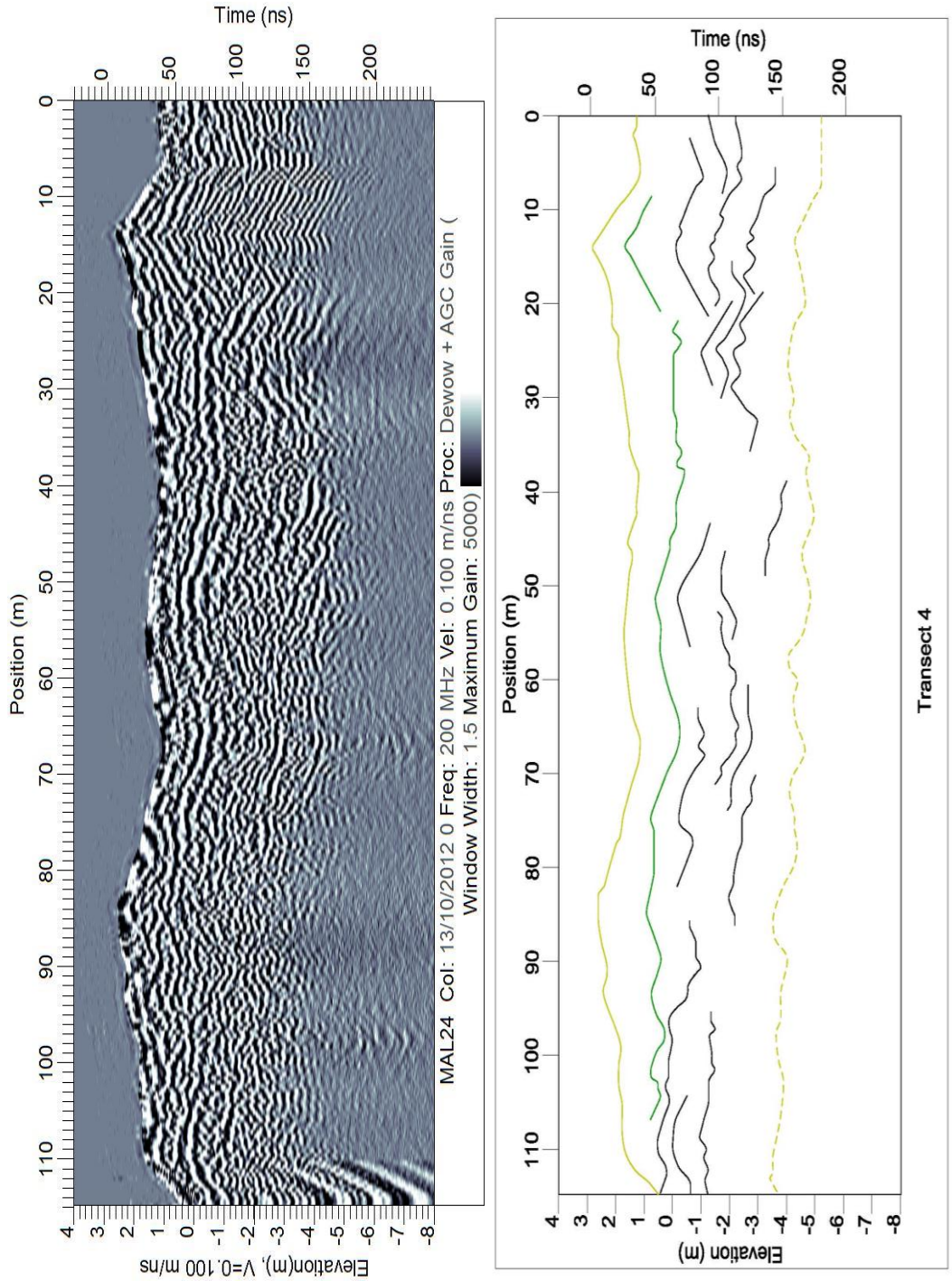
Time (ns)
Position (m)
Elevation(m), V=0.100 m/ns
MAL24 Col: 13/10/2012 0 Freq: 200 MHz Vel: 0.100 m/ns Proc: Dewow + AGC Gain (
Window Width: 1.5 Maximum Gain: 5000)
Time (ns)
Position (m)
Elevation (m)
Transect 4

Transect 4

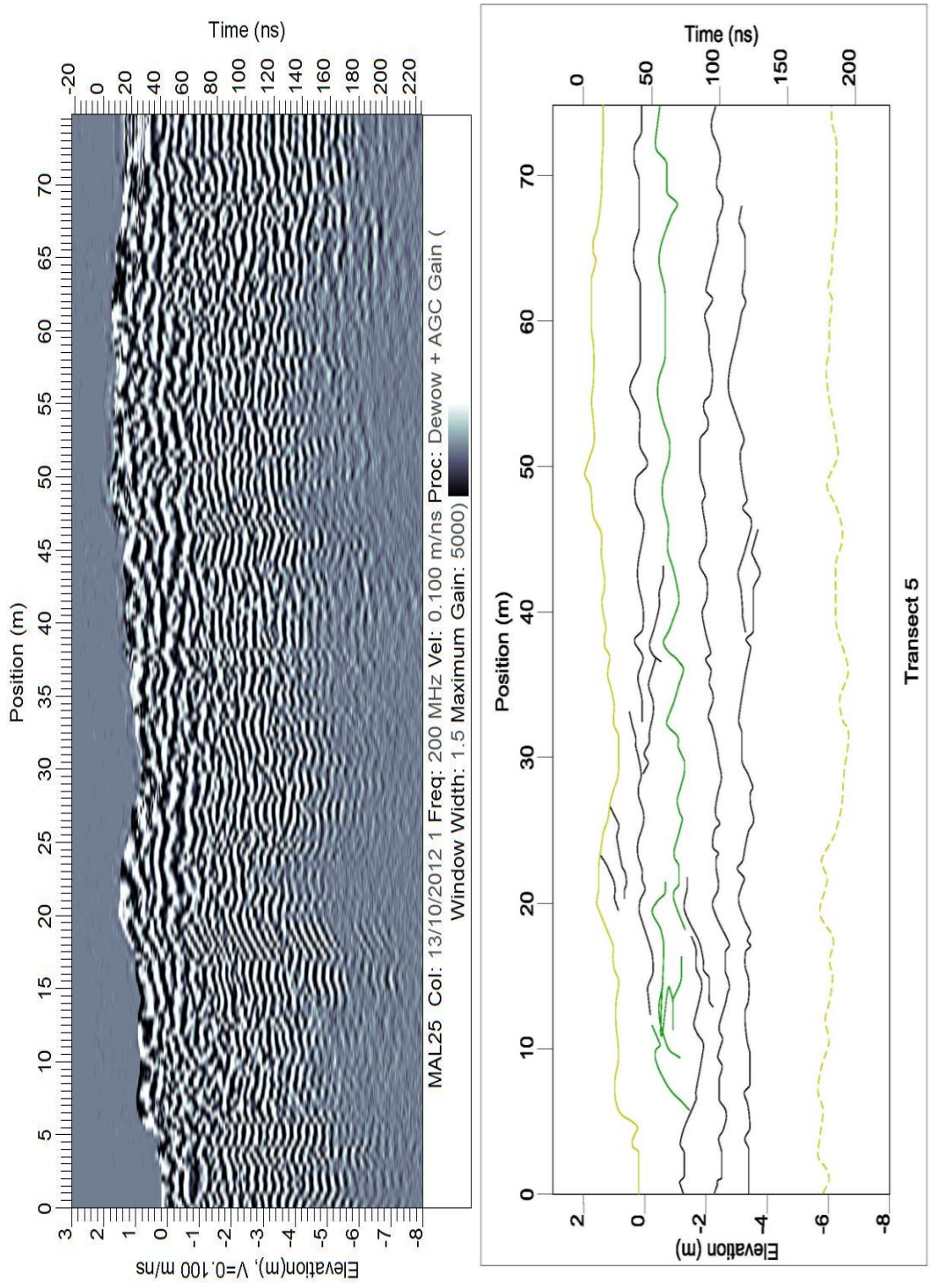
Time (ns)
Position (m)
Elevation(m), V=0.100 m/ns
MAL25 Col: 13/10/2012 1 Freq: 200 MHz Vel: 0.100 m/ns Proc: Dewow + AGC Gain (
Window Width: 1.5 Maximum Gain: 5000)
Time (ns)
Position (m)
Elevation (m)
Transect 5

Transect 5

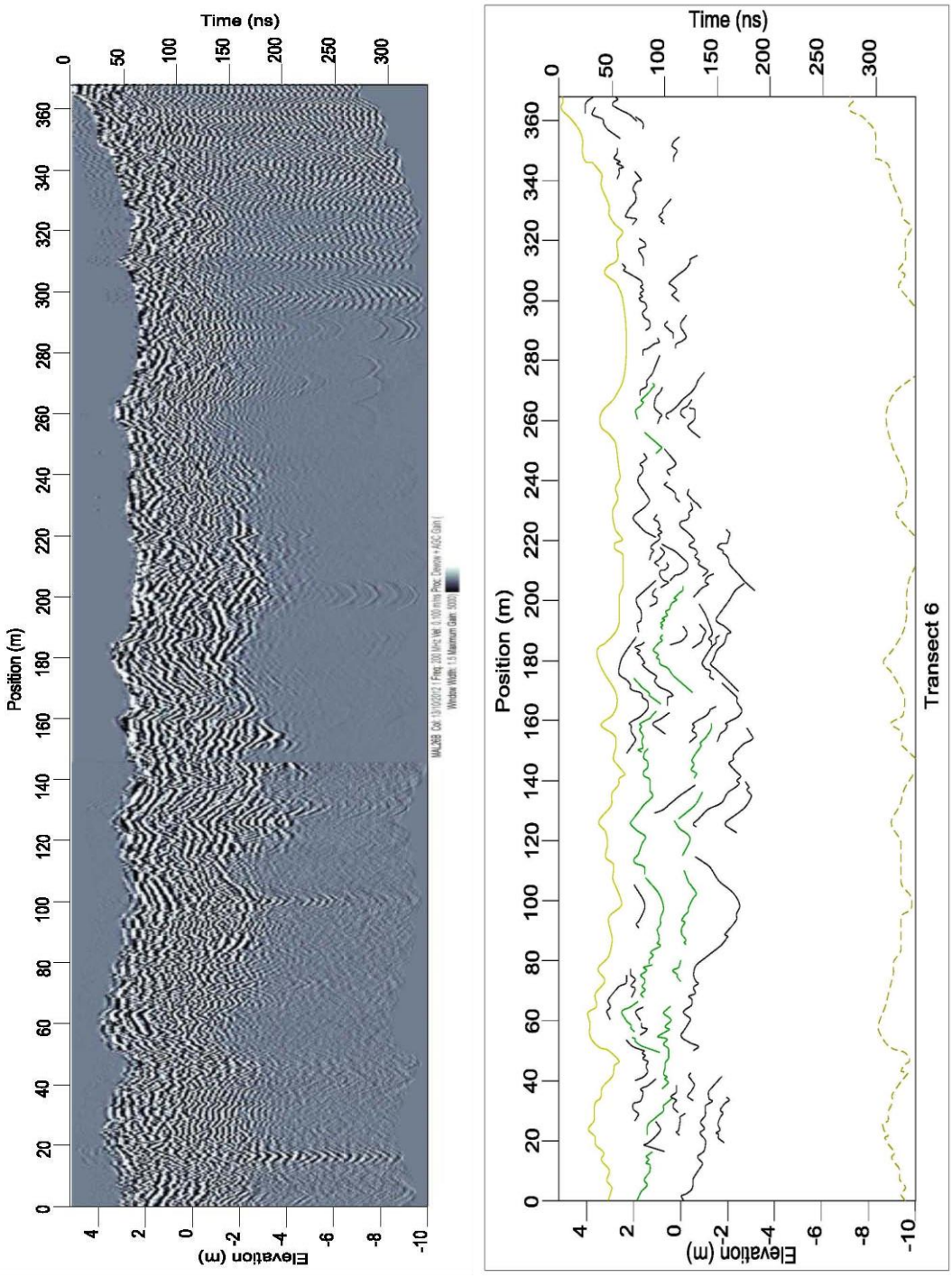

Transect 6

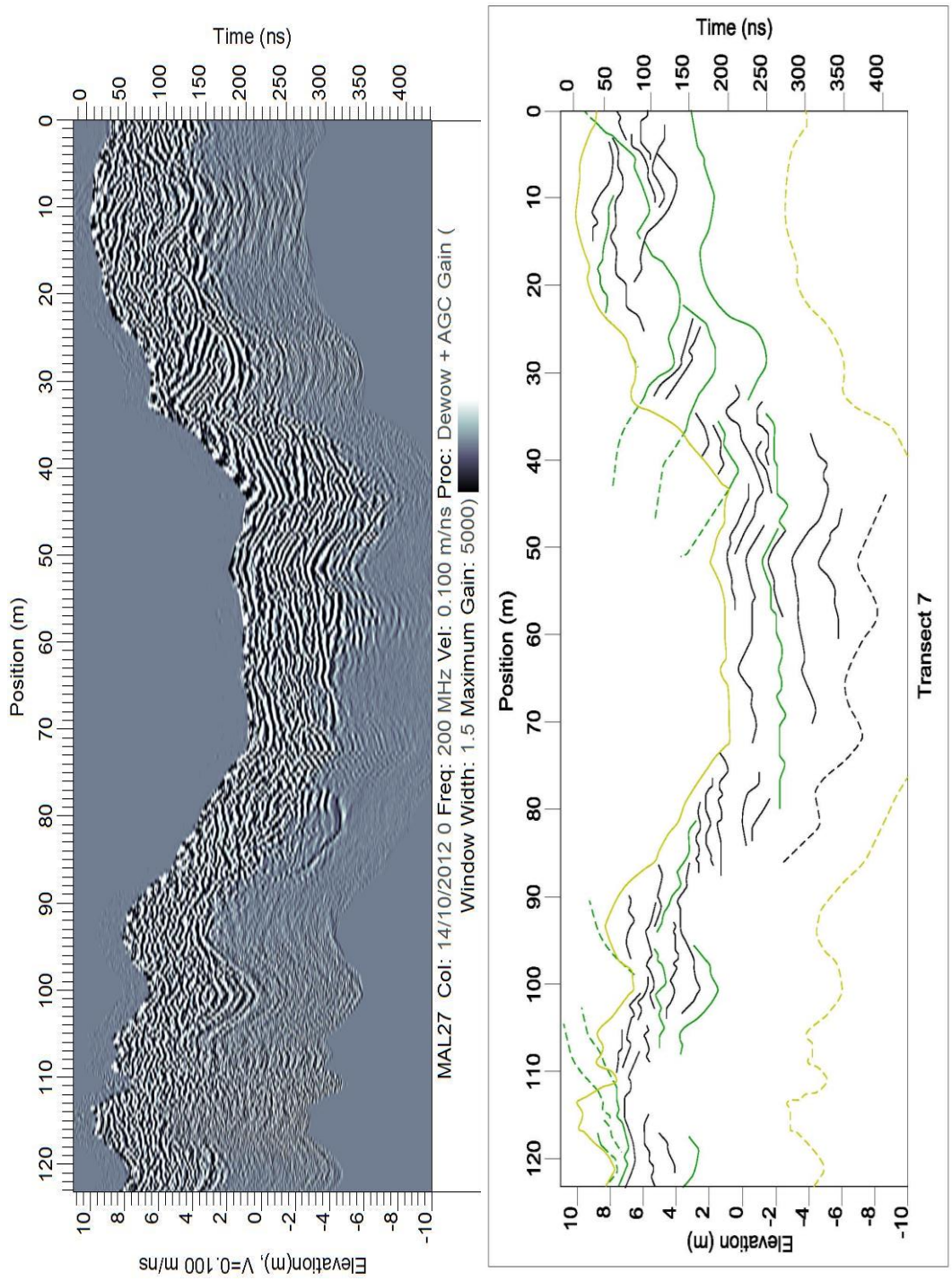
Time (ns)
Position (m)
MAL27 Col: 14/10/2012 0 Freq: 200 MHz Vel: 0.100 m/ns Proc: Dewow + AGC Gain (
Window Width: 1.5 Maximum Gain: 5000)
Elevation(m), V=0.100 m/ns
Time (ns)
Position (m)
Elevation (m)
Transect 7

Transect 7

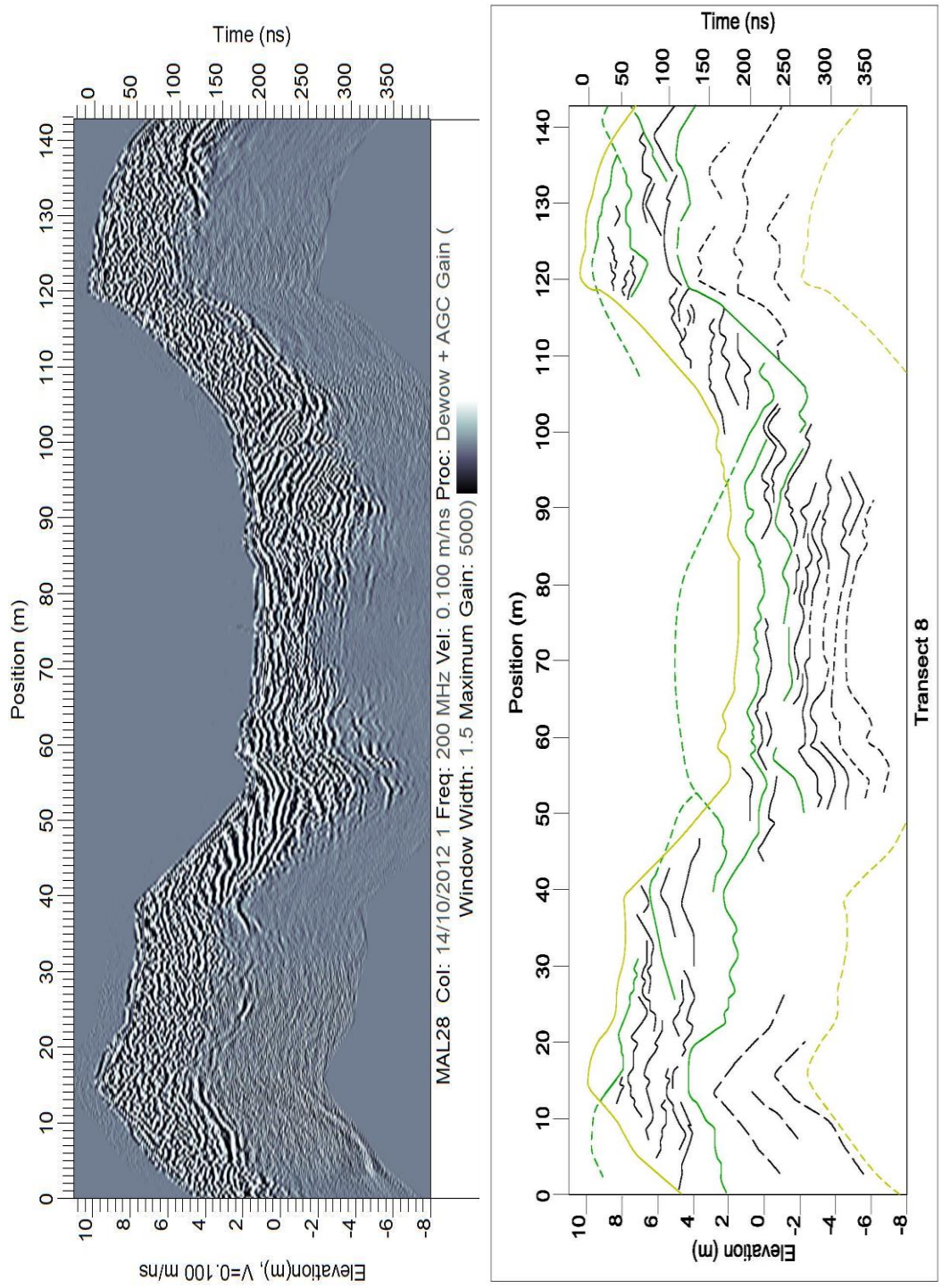
Time (ns)
Position (m)
Elevation(m), V=0.100 m/ns
MAL28 Col: 14/10/2012 1 Freq: 200 MHz Vel: 0.100 m/ns Proc: Dewow + AGC Gain (
Window Width: 1.5 Maximum Gain: 5000)
Time (ns)
Position (m)
Elevation (m)
Transect 8

Transect 8

APPENDIX 2. STUDY SITE 2 GPR PROFILES

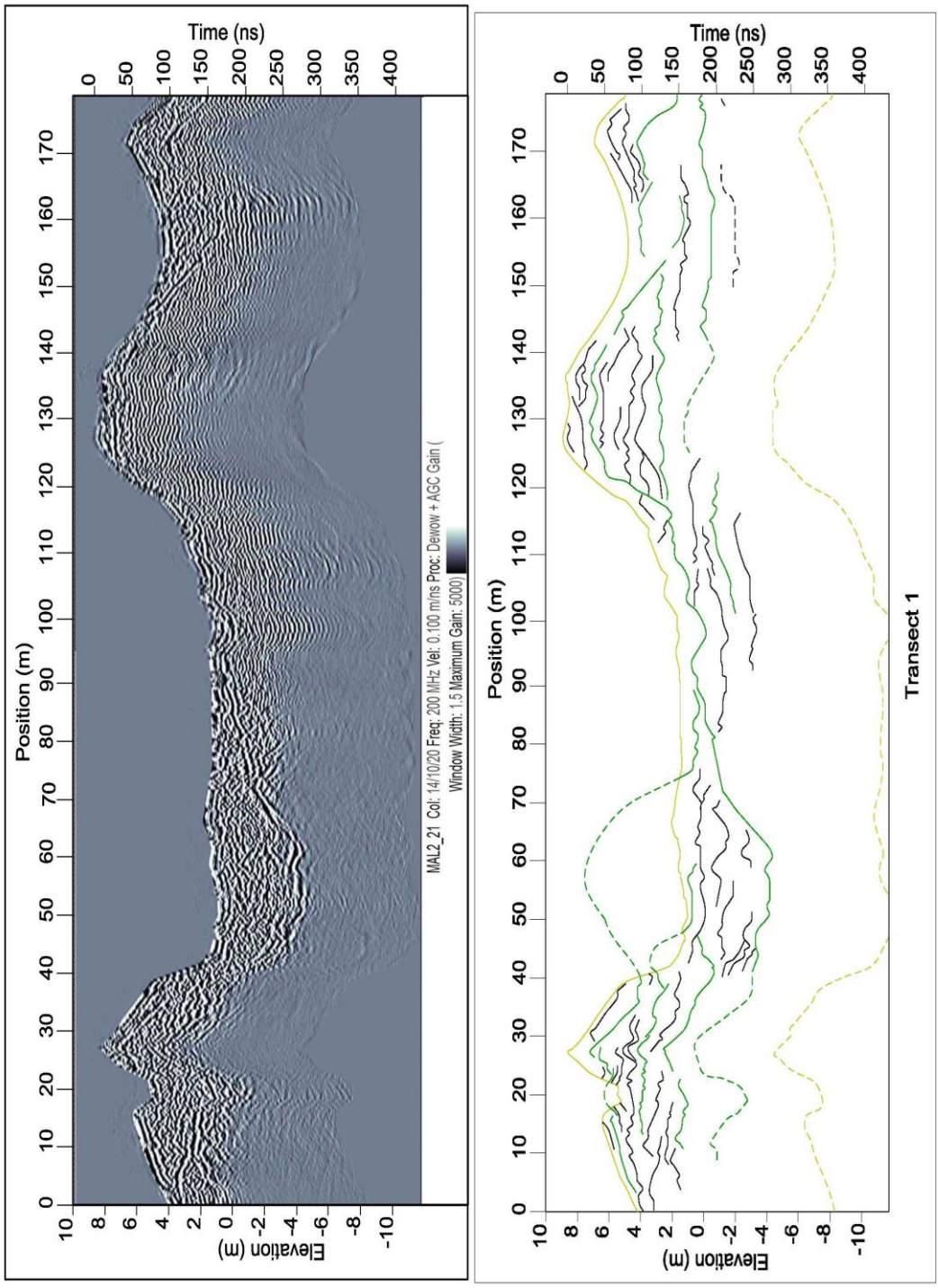

Transect 1

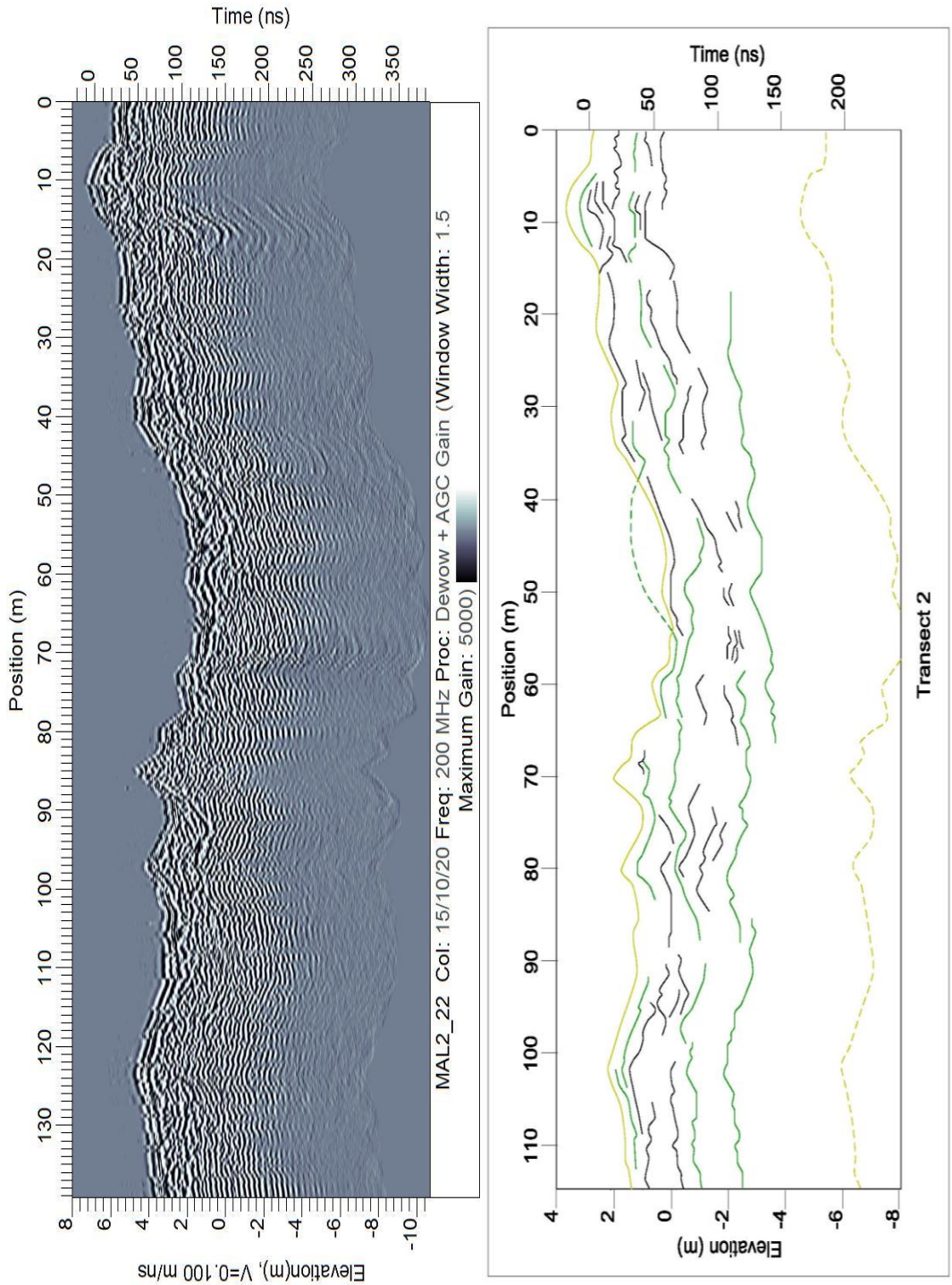
Time (ns)
Position (m)
Elevation(m), V=0.100 m/ns
MAL2_22 Col: 15/10/20 Freq: 200 MHz Proc: Dewow + AGC Gain (Window Width: 1.5
Maximum Gain: 5000)
Time (ns)
Position (m)
Elevation (m)
Transect 2

Transect 2

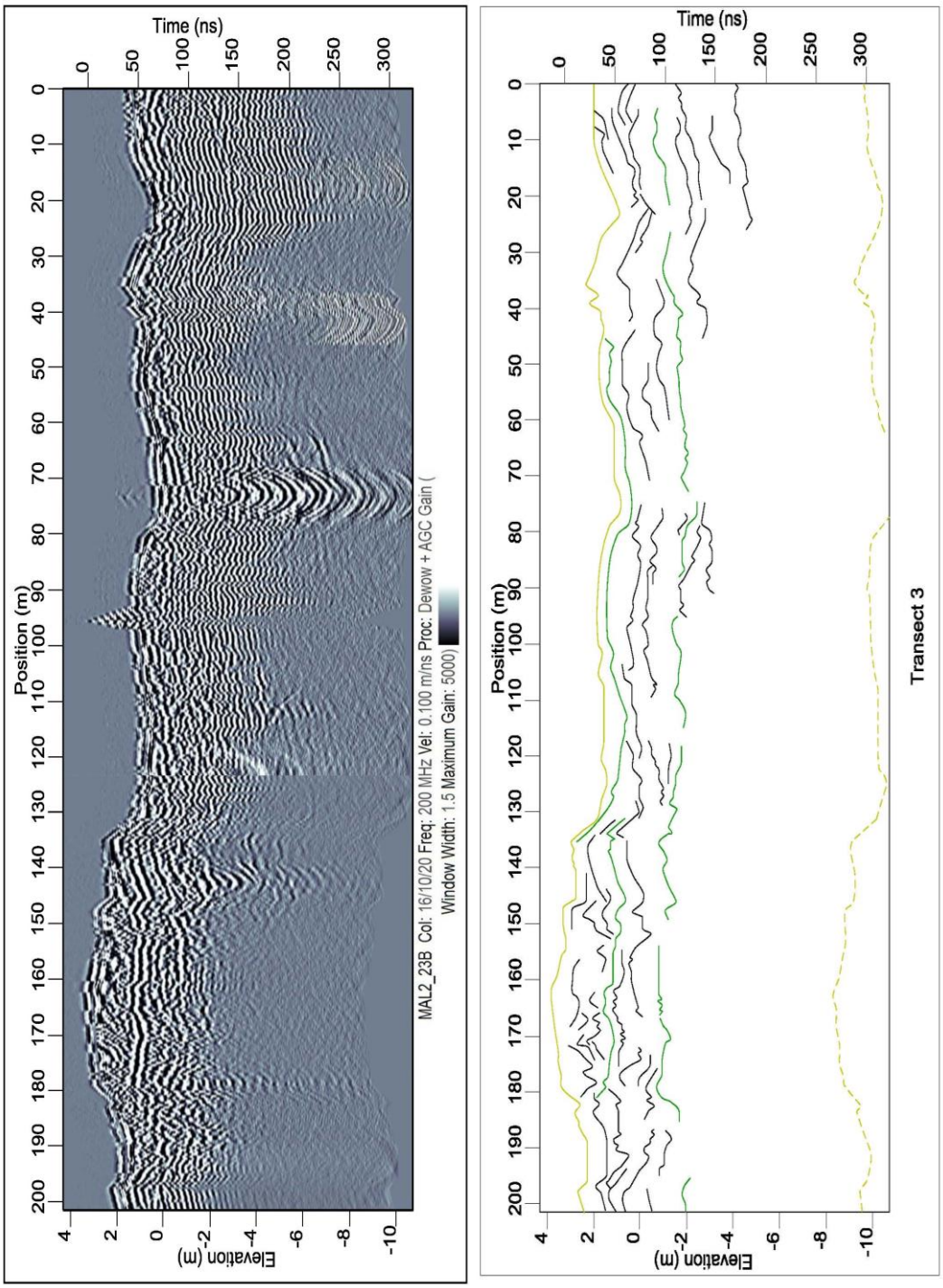
Time (ns)
Position (m)
Elevation (m)
MAL2_23B Col: 16/10/20 Freq: 200 MHz Vel: 0.100 m/ns Proc: Dewow + AGC Gain (
Window Width: 1.5 Maximum Gain: 5000)
Transect 3

Transect 3

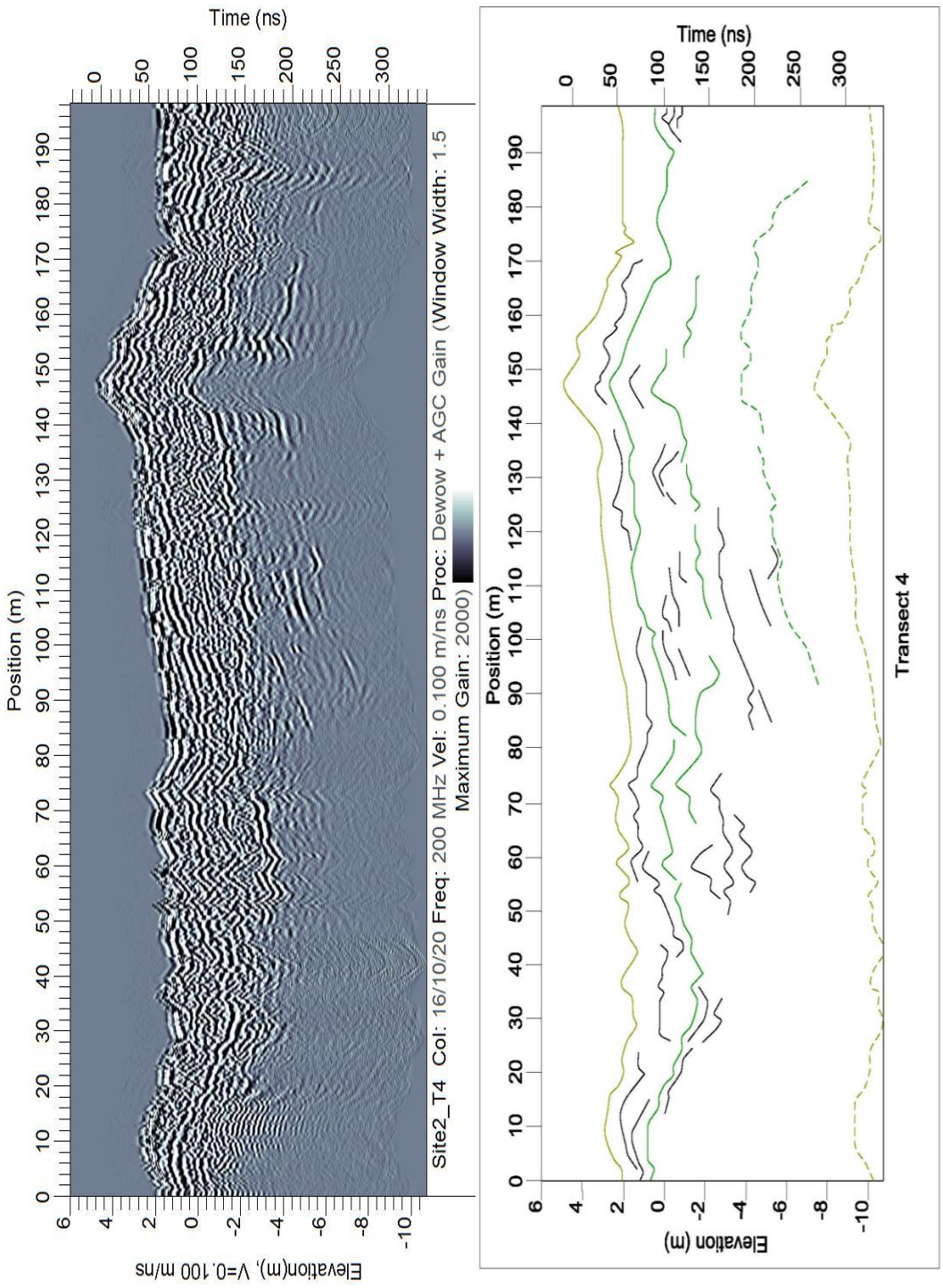
Time (ns)
Position (m)
Elevation(m), V=0.100 m/ns
Site2_T4 Col: 16/10/20 Freq: 200 MHz Vel: 0.100 m/ns Proc: Dewow + AGC Gain (Window Width: 1.5
Maximum Gain: 2000)
Time (ns)
Position (m)
Elevation (m)
Transect 4

Transect 4